Arborescent Polypeptides for the Targeted and Controlled Release of Drugs

by

Jun-Zhi Wang

A thesis

presented to the University of Waterloo

in fulfilment of the

thesis requirement for the degree of

Master of Science

in

Chemistry

Waterloo, Ontario, Canada, 2022

Author's Declaration

I hereby declare that I am the sole author of this thesis. This is a true copy of the thesis, including any required final revisions, as accepted by my examiners.

I understand that my thesis may be made electronically available to the public.

Abstract

Amphiphilic block copolymer micelles are commonly used as drug delivery agents, but these micelle structures tend to dissociate upon dilution. In contrast, arborescent copolymers are highly branched unimolecular micelles that remain stable under diluted conditions. This thesis work deals with the synthesis and the characterization of pH-responsive arborescent copolymer micelles containing a poly(γ-benzyl L-glutamate) (PBG) core, a poly(N^{ε}-carbonylbenzoxy L-lysine) (PZLys) inner layer, and a poly(ethylene glycol) (PEG) shell. One of the PEG chain ends was modified with an aldehyde group to couple with the amine groups of deprotected PLys chains and form imine bonds, allowing cleavage of the PEG chains under acidic conditions.

The arborescent micelles were synthesized by a generation-based grafting scheme. Linear PBG was prepared by ring-opening polymerization of γ-benzyl L-glutamate N-carboxyanhydride with *n*-hexylamine as initiator. A fraction of the benzylic protecting groups was removed with HBr, to expose free carboxylic acid groups which were coupled with the amine terminus of other PBG chains to form a generation zero arborescent structure (G0PBG). This deprotection and coupling reaction was repeated using either PBG or PZLys chains to obtain higher-generation arborescent copolymers, G0PBG-*g*-PZLys and G1PBG-*g*-PZLys. The protecting groups of PZLys were then removed with HBr, and the PLys segments were coupled with aldehyde-terminated PEG chains.

Arborescent structures with narrow molecular weight distributions ($M_w/M_n < 1.10$) were obtained up to generation G2, with molecular weights increasing exponentially for successive generations. In the deprotection of the Z groups on arborescent PBG-*g*-PZLys, the remaining benzylic protecting groups in the PBG core were also inadvertently deprotected. As a result, dynamic light scattering (DLS) measurements in water revealed the presence of aggregated species,

attributed to electrostatic intermolecular interactions between the lysine and glutamic acid units. More consistent size and zeta potential measurement were obtained in phosphate buffered saline (PBS) and 0.1 M HCl solutions, to protonate the amine and carboxyl groups of G0PBG-*g*-PLys. In PBS, the size and zeta potential were found to be 8.1 nm and 13 mV for G0PBG-*g*-PLys, and 13.6 nm and 21 mV for G1PBG-*g*-PLys, respectively. To avoid aggregation under conditions closer to neutrality, it is suggested that an alternate protecting group be used for the PLys chains, to allow full deprotection of the PLys chains without affecting the PBG units.

Imine formation between primary amines and aldehydes was found to be difficult. When a small-molecule amine was reacted with aldehyde-terminated PEG, almost quantitative yield was achieved at room temperature without removal of the water by-product. For linear PLys, drying agents were needed to drive the equilibrium towards imine formation and only 24% of the PEG chains were coupled. For the arborescent structures only a low imine yield was achieved, even by heating and stirring with a drying agent. Lower accessibility of the amine groups is considered to be the main cause for the decreased imine formation efficiency in linear PLys and the arborescent structures.

Acknowledgements

I would like to express my sincere gratitude to Professor Mario Gauthier for giving me the opportunity to complete my Master's studies in his research group. I really appreciated his patient and professional guidance and supervision throughout the project. It has been a wonderful experience being his student for the past two years, during which I have learned from him not only about polymer chemistry, but also scientific thinking when conducting research. I would also like to thank Professor Jean Duhamel and Professor Michael Tam for being my committee members and providing feedback on my thesis.

I would like to thank the current and past Gauthier lab members Natun Dasgupta, Deepak Vishnu Dharmangadan, Joanne Fernandez, Benjamin Hisey, Nicholas Lanigan and Dirceu Pereira dos Santos, as well as the Duhamel lab members Abdullah Ba Salem, Remi Casier, Franklin Frasca, Damin Kim, Alex Liu, Hunter Little, Kristijian Lulic, Sanjay Patel, Janine Thoma and Zehou You, for their company and for making the lab a very friendly environment throughout my graduate studies.

I would like to thank all my friends and family for their love, care and support, especially during the challenging times of a global pandemic. Lastly, I would like to thank God for providing me strength and encouragement throughout this journey.

Table of Contents

List of Figures

List of Tables

List of Schemes

List of Abbreviations and Symbols

ATRP	Atom transfer radical polymerization
BAIB	Bis(acetoxy)iodoobenzene
Boc	*tert*-Butyloxycarbonyl
BTF	Benzotrifluoride (α,α,α-trifluorotoluene)
BzGlu	γ-Benzyl L-glutamate
CMC	Critical micelle concentration
CuAAC	Cu(I)-catalyzed azide-alkyne cycloaddition
DCC	Dicyclohexylcarbodiimide
DCM	Dichloromethane
DIB	1,3-Diisoproprenylbenzene
DIC	*N*,*N*'-Diisopropylcarbodiimide
DMAP	4-Dimethylaminopyridine
DNA	Deoxyribonucleic acid
DOX	Doxorubicin
EPR	Enhanced permeability and retention

FmBA	4-Formylbenzoic acid
GPC	Gel permeation chromatography
Gx	Generation x (of dendritic polymer)
HMES	4-(1-Hydroxy-1-methylethyl)styrene
HOBt	*N*-Hydroxybenzotriazole
MALLS	Multi-angle laser light scattering
M_n	Number-average molecular weight
M_w	Weight-average molecular weight
MWD	Molecular weight distribution
NCA	*N*-Carboxyanhydride
NMR	Nuclear magnetic resonance
P2VP	Poly(2-vinylpyridine)
PAMAM	Polyamidoamine
PBAE	Poly(β-amino ester)
PBG	Poly(γ-benzyl L-glutamate)
PBLA	Poly(β-benzyl L-aspartate)

PBS	Phosphate buffered saline
PDI	Polydispersity index
PEI	Poly(ethylene imine)
PEO	Poly(ethylene oxide)
PEG-CHO	Aldehyde-terminated poly(ethylene glycol)
PEG-Bz-CHO	Methoxy poly(ethylene glycol) benzaldehyde
PGlu	Poly(L-glutamic acid)
PIP	Polyisoprene
PLA	Poly(lactic acid)
PLL	Poly(L-lysine)
PLys	Polylysine
PPO	Poly(propylene oxide)
PS	Polystyrene
PTFE	Polytetrafluoroethylene
PTX	Paclitaxel
PZLys	Poly(N^{ε}-carboxybenzoxylysine)

SEC	Size exclusion chromatography
SN-38	7-Ethyl-10-hydroxyl-camptothecin
TEA	Triethylamine
TEMPO	2,2,6,6-Tetramethylpiperidine-1-oxy radical
TFA	Trifluoroacetic acid
TFBA	Trifluorobenzaldehyde
THF	Tetrahydrofuran
X_n	Number-average degree of polymerization
Z	Benzyloxycarbonyl group
ZLys	N^{ε}-benzyloxycarbonyl-L-lysine

1 Introduction

1.1 Cancer and Challenges in Cancer Treatments

Cancer is one of the leading causes of death around the world. According to a report by the World Health Organization, cancer has taken 9.6 million lives around the world in 2018.[1] Despite phenomenal medical advances over the past few decades, cancer still remains a great challenge to scientists around the world. Cancer is a family of diseases causing the uncontrolled growth of cells in certain parts of the body due to genetic damage. The rapid growth leads to the formation of tumours, which can hinder the growth of healthy tissues in the surrounding regions. Localized cancerous tumours can be removed by surgery and radiotherapy,[2] but cancer cells can also travel through the circulatory or lymphatic systems and infect other distant organs in the body through a process known as metastasis.[3] In these metastatic cancers, surgical procedures are no longer effective; drug and gene therapy are currently the most common and effective methods for treating these forms of cancer.

While therapeutic drugs can be very effective at killing cancer cells, they suffer from significant limitations. First of all, many of the drugs cannot distinguish between cancer and healthy cells, particularly rapidly dividing cells. Indeed, cancer drugs are known to cause damage to cells in bone marrow, the digestive system, and hair follicles.[4] Furthermore, when drugs are administered to patients, they tend to distribute themselves more or less evenly throughout the body, resulting in a very small fraction of the drugs being actually delivered to the tumour site. A high drug dosage is required to achieve the desired therapeutic effect, which decreases the efficacy of the treatments. Furthermore, most drug molecules are hydrophobic and have limited solubility in the plasma, which can cause them to be eliminated rapidly from the body. Finally, drugs are

foreign materials recognized by the immune system, which can trigger undesired immune responses in the body of the patient.

Since cancer is usually caused by abnormalities in the genetic material, another valuable strategy to treat these diseases is gene therapy.[5] This typically involves the delivery of genetic material into the cell nuclei, to silence the expression of genes coding for the disease-causing proteins.[6] Unfortunately, similarly to traditional drug therapy, the direct delivery of nucleic acid sequences into cells is highly inefficient. Many of the challenges encountered in drug therapy, such as undesired immunological response and lack of target specificity, are also common in gene therapy.[6] In addition, free nucleic acids have limited stability in the circulatory system due to the presence of extracellular nucleases in the plasma causing their rapid degradation. The negatively charged nucleic acids also have repulsive electrostatic interactions with the phospholipid cell membranes, which limits their ability to enter cells.[7]

1.2 Drug and Gene Delivery Systems

Many of the challenges mentioned above can be addressed using drug or gene delivery systems. These involve encapsulating therapeutic agents, such as drug molecules or nucleic acids, in nanocarriers.[8] The size, composition, physical and chemical properties of these nanocarriers can be designed to provide benefits over conventional drug or gene therapies. If the therapeutic agents are encapsulated in a hydrophilic material, the nanocarriers can significantly enhance their solubility and increase their circulation time. Drug molecules or genes can be protected further with a shell of biocompatible material, to minimize immunological response. Encapsulating a drug in a carrier also provides control over the pharmacokinetics, allowing the drug molecules to be

released over an extended time period. This can decrease significantly the required frequency of drug administration and enhance patient compliance. Cationic delivery materials are preferred for gene delivery systems, because of the interactions between the gene-loaded nanocarriers and anionic phospholipid membranes. This enhances the cellular uptake of nucleic acids and promotes their endosome escape via the "proton sponge effect".[9] Lastly, drug- and gene-carrying materials can be designed to be responsive to changes in their surrounding environment such as the temperature,[10] pH[11] or redox conditions, to achieve targeted delivery.[12] Furthermore, the surface of drug carriers can be modified with ligands that specifically bind to receptors found on the surface of the targeted cancer cells.[13]

Another important, albeit disputed concept in drug and gene delivery is the so-called enhanced permeability and retention (EPR) effect. This refers to the tendency of nanoparticles with a size between 10–100 nm to accumulate in tumours,[14] due to a combination of hyperpermeability of the vasculature and poor lymphatic drainage in tumour tissues. Hyperpermeability refers to the fact that blood vessel walls near cancerous tumours are much more permeable than those in healthy tissues, due to more loosely packed endothelial cells lining the blood vessels.[12] Therefore, nanoparticles incapable of permeating through the walls of normal blood vessels may be able to extravasate from cancer vasculature and accumulate in nearby tumours. The tumours also have deficient lymphatic drainage, such that nanoparticles arriving at tumour sites may be retained for an extended time period, favouring the release of drugs or genes from the nanocarriers.[15] An illustration of this effect can be found in **Figure 1.1**. Consequently, when nanocarriers are used to carry drugs or genes, nanoparticles of a suitable size may allow higher accumulation of therapeutic agents in tumours via the EPR effect. This effect has been well documented in many animal models, but studies investigating the effect in humans have generated mixed results.[16,17] On the other hand,

stimuli responsiveness and the incorporation of surface ligands in drug delivery systems has definitely been shown to favour enhanced nanocarrier accumulation in tumours.[18]

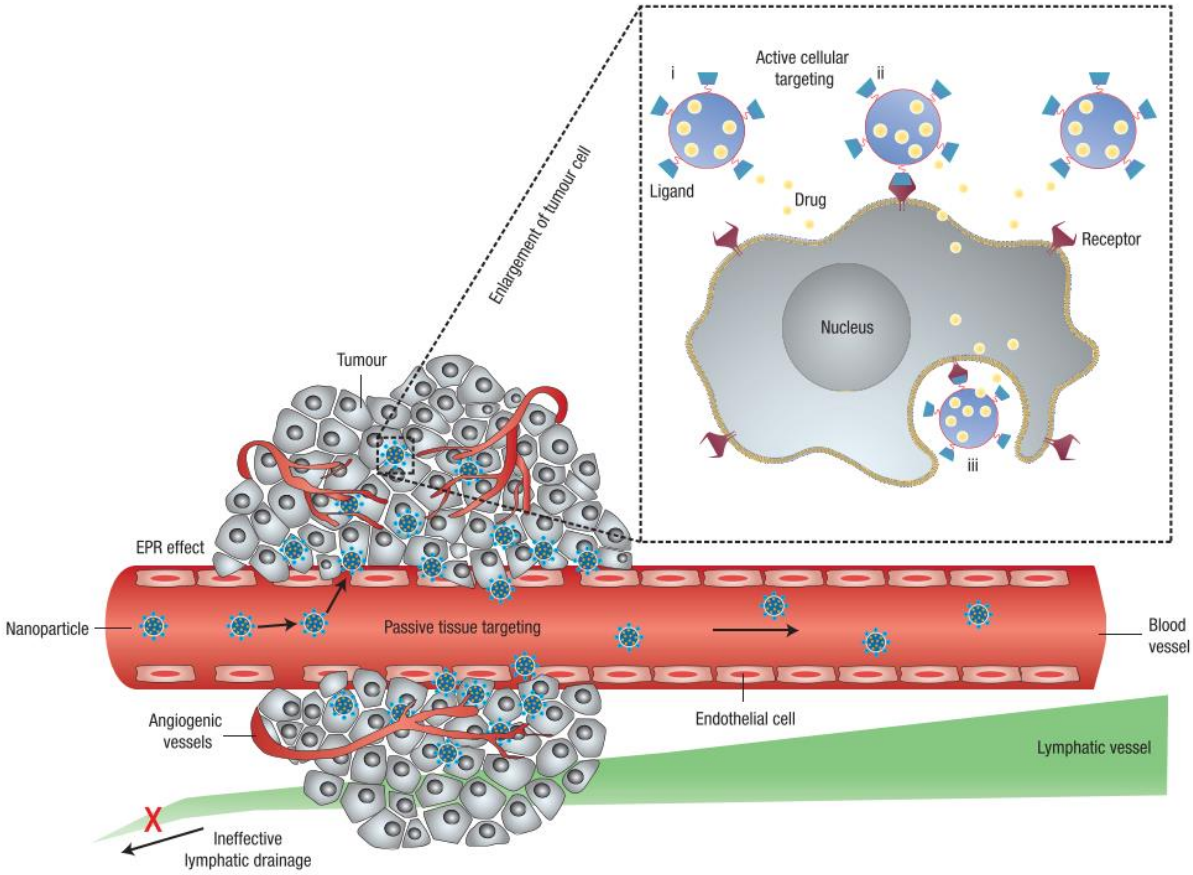

Figure 1.1 Mechanisms of drug carrier accumulation inside tumours via active cellular targeting and the passive enhanced permeation and retention effect.

Reprinted with permission from reference 19. Copyright 2007 Macmillan Publishers Ltd.

A wide range of materials have been used as drug delivery systems including liposomes,[20] metallic nanoparticles,[21] and polymer micelles.[22] For gene delivery, engineered viral vectors are commonly used to carry nucleic acids to target cells. Since viruses can gain access to cells effectively, therapeutic genes can be incorporated into their viral genome, and the virus can be used to infect the host cells and deliver the genes inside of them. Despite their efficiency, virus-based gene delivery techniques suffer from limited gene carrying capacity, toxicity, and immunogenicity.[23] In recent years, many non-viral gene delivery systems have been developed using lipids,[23] cationic polymers,[24] and saccharides.[25] Among these materials, polymer micelles are very popular for drug and gene delivery because of the great versatility in their design and the extent of control achieved over their morphology, composition, internal structure, and their physical and chemical properties. When used as gene delivery systems, polymers with cationic moieties can condense nucleic acids, protect them from degradation by plasma enzymes, and allow electrostatic interactions with the negatively charged cell membranes.[6, 26]

1.3 Polymer Micelles

The most common polymer micelles are derived from amphiphilic block copolymers, incorporating hydrophilic and hydrophobic chain segments. These block copolymers can self-assemble in aqueous solutions into spherical micelles with a hydrophobic core and a hydrophilic corona. One of the polymers most commonly used for the corona-forming segment of block copolymer micelles is poly(ethylene glycol) (PEG), also called poly(ethylene oxide) (PEO). The PEG chains are highly biocompatible and effectively prevent the aggregation of polymer micelles.[27] Other common hydrophilic materials serving as the corona-forming block in polymer

micelles include poly(vinyl alcohol),[28] poly(acrylic acid),[29] and poly(*N*-(2-hydroxypropyl) methacrylamide).[30] The hydrophobic core-forming segment not only stabilizes the micelle structure through hydrophobic interactions with other block copolymer chains, but also provides a favourable environment for hydrophobic drug molecules. Some of the polymers utilized for the core segment in block copolymer micelles include poly(propylene oxide),[31] poly(ε-caprolactone),[32] and poly(lactic acid) (PLA).[33]

Many block copolymers have been studied as drug nanocarriers. For example, Pişkin *et al.* synthesized PEG-*b*-PLA block copolymers and investigated their potential as drug carriers.[33] The micelles formed in aqueous solutions were shown to encapsulate the drug adriamycin within their core. Triblock PEO-*b*-poly(propylene oxide) (PPO)-*b*-PEO copolymers synthesized by Kadam *et al.* were likewise used to load hydrochlorothiazide within their core.[34] Besides hydrophobic interactions between the block copolymer chains, interactions between the polymer nanocarrier and the drug cargo can provide additional stabilization to the micelle structure and enhance drug loading. For example, Kataota *et al.* synthesized PEG-*b*-poly(β-benzyl L-aspartate) (PBLA) and loaded doxorubicin (DOX) within the PBLA core of the resulting micelles.[35] It was shown that the structure of the drug-loaded polymeric micelles was stabilized not only via hydrophobic interactions between the block copolymer chains, but also through additional π–π interactions between the benzylic groups of PBLA and the aromatic DOX molecules.[36] Many of these block copolymer drug delivery systems have been proven effective in *in vivo* drug delivery experiments and have entered clinical trials. For example, NK105 is a block copolymer with PEG as hydrophilic segment and modified polyaspartate as hydrophobic segment. The carboxyl groups of the polyaspartate block were modified with 4-phenyl-1-butanol to increase drug-polymer interactions. In a clinical study, NK105 micelles loaded with paclitaxel (PTX) were found to yield a higher

plasma concentration and slower elimination from the body as compared with free PTX.[37] The promising results obtained with NK105 have led to phase III clinical trials.[36]

While many block copolymer micelles have been very successful as drug delivery vehicles to enhance drug accumulation at tumour sites, a significant challenge remains with these drug delivery systems. In these micelles, the structure is usually stabilized by interactions between the hydrophobic segments of block copolymer molecules. The stability of the structure is due to a balance between decreased entropy of the block copolymer as compared with their free polymer form, and the decreased interfacial energy between the hydrophobic domains and the aqueous medium.[9] Because of this, a minimum concentration known as the critical micelle concentration (CMC) is required to maintain the structural integrity of these micelles. For the same reason, when these drug carriers are administered to patients, the rapid decrease in polymer concentration due to dilution in the bloodstream may lead to their dissociation, causing premature drug release.

Many methods have been used to increase the stability of micelle structures. For example, crosslinking the block copolymer chains allows the micelles to remain intact upon dilution. In a study by Iijima *et al.*, PEG-*b*-PLA micelles were synthesized with a terminal methacryloyl group at the PLA end, which was subsequently polymerized to create crosslinked micelle structures.[35] The crosslinked micelles exhibited enhanced stability in the presence of sodium dodecyl sulfate. In another study by Kim *et al.*, a PEG-*b*-poly(L-glutamic acid) (PGlu) block copolymer was hydrophobically modified by grafting a phenylalanine methyl ester group to the PGlu segment.[38] The core-forming modified PGlu segment was then crosslinked with cystamine. The micelles displayed a higher drug loading capacity for DOX and more gradual controlled drug release as compared with their non-crosslinked counterparts. Other attempts to stabilize micellar structures involved electrostatic interactions. Polymer micelles of PLys-*b*-PLA with a cationic PLys corona

were thus coated with a layer of anionic poly(sodium hyaluronate).[39] The electrostatic interactions between the PLys and the poly(hyaluronic acid) segments made the micelles more resistant to dissociation, as the poly(hyaluronic acid)-coated micelles displayed higher stability and slower drug release as compared with bare PLys-*b*-PLA micelles.

While these methods were effective at stabilizing micelle structures and controlling their drug delivery profile, there are drawbacks associated with these strategies. For crosslinked micelles, the introduction of a crosslinker can potentially result in changes in the physiological properties of the micelles and the drug. Biodegradability and the drug release profile may also be compromised after crosslinking.[40] For micelles stabilized through electrostatic forces, the stability of the micelles can be disrupted by salts.[41] When these drug carriers enter the circulatory system, the micelle structure may thus still dissociate prematurely due to the presence of metal salt ions in the plasma such as sodium, potassium, magnesium and calcium. To address this issue, an alternate strategy to stabilize polymer micelles was developed in the form of unimolecular micelles.

1.4 Unimolecular Micelles

Unimolecular micelles are typically derived from dendritic polymers, which are polymers containing multiple levels of branching. The branching sites can be located either on individual monomer units or on short polymer chains, and used to couple other monomers or short polymer chains to form the branched structures. There are three main types of dendritic polymers, namely dendrimers, hyperbranched polymers, and arborescent (or dendrigraft) polymers, classified according to their architecture as shown in **Figure 1.2**. Each of these dendritic structures has its own distinct features and properties.

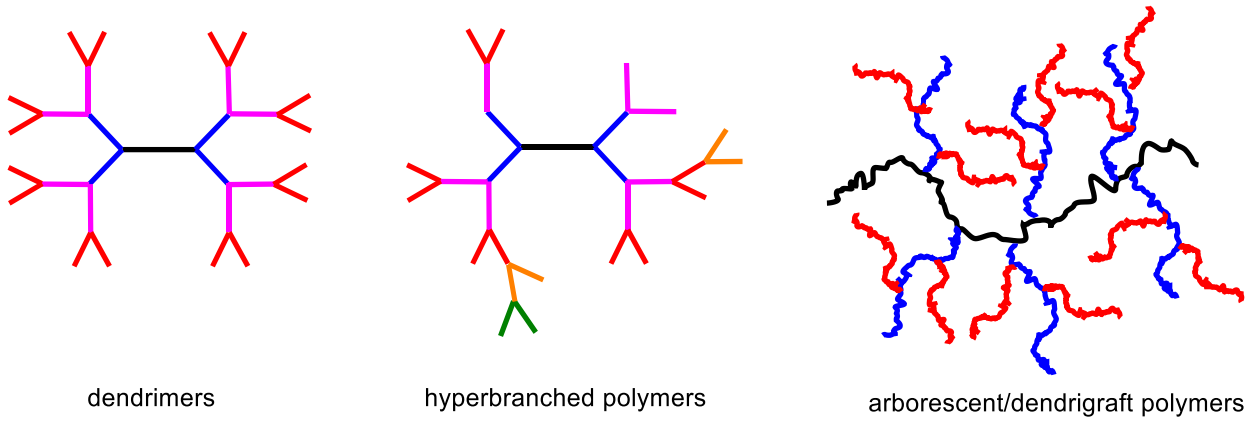

Figure 1.2 Architecure of differents types of dendritic polymers.

1.4.1 Dendrimers

Dendrimers are constructed from a monomer with core functional groups and multiple monomers with branching functional groups. The branching monomers are first synthesized in a protected form for selective coupling with the core functional groups, such that branching can be introduced in the molecules. The functional groups on the branching monomers can then be activated (deprotected), such that the coupling reaction with the branching monomers can be repeated to increase the branching functionality. Repetition of these cycles of activation and coupling reactions leads to structurally highly-defined branched macromolecules. The most famous example of dendrimers is the polyamidoamine (PAMAM) system synthesized by Tomalia *et al.* in 1985.[42] An example of a synthetic scheme used for PAMAM dendrimers is shown in **Scheme 1.1** The synthesis starts from an ethylenediamine core. The amine groups serve in a Michael addition reaction with methyl acrylate to generate a branched structure with four amide branching sites, and four methyl ester end groups. A large excess of ethylenediamine is then

reacted with the substrate to yield a G0 PAMAM dendrimer, with four peripheral amine groups. After removal of the excess ethylenediamine, a further cycle of Michael addition with methyl acrylate and condensation with ethylenediamine generates a G1 dendrimer with eight amine functional groups at their periphery, and so on for higher generation dendrimers.

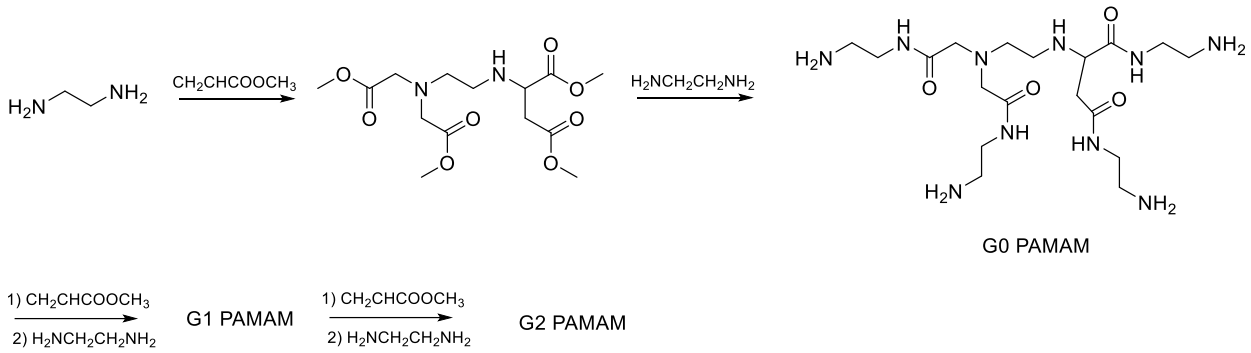

Scheme 1.1 Synthesis of PAMAM dendrimers.

Reprinted with permission from reference 43. Copyright 1985 Springer Nature.

These polymers have a highly defined molecular structure, with internal cavities allowing drug encapsulation. In work by Kojima *et al*., G3 and G4 PAMAM dendrimers were synthesized and poly(ethylene glycol) monomethyl ether was grafted onto the dendrimers through their peripheral amine groups.[44] DOX molecules were successfully loaded into the hydrophobic core of these unimolecular micelles. The drug encapsulation ability was found to be related to the size of the PAMAM core and the length of the PEG chains in the shell. In addition to physical encapsulation, drugs can be covalently attached to the polymers through covalent bonds. In work by Patri *et al.*, G5 PAMAM dendrimers were synthesized as drug carriers for methotrexate.[45] The drug molecules were loaded in the dendrimer either by inclusion complexation or covalent bonding,

but it was found that covalently bonded methotrexate had a significantly slower release profile in phosphate buffered saline (PBS). Besides PAMAM, many other types of dendrimers have been used as drug carriers. For example, Morgan *et al.* synthesized dendrimers from succinic acid and glycerol and utilized them as drug carriers for 10-hydroxycaptothecin. The drug-loaded dendrimers enabled a 16-fold increase in cellular uptake and a more than doubled cytotoxic activity.[46] Even though promising results have been obtained with dendrimer-based drug carriers, one significant drawback of these systems is that they involve tedious synthetic procedures. Many cycles of activation, coupling and purification steps are required to synthesize dendrimer micelles, even for small sizes. This hinders the potential clinical applications of dendrimers significantly.

1.4.2 Hyperbranched Polymers

Similarly to dendrimers, hyperbranched polymers are also constructed from low-molecular weight polyfunctional monomer building blocks. However, instead of using cycles of functional group activation and coupling reactions, they are synthesized by direct polycondensation of unprotected monomers in one-pot schemes. One of the first hyperbranched polymers reported was polyphenylene, synthesized by Kim in the late 1980s from 3,5-dihalophenyl Grignard reagents and 3,5-dihalophenylboronic acid monomers.[47] The hyperbranched polymer structures were obtained through metal-catalyzed aryl-aryl coupling between the monomers as shown in **Scheme 1.2**.

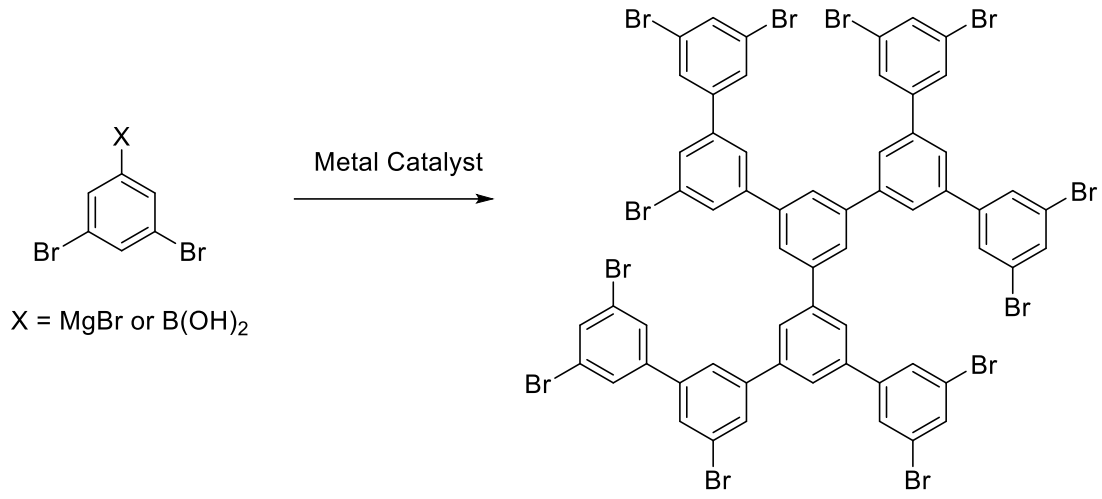

Scheme 1.2 Synthesis of polyphenylene hyperbranched polymers.

Adapted with permission from reference 47. Copyright 1990 American Chemical Society.

An example of hyperbranched unimolecular micelles used for drug delivery purposes is the Boltorn hyperbranched polyesters, constructed from bis(methylol)propionate as monomer. The group of Nystrom synthesized G3 (B30) and G4 (B40) Boltorn polymers and the peripheral hydroxyl groups were coupled with PEG chains.[48] When the micelles were utilized as nanocarriers for DOX, the drug-loaded micelles exhibited prolonged release profiles and higher cytotoxicity as compared with the free drug.

The synthesis of hyperbranched polymers is much simpler than dendrimers, as no pre-activation of the monomers is required for each generation. However, since the monomers react with each other in a random fashion, the structure of hyperbranched polymers contains many defects.

1.4.3 Arborescent Polymers

The third type of dendritic polymer architecture is arborescent polymers, also known as dendrigraft polymers. The arborescent polymers were developed concurrently by Gauthier and Möller,[49] and by the group of Tomalia.[50] These polymers combine some of the characteristics of dendrimers and hyperbranched polymers. Similarly to dendrimers, arborescent polymers are synthesized in generation-based schemes, but instead of using low-molecular-weight monomers, arborescent polymers utilize short polymer chains as building blocks. In this way, high molecular weight polymers are obtained after relatively few activation and coupling reaction cycles, providing a much simpler and more economical approach to the synthesis of dendritic polymers. These polymers have a less defined molecular architecture than dendrimers, but by controlling the number of coupling sites on the substrates and the molecular weight of the polymer chains grafted in each generation, relatively precisely controlled architectures and molecular weights can still be achieved, with polydispersity indices $M_w/M_n \approx 1.1$.[51]

Arborescent polymers can be obtained by three different methods, namely "grafting onto", "grafting from", and "grafting through" strategies. In the "grafting onto" technique, arborescent polymers are constructed by coupling pre-synthesized polymer chains with a linear or arborescent substrate. An example of this technique is the arborescent polymers synthesized by Gauthier and Möller in 1991.[49] In this case, linear polystyrene (PS) chains of uniform size were synthesized by anionic polymerization with *sec*-butyl lithium as initiator. The quenched chains were then chloromethylated to introduce chloromethyl groups on some of the styrene units, to serve as coupling sites. Linear PS serving as side chains were again synthesized by anionic polymerization, but the chain ends were not quenched. They were rather reacted with 1,1-diphenylethylene, to cap the chains and prevent side reactions, and added to the solution containing the chloromethylated

PS substrate to generate a G0 arborescent PS (**Scheme 1.3**). The chloromethylation and grafting cycles were repeated to obtain G1 and G2 arborescent polymers in high yield (> 90%) and with relatively narrow molecular weight distributions ($M_w/M_n \approx 1.1 - 1.3$). Since then, arborescent copolymer micelles with a core-shell morphology were also developed, including arborescent PS-*g*-PEO and PS-*g*-poly(2-vinylpyridine) (P2VP).[52,53]

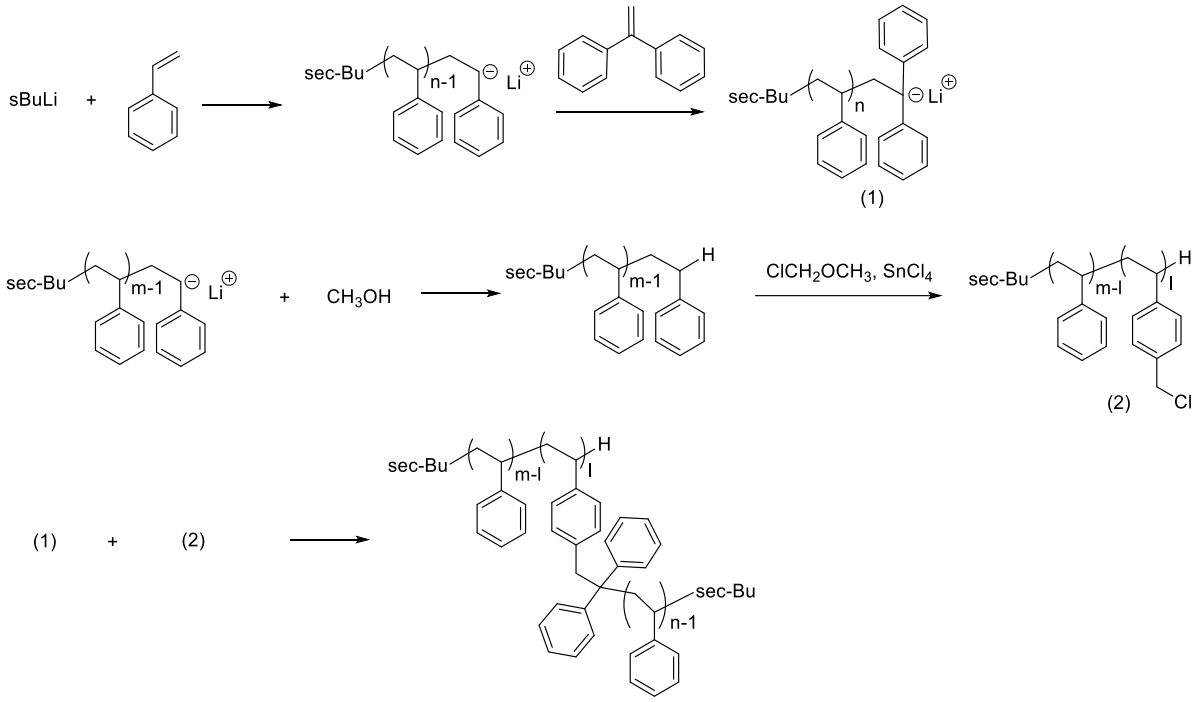

Scheme 1.3 Synthesis of arborescent polystyrene using chloromethyl coupling sites.

Reproduced with permission from reference 49. Copyright 1991 American Chemical Society.

Activation of the PS substrates was achieved initially through chloromethylation with chloromethyl methyl ether, but that compound is a suspected carcinogen, which stimulated the development of alternate activation and coupling reactions.[54] Li and Gauthier developed a novel

method to activate the *para*-position of styrene units by acetylation with acetyl chloride and $AlCl_3$.[55] By this method, arborescent PS and PS-*g*-P2VP of up to the second generation were synthesized successfully with narrow molecular weight distributions ($M_w/M_n < 1.1$).[55,56] For diene monomers such as 1,3-butadiene and isoprene, arborescent structures were also obtained by epoxidation of the residual double bonds, followed by coupling with pre-synthesized "living" anionic polymers serving as side chains. In work by Yuan and Gauthier, the polymerization of isoprene in hexane yielded a mixture of 1,4- and 3,4-isoprene repeating units (**Scheme 1.4**). Due to their high electron density, the alkene units within the chains could be epoxidized to serve as coupling sites for "living" polyisoprenyllithium chains.[57] A similar strategy was used subsequently by Zhang *et al.* to synthesize arborescent polybutadiene.[58] More recently, Cu(I)-catalyzed alkyne-azide cycloaddition (CuAAC) reactions were implemented in the synthesis of arborescent PS. In this case, linear PS chains were functionalized with acetylene groups on a fraction of the styrene units, and coupled with azide-terminated PS chains to yield arborescent PS. Arborescent PS molecules of generations G0 and G1 were obtained by that method with M_w/M_n = 1.08 and 1.38, respectively.[59]

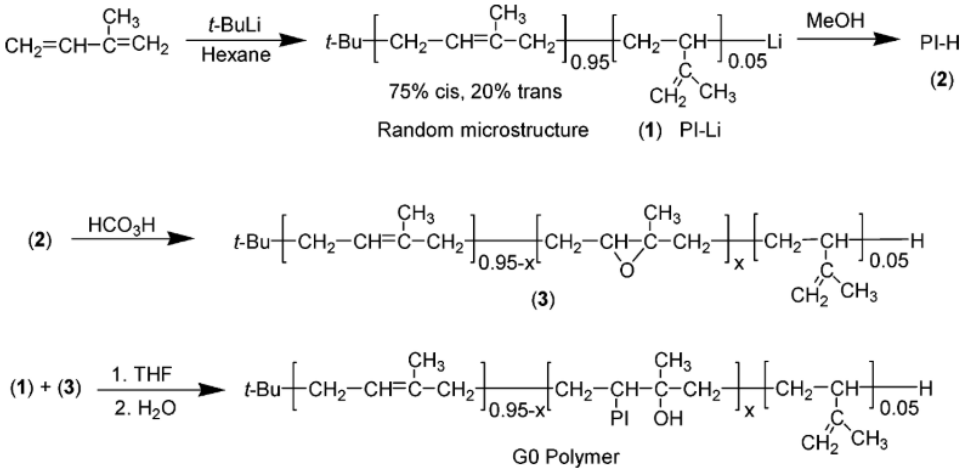

Scheme 1.4 Synthesis of arborescent polyisoprene using epoxide coupling sites.

Reprinted with permission from reference 57. Copyright 2005 American Chemical Society.

In the "grafting from" technique, several initiating sites for the monomer to be grafted are created on a substrate polymer. The substrate then serves as macroinitiator for the growth of several polymer side chains to create a branched architecture. If the substrate functionalization and side chain growth processes can be repeated, arborescent polymers are obtained. In work by Yuan and Gauthier, arborescent polystyrene molecules were obtained using 1,3-diisopropenylbenzene (DIB) to introduce latent initiating sites.[60] DIB was first copolymerized with styrene to yield a linear styrene-DIB copolymer substrate, and the pendent isopropenyl groups were activated with *sec*-butyllithium to initiate the growth of the side chains (**Scheme 1.5**). Due to a significant difference in reactivity between the two isopropenyl groups on DIB, this synthetic procedure could be performed in a one-pot process. In other work from the group of Dhamodharan, linear PS chains were partially brominated through allylic bromination and utilized as macroinitiators for the polymerization of PS side chains via atom transfer radical polymerization (ATRP).[61] Besides PS,

other polymers have been used in the synthesis of arborescent polymers. For example, Feng *et al.* synthesized arborescent PEO starting from a 1,1,1-tris(hydroxymethyl)ethane precursor.[62] Three PEO chains were grown from hydroxyl groups on the precursor, and each terminal hydroxyl group on the PEO chains was modified to introduce two new hydroxyl groups and initiate the polymerization of ethylene oxide, to yield higher generations of arborescent PEO.

Arborescent micelle structures with a core–shell morphology, incorporating different building blocks, were also obtained by combining the "grafting onto" and "grafting from" techniques.[52] An arborescent polystyrene substrate was first synthesized by the "grafting onto" technique described earlier. For the last coupling reaction, linear PS chains were synthesized using (6-lithiohexyl)acetaldehyde acetal, so as to introduce acetal-protected hydroxyl groups at the periphery of the arborescent PS substrate. After acid hydrolysis of the acetal groups, the peripheral alcohols were deprotonated and used to initiate the polymerization of ethylene oxide, thus generating a shell of hydrophilic PEO segments encapsulating the hydrophobic PS core.

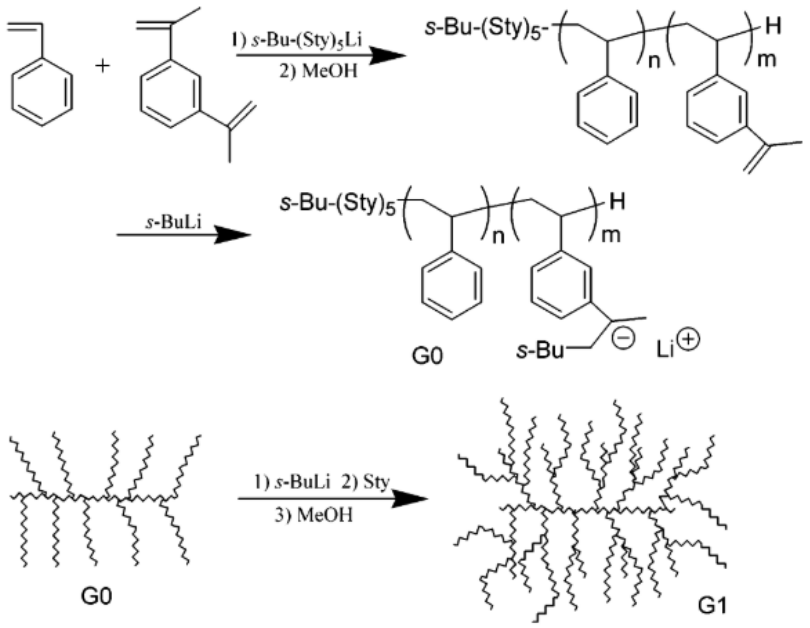

Scheme 1.5 Synthesis of arborescent polymers from diene monomers.

Reprinted with permission from reference 60. Copyright 2006 American Chemical Society.

The less common "grafting through" technique requires the use of an inimer – a difunctional molecule that has a functional group allowing its polymerization, and another one serving as branching point, by initiating the polymerization of additional monomers. An example of the "grafting through" technique was provided by the group of Puskas, for arborescent polyisobutylene synthesized by a one-pot technique using 4-(1-hydroxy-1-methylethyl)styrene (HMES) as inimer.[63] The vinyl group of HMES can copolymerize with styrene, while the hydroxyl group can serve as initiating site to generate polyisobutylene side chains. In this manner, arborescent polymers with a polystyrene core and a polyisobutylene corona were obtained. The

architecture obtained by this strategy is similar to a hyperbranched polymer, except that branching sites are separated by short polymer segments rather than present on each monomer residue.

Both the “grafting from” and “grafting through” techniques suffer from a major limitation, in that the core polymer and the side chain polymers cannot be characterized individually. This can limit the characterization of the internal architecture of the arborescent polymers obtained. In a “grafting onto” approach, in contrast, the polymer chains serving in every grafting step of the substrate synthesis can be characterized before the grafting reactions. In this way, more detailed information is obtained about the internal architecture of arborescent polymers. Consequently, the “grafting onto” technique was preferred for the synthesis of the arborescent architectures with potential applications in drug and gene delivery in this project.

1.5 Targeted Drug and Gene Delivery

Many criteria need to be taken into consideration in the design of targeted drug delivery systems. First of all, the material used for the delivery system must be non-toxic, and ideally biocompatible so as not to trigger any inflammatory response or allergic reaction. In addition, the carrier material should be biodegradable so it can be cleared from the body after the delivery process. More importantly, to achieve targeted delivery, a triggered release mechanism should be incorporated in the design of the carrier, so that it can release its cargo over an extended time period, but also selectively at desired sites.

A common strategy to achieve targeted delivery is to synthesize nanocarriers responsive to external stimuli. For example, since tumour cells are known to exhibit a more acidic extracellular

environment as compared with healthy tissues, designing pH-responsive nanocarriers allows the specific delivery of genes or drugs at tumour sites.[64] Tumour cells are also found to contain a higher concentration of glutathione than normal tissues.[64] Many redox-sensitive drug-delivery systems, such as block copolymer micelles with a disulfide linkage between the hydrophilic and hydrophobic chain segments,[65] or micelles reversibly crosslinked with disulfide bonds,[66] have been designed so as to dissociate and release a drug under reducing conditions. Drug delivery systems responsive to light irradiation have also been synthesized. After the drug delivery system is administered, exposure of the tumour area to light triggers bond cleavage[67] or the isomerization[68] of specific functional groups in the micelles, to induce their dissociation and the release of the drug. In the following section, some pH-responsive drug and gene delivery systems are described in more detail.

1.5.1 pH-Responsive Delivery Systems

Designing pH-responsive nanocarriers that release their cargo under acidic conditions is a common strategy to achieve targeted delivery. Due to the rapid proliferation of cancerous tumours, the cells cannot receive sufficient oxygen supply from the local circulatory system. As a result, tumour cells rely on anaerobic glycolysis as their energy source and generate a high concentration of lactic acid.[64] This causes the extracellular environment of cancerous cells to be slightly more acidic (pH ~ 6.5) than normal cells (pH ~ 7.4).[12] Drug carriers can be designed to release their cargo under these conditions. Poly(β-amino ester) (PBAE) is a highly biodegradable polymer commonly used for gene delivery. Drug- or gene-loaded PBAE is stable under neutral conditions, but undergoes rapid dissolution in acidic environments.[12] Paclitaxel-loaded PBAE was thus found

to favour drug accumulation in tumours as compared with paclitaxel-loaded, non-pH-responsive poly(caprolactone).[69] In another investigation, PBAE was used as a vehicle for the *in vivo* delivery of a minicircle DNA. The injection of DNA-loaded PBAE led to a two-fold increase in protein expression as compared with injection of the gene alone.[70] Another method to achieve pH-triggered drug release is to conjugate the drug with polymer micelles through acid-labile covalent bonds such as hydrazine, imine, and acetal bonds. In work by Bae *et al.*, doxorubicin molecules were conjugated with PEG-*b*-poly(aspartic acid) micelles via hydrazone bonds.[71] The drug was released from the micelles in acidic environments, while negligible release was observed at physiological pH. Polymer micelles can also be designed so that the micelle structure is disrupted in acidic environments.[11] In work by the group of Bae, poly(L-histidine)-*b*-PEG micelles were found to remain stable at neutral pH but to dissociate under acidic conditions, upon protonation of the imidazole group of histidine.[72] For micelles loaded with doxorubicin, higher cytotoxicity to HeLa cells was observed at pH 5.0 as compared with pH 7.4.[73] Micelles can also be constructed with an acid-labile linkage between the hydrophobic and hydrophilic segments of a block copolymer. Zhang *et al.* thus synthesized dextran-retinal block copolymers with a hydrazone linkage. Under acidic conditions, the hydrazone linkage was cleaved and the micelle structure was disrupted. In an *in vitro* study, when DOX was loaded into the micelles, much more rapid release was observed at pH 5.0 as compared with pH 7.4.[74]

1.5.2 Cationic Delivery Systems

Another particularly useful strategy for targeted delivery is the design of cationic nanocarriers to enhance the cellular uptake of drug molecules and genes. In targeted delivery,

internalization of the therapeutic agent is usually achieved by endocytosis,[5] so interactions between the cell membrane and the nanocarrier are especially important. Cationic polymers exhibit strong electrostatic interactions with the slightly anionic phospholipid cell membranes, thus allowing drug/gene accumulation inside the cells. Cationic polymers are particularly beneficial for the delivery of genetic material, because cell internalization of nucleic acids is especially difficult due to repulsive electrostatic interactions between the nucleic acids and the cellular membrane. After cell internalization, the more acidic environment in endosomes can protonate cationic polymers and create a significant charge differential across the endosomal membrane. More fluids enter the endosome through osmosis and eventually cause the endosome to burst, allowing the nucleic acids to enter the cell nucleus. This phenomenon is known as the "proton sponge effect". Cationic polymers can also shield nucleic acids from enzymes present in the plasma, such as nucleases, thereby increasing their circulation time.[75] Many cationic polymers have been used as gene delivery vehicles, but particularly poly(ethylene imine) (PEI), PBAE, and poly(L-lysine) (PLL).

Among these, the most common cationic polymer used for gene delivery is PEI. This polymer has a large number of amine groups that are protonated (positively charged) under physiological conditions. There are multiple examples of linear or dendritic PEI (**Scheme 1.6**) used as cationic gene delivery agents. In an investigation by Venkiteswaran, for example, breast cancer cells were successfully transfected with luciferase reporter genes complexed with linear PEI.[76] While PEI is an excellent carrier to deliver genes across cell membranes, it suffers from low biodegradability and high cytotoxicity.[77] Modifications to PEI molecules were necessary to obtain more biocompatible materials. In a study by Lee *et al.*, disulfide linkages were introduced in linear PEI. The resulting poly(ethyleneimine sulfide) had transfection efficiencies similar to unmodified PEI, but also significantly higher degradability and lower cytotoxicity.[78] Another common

modification of PEI is heparin-conjugated PEI (HPEI). The HPEI system displayed similar transfection efficiency, but much better blood compatibility and lower cytotoxicity than unmodified PEI. In work of Gou *et al.*, HPEI-gene conjugates successfully inhibited the metastasis of carcinoma.[79] Liu *et al.* used hyperbranched PEI grafted with PCL-*b*-PEG copolymer to obtain amphiphilic structures. Folic acid was then conjugated with the PEG chain ends to obtain PEI-*g*-PCL-*b*-PEG-Fol for the targeted delivery of silencing RNA (siRNA) to ovarian cancer cells (**Scheme 1.7**).[80] The siRNA-loaded micelles exhibited higher gene silencing efficiency, and a 6-fold increase in bioavailability as compared with siRNA loaded in unmodified PEI. Other biocompatible materials have been used to modify PEI, including chitosan,[81] pullulan,[82] and short peptides chains.[83]

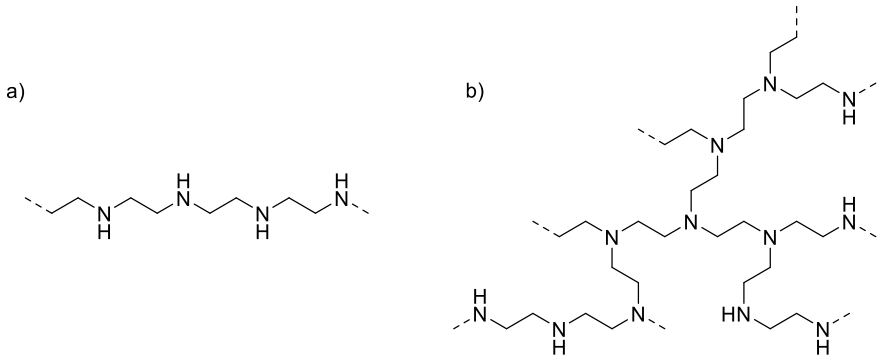

Scheme 1.6 Structure of linear and dendritic PEI.

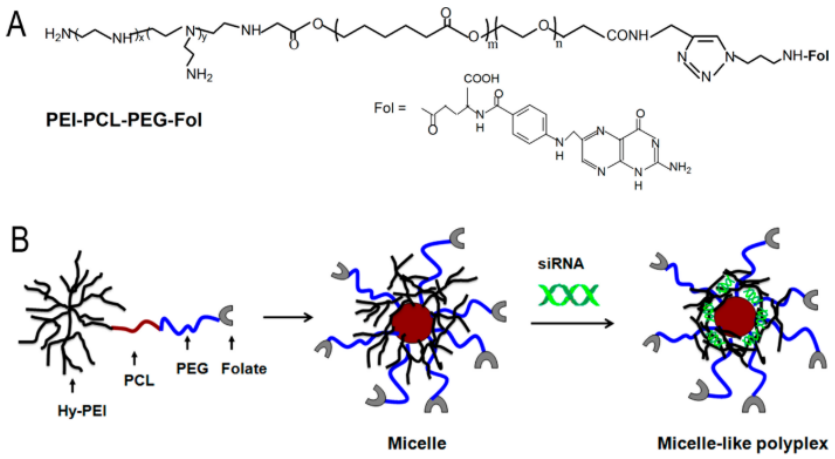

Scheme 1.7 Synthesis of PEI-*g*-PCL-*b*-PEG-Fol for targeted delivery of silencing RNA.

Reprinted with permission from reference 80. Copyright 2016 American Chemical Society.

Another useful type of cationic polymer for gene delivery is poly(β-amino esters) (PBAE), synthesized through Michael addition reactions of primary amines with acrylates.[84] Similarly to PEI, PBAE can be synthesized with linear, branched, or crosslinked structures (**Scheme 1.8**). The chain ends or periphery of these PBAEs must be modified with amine groups to obtain positively charged polymers. The group of Green developed many types of linear PBAEs and compared their gene-loading capability using enhanced green fluorescence protein and found that PBAE with a molecular weight of 25000 g/mol could encapsulate up to 120 plasmids per molecule, as compared with 90 plasmids for a PEI molecule with a similar molecular weight.[85] The gene-loaded PBAE molecules were successfully used to transfect brain tumour-initiating cells with high specificity and without damaging healthy cells, both *in vivo* and *in vitro*.[86] In work by Keeney *et al.*, a PBAE library was prepared and used to transfect minicircle DNA into mouse embryonic fibroblasts.[70] The transfection efficiency of DNA-loaded PBAE was significantly higher than for naked

minicircle DNA, and comparable with or even higher than for the commercial gene delivery agent Lipofectamine. In work by the group of Wang, branched PBAE was synthesized and shown to display superior gene transfection efficiency as compared with linear PBAE.[87] PBAE may also be modified to be bio-reducible through a disulfide-containing acrylate monomer. The modified PBAE, loaded with micro RNA and used to transfect glioblastoma cells, enhanced cellular uptake and prolonged the survival of tumour-bearing mice *in vivo* as compared with non-reducible PBAE.[88] A peptide-terminated PBAE developed by Borrös *et al.* also yielded enhanced transfection efficiency, due to enhanced interactions between the peptide and the target cells.[89]

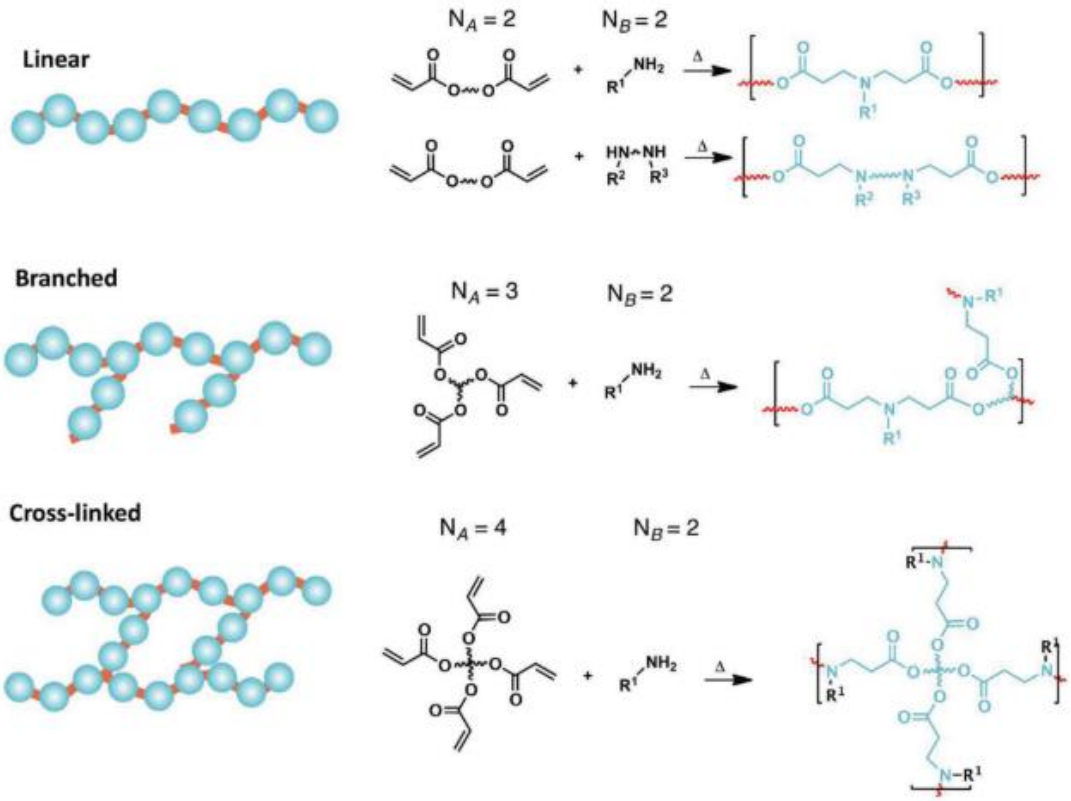

Scheme 1.8 Synthesis of PBAE with different topologies.

Reprinted with permission from reference 84. *Copyright 2019 John Wiley and Sons.*

PLL is another polymer commonly used as gene delivery agent. The amine groups of lysine are protonated and positively charged at physiological pH, allowing interactions with negatively charged nucleic acids. Kodama *et al.* thus synthesized dendrigraft PLL and complexed the polymer with plasmid DNA.[90] Anionic poly(γ-glutamic acid) (PGA) was also added to the complex to reduce its toxicity. The cellular uptake of the dendrigraft PLL-DNA-PGA complex was found to be higher for the PLL-DNA complex. PLL was also used to modify the common gene transfection agent PEI to improve its transfection efficiency. In work by Tian *et al.*, PLL chains were grown from a branched PEI structure, with the peripheral amine groups of PEI serving as macroinitiator.[91] The PLL-decorated PEI was used to transfect HeLa cells with Caspase-3, a gene that induces apoptosis. In the study, higher transfection efficiency, lower cytotoxicity, and higher cellular uptake were observed for the PLL-decorated PEI as compared with bare PEI. Stimuli-responsive PLL-based gene delivery systems have also been reported. For example, a pH-sensitive poly(L-histidine)-*g*-PLL (PLH-*g*-PLL) comb-shaped polymer was synthesized and successfully used in the transfection of 239T cells with plasmid DNA.[92] The copolymer yielded enhanced transfection as compared with pure PLL, due to disruption of the endosome membrane by the protonated histidine units under acidic conditions.

1.6 Arborescent Polypeptides

Among the many materials currently used for drug delivery, polypeptides provide many benefits. Since peptides are naturally synthesized in the body, they are highly biocompatible and biodegradable in many cases. Polypeptides consists of amino acids with different physical

properties such as hydrophilicity and acidity, which can be useful in designing drug delivery systems. Furthermore, amino acids contain many different functional groups such as amines, hydroxyl and carboxyl groups, which provide great versatility in designing these polypeptides.[93] Many polypeptides have already been used as drug-carrying vehicles for therapeutic agents. For example, DOX loaded in PEG-*b*-PBLA block copolymer micelles produced considerably higher anti-tumour activity than the free drug.[35] DOX molecules can be conjugated with PEG-*b*-poly(aspartic acid) via the side chain carboxyl groups, and additional DOX molecules can be loaded through π-π interactions. This formulation, under the name NK911, has entered Phase II clinical trials.[36] SN-38, also known as 7-ethyl-10-hydroxyl-camptothecin, is a drug used to treat colon and small intestine cancer. The drug was conjugated with PEG-*b*-poly(L-glutamic acid) (PEG-*b*-PGlu) using the phenol group of SN-38 and carboxyl groups of the PGlu segments. The resulting drug delivery system, denoted as NK012, produced a significantly increased accumulation in tumours and enhanced antitumour activity.[94] Many Phase II clinical studies of NK102 in the treatment of different types of cancer are underway around the world.[36]

Designing polypeptides with an arborescent structure would combine the benefits of arborescent polymers and polypeptides, to create biodegradable drug delivery agents with a relatively well-defined structure, obtained through economical synthetic procedures. Different polypeptides with arborescent structures have been obtained, starting with Klok *et al.*, by a "grafting from" technique.[95] Linear PLL was first obtained by ring-opening copolymerization of N^{ε}-Boc- and N^{ε}-Z-protected lysine NCAs. The Z group was cleaved to expose a fraction of the side-chain amines to serve as initiating sites and generate a branched structure. Repetition of deprotection and polymerization cycles successfully yielded higher generation arborescent PLLs. Unfortunately, this arborescent system suffered from broad molecular weight distributions (M_w/

M_n = 1.43–1.64), due to the inadvertent deprotection of some of the side chain amines in the lysine units in the grafting step. Collet *et al.* modified the Klok procedure using N^{ε}-trifluoroacetyl-protected lysine NCA monomer. After obtaining the linear polylysine, the trifluoroacetyl protecting groups were removed to expose the free amine and initiate the growth of side chains upon addition of monomer.[96] Improved polydispersities of M_w/M_n = 1.36–1.46 were obtained by that approach (**Scheme 1.9**).

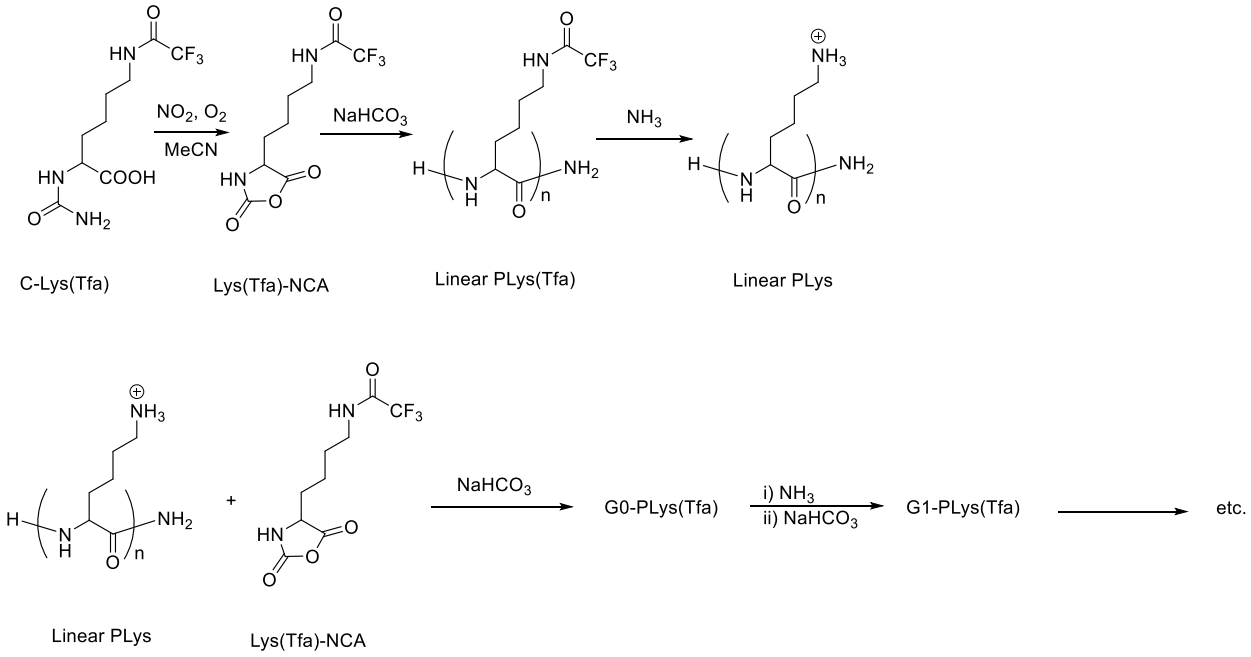

Scheme 1.9 Synthesis of arborescent PLLs.

Reprinted with permission from reference 96. Copyright 2010 European Chemical Societies.

The first arborescent polypeptides of uniform size were synthesized by Whitton and Gauthier in 2013.[97] In this work, arborescent poly(γ-benzyl L-glutamate) (PBG) was synthesized by a "grafting onto" strategy. Linear PBG was synthesized using *n*-hexylamine as initiator for γ-

benzyl L-glutamic acid NCA, and a portion of the benzylic protecting groups was removed with HBr. Additional PBG segments serving as side chains were then grafted onto the substrate via their N-terminus in a peptide coupling reaction (**Scheme 1.10**). By controlling the deprotection level, and the size of the polymer substrate and the side chains, narrow MWDs ($M_w/M_n < 1.06$) were obtained for up to G3 arborescent polymers, which was a significant improvement from the earlier "grafting from" approach. In later work, hydrophilic chains were grafted on the arborescent PBG substrates to create amphiphilic structures.[98] Chains of polyglycidol, PEO, or PGlu were grafted either randomly or at carboxyl chain-ends of the arborescent PBG substrates (**Scheme 1.11**). Chain-end coupling of the hydrophilic segments led to decreased aggregation of the unimolecular micelles, presumably due to their better-defined core–shell structure. This work demonstrated great promise for arborescent polypeptide micelles as potential drug delivery vehicles. In a more recent investigation, alkyne groups were introduced either randomly or at the chain ends of arborescent PBGs. Azide-terminated PEO or polyglycidol chains were then grafted onto the substrates using the CuAAC "click" reaction to obtain amphiphilic micelles with significantly improved grafting yield, while maintaining relatively narrow molecular weight distributions.[99]

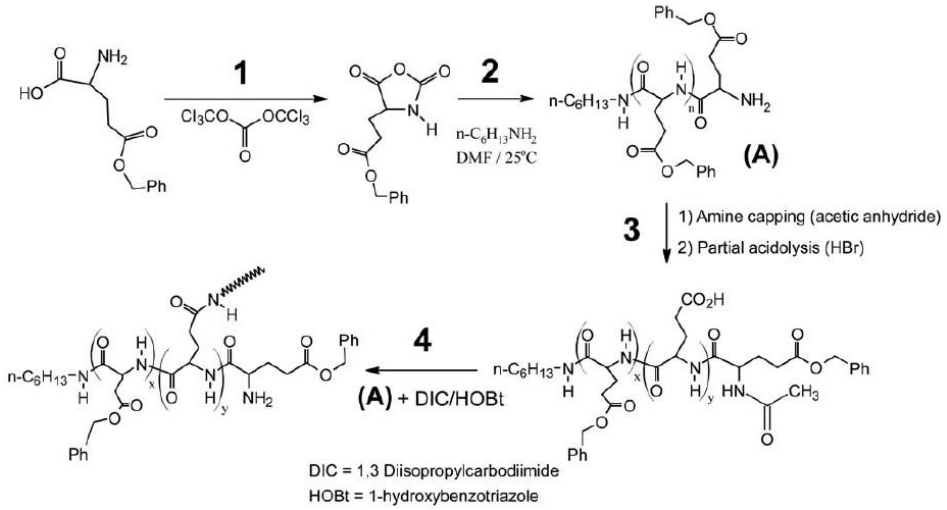

Scheme 1.10 Synthesis of arborescent PBG.

Reprinted with permission from reference 98. Copyright 2013 John Wiley and Sons.

Alsehli and Gauthier demonstrated that DOX could be loaded in arborescent amphiphilic PBG-*g*-PEO micelles either via hydrophobic interactions, electrostatic interactions, or covalent conjugation through pH-sensitive hydrazone bonds.[100] All these methods yielded promising results for pH-controlled drug release, but the micelle structures with pH-sensitive hydrazone bonds showed the strongest pH-dependent drug release behaviour. Drug release from the hydrazone-linked PBG-PEO-DOX was indeed limited to 5 and 7 % after 50 h at pH 7.4 for G1 and G2 polymers, respectively, and increased to 42 and 57 % at pH 5.5.

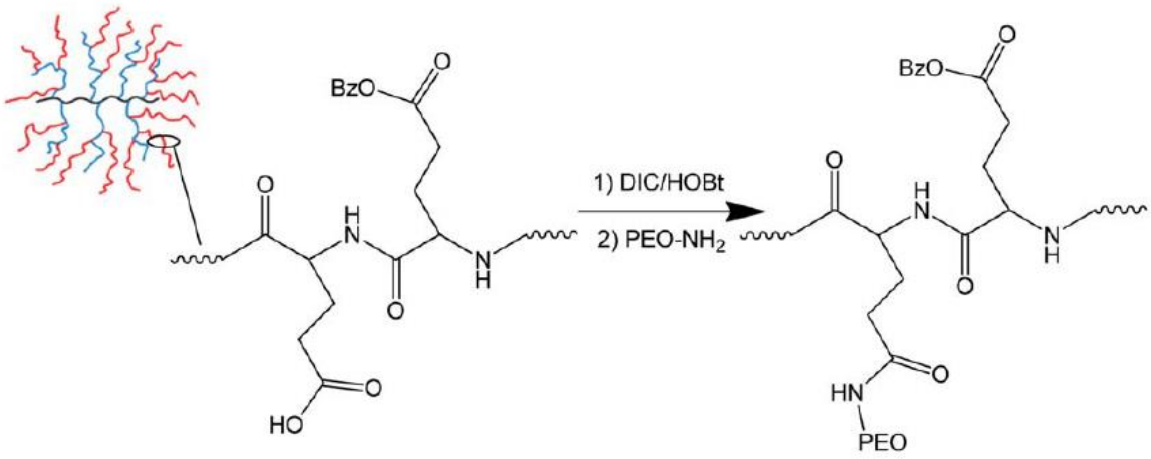

Scheme 1.11 Synthesis of arborescent PBG-*g*-PEO micelles as drug delivery agents.

Reprinted with permission from reference 100. Copyright 2013 John Wiley and Sons.

These results show that arborescent polypeptides are very promising drug delivery systems. Cationic polymers, and particularly polymers that are pH-responsive, are known to be highly desirable to favour drug accumulation inside tumour cells. Therefore, the project described in this thesis focused on the development of pH-responsive arborescent polypeptides with cationic moieties as potential drug delivery agents.

1.7 Project and Thesis Outline

The main goal of the current project was to synthesize and characterize pH-sensitive arborescent polymer micelles containing a PBG core, a PLys inner layer, and a cleavable PEG shell. The PBG core provides a hydrophobic environment for loading drugs. The amine groups on

the polylysine chains have a pKa value of approximately 10.53.[101] Therefore, the PLys inner layer should be protonated under physiological conditions and favour cellular uptake via electrostatic interactions with the cellular membranes. In gene delivery, the positive charges of PLys was also demonstrated to be highly effective in shielding negatively charged DNA from plasma components, resulting in the increased accumulation of genes in target cells and enhanced gene transfection.[5,102] The PEG shell can minimize interactions of the PLys component with proteins and increase the stability of the micelles in the circulatory system. The PEG shell and the PLys inner layer are connected via a pH-sensitive imine bond. This should allow the polymer drug carrier to remain stable under physiological conditions. In the acidic environment of tumour tissues, however, the PEG chains would be cleaved to expose the positively charged amine groups, allowing the drug carrier to penetrate the cellular membrane more easily to release its cargo. An illustration of this drug release mechanism is shown in **Scheme 1.12**.

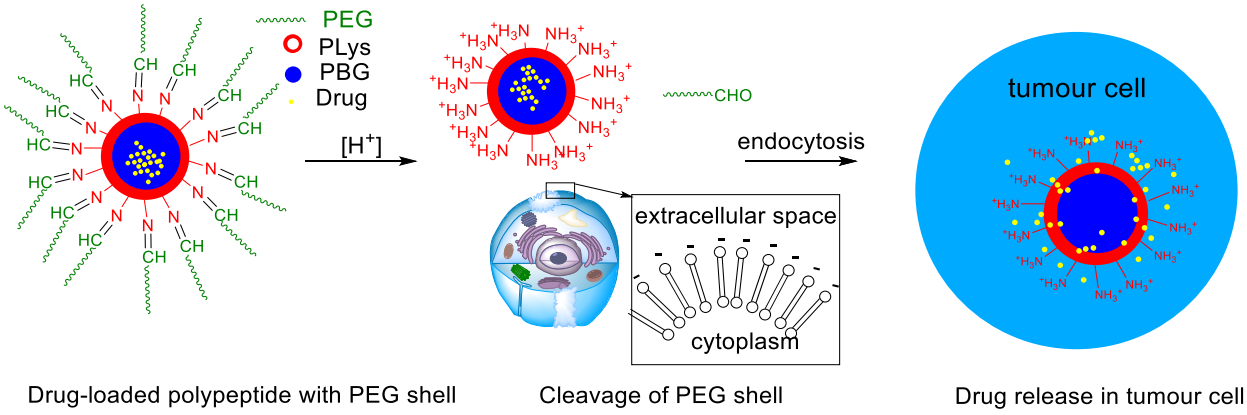

Scheme 1.12 pH-stimulated cleavage of PEO chains and cellular uptake of arborescent PBG-*g*-PLys-*g*-PEO.

The PBG core was prepared by an already established method,[97] starting with the ring-opening polymerization of BzGlu NCA. A fraction of the benzylic protecting groups on PBG was cleaved to expose free carboxylic acid moieties as coupling sites for amine-terminated PBG serving as side chains, to obtain a G0PBG arborescent structure. The partial deprotection and grafting reactions were repeated to obtain the following generation of arborescent PBG (G1PBG). Similarly, the polymerization of N^{ε}-carbobenzoxy-L-lysine (ZLys) NCA yielded linear chains of poly(Z-lysine) (PZLys). To incorporate the PLys segments, G0 and G1 arborescent PBG substrates were partially deprotected and coupled with the amine-terminated PZLys chains. To build a PEG shell, PEG monomethyl ether was functionalized with an aldehyde group. The Z protecting groups of the PZLys chains were then removed to generate free amine functionalities, which could be coupled with the PEG chain segments through the formation of a pH-sensitive imine bond. The detailed strategy for this project is provided in **Scheme 1.13**.

The materials synthesized were characterized by standard techniques including ^{1}H NMR spectroscopy and gel permeation chromatography (GPC), but also by dynamic light scattering (DLS) and zeta potential measurements, among others to determine the influence of core shielding by the PEG chains on the properties of the micelles.

Following the review of relevant literature provided in this Introduction, the experimental procedures used to carry out the work are described in Chapter 2. The results obtained in the analysis of the products synthesized, and their significance are discussed in Chapter 3. The main conclusions that can be drawn from the work completed are provided in Chapter 4, before a list of references cited in Chapter 5.

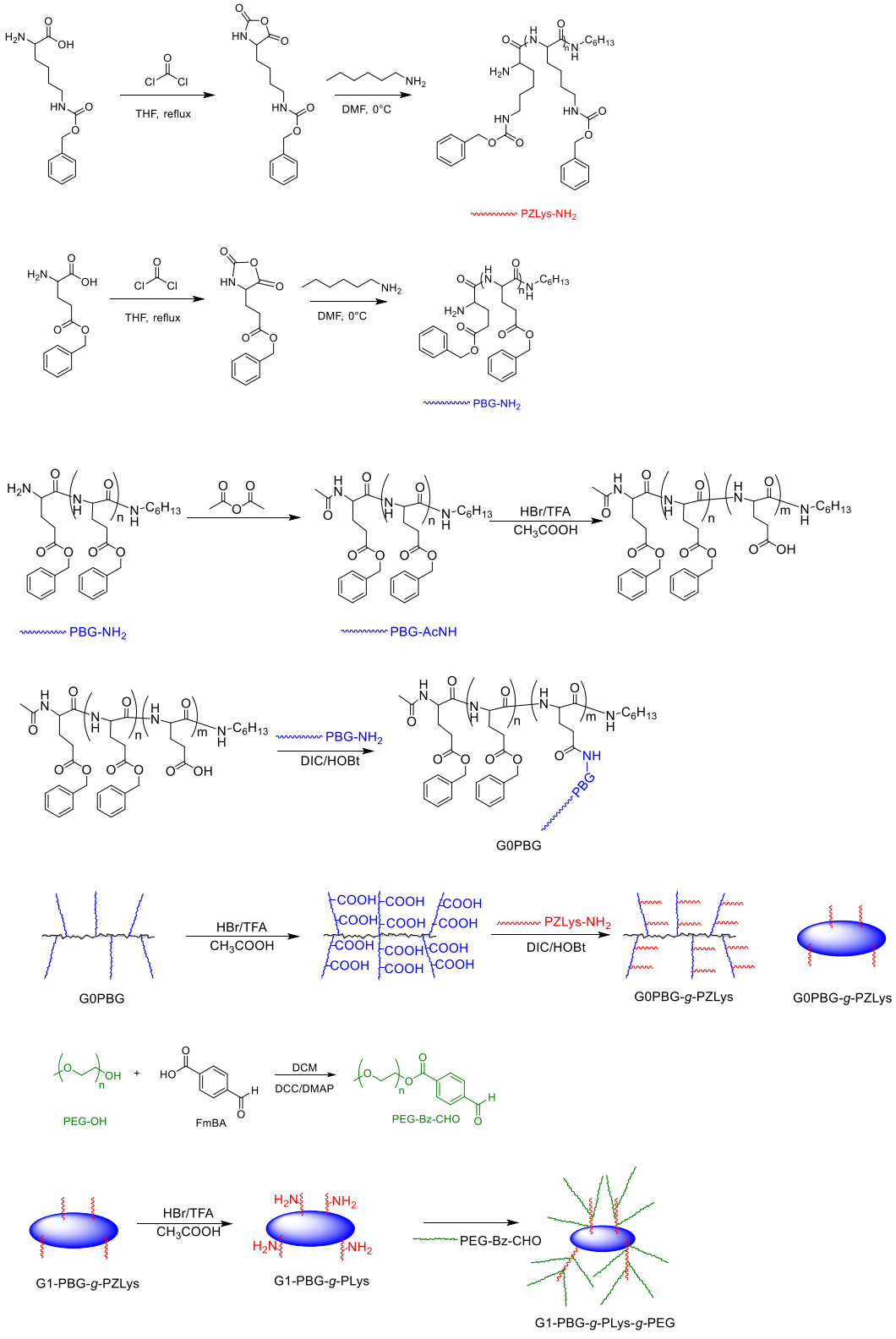

Scheme 1.13 Overall scheme for the synthesis of arborescent PBG-*g*-PLys-*g*-PEG.

2 Experimental Procedures

2.1 Materials and Characterization

N,*N*'-Dimethylformamide (DMF; Aldrich, >99.8%) was stirred with calcium hydride (CaH_2) overnight before it was fractionally distilled under reduced pressure and stored in the dark to prevent photodegradation.[103] Dichloromethane (DCM; Aldrich, >99.8%), dimethyl sulfoxide (DMSO; Aldrich, >99.9%), and *n*-hexylamine (Aldrich, 99%) were stirred with CaH_2 overnight and distilled under reduced pressure. Tetrahydrofuran (THF; Aldrich, >99.8%) was distilled from sodium/benzoquinone ketyl under N_2 atmosphere. Phosgene (Aldrich, 15% solution in toluene), *N*-*N*'-diisopropylcarbodiimide (DIC; Aldrich, >98.0%), deuterated dimethyl sulfoxide (DMSO-d_6; Aldrich, 99.9% atom D), deuterated chloroform ($CDCl_3$; Aldrich, 99.8% atom), hydrobromic acid (HBr; Aldrich, 33% solution in acetic acid), trifluoroacetic acid (TFA; Aldrich, 99%), methanol (Aldrich, >99.9%), diethyl ether (Aldrich, 99%), dichloromethane (Aldrich, >99.8%), *n*-hexane (Aldrich, >98.5%), bis(acetoxy)iodoobenzene (BAIB; Aldrich, 98%), 4-formylbenzoic acid (FmBA; Aldrich, 97%), *N*,*N*'-dicyclohexylcarbodiimide (DCC; Aldrich, 98%), 4-(dimethylamino)pyridine (DMAP; Aldrich, 99%), 2,2,6,6-tetramethylpiperidine-1-oxy radical (TEMPO; Aldrich, 98%), trifluorotoluene (BTF; Aldrich, >99%), and 4-trifluorobenzaldehyde (TFBA; Aldrich, 98%), BzGlu (Chem-Impex, 99.1%), ZLys (Bachem), *N*-hydroxybenzotriazole (HOBt; TCI, >97%), triethylamine (TEA; Alfa Aesar, 99%), poly(ethylene glycol) monomethyl ether (PEG-OH; M_n = 5000 g/mol, Polysciences Inc.), and acetic anhydride (Caledon Laboratories, Reagent Grade) were used as received from suppliers. Spectra/Por dialysis membranes (MWCO = 1 kD) were purchased from Spectrum Laboratories.

^{1}H NMR spectroscopy was used to confirm the structure of the monomer and polymer samples, to determine the degree of polymerization of the polymers, and to calculate the deprotection level of the polymer grafting substrates. The spectra were acquired on a Bruker 300 MHz spectrometer at room temperature. ^{19}F NMR spectroscopy on the same instrument served to determine the primary amine functionality level of the PBG chains. Analytical size exclusion chromatography (SEC) was performed on a system including a Hewlett Packard G1311A quaternary pump, a Hewlett Packard G1313A autosampler, a 100 μL injection loop, two 300 mm × 7.8 mm Jordi Resolve DVB Mixed Bed columns (Model A15076) with a polystyrene molecular weight range of 200 – 3,000,000 g/mol, and a Waters 410 differential refractometer. The analysis was performed in DMF with 0.1% w/w lithium chloride at a flow rate of 0.9 mL/min and 45 °C. Preparative SEC was carried out on a system consisting of a Waters 515 HPLC pump, a Rheodyne model 7125 injector with a 2 mL injection loop, a 250 mm × 22 mm Jordi Gel DVB column with a pore size of 10^3 Å and a polystyrene molecular weight range of 100 – 50,000 g/mol, and a Waters R401 differential refractometer. The separation was performed in DMF with 0.2 g/L LiCl, at a flow rate of 2.0 mL/min and room temperature. Dynamic light scattering measurements were used to determine the size and the zeta potential of the arborescent polymers on a Malvern Nano ZS90 instrument with a 633 nm He-Ne laser at 25 °C. The samples were prepared by dissolution at a concentration of 1 mg/mL in different media including deionized water, PBS, 10% PBS in 1 mM HCl, 20% PBS in 10 mM HCl, and 0.1 M HCl.

2.2 Synthesis of BzGlu NCA

The amino acid NCA monomers used in this project were synthesized using a phosgene solution in toluene, according to a procedure adapted from Kramer *et al.*[104] Briefly, BzGlu (10.0 g, 42.1 mmol) was dispersed in 300 mL of dry tetrahydrofuran (THF) and stirred under reflux in a 3-neck round-bottom flask fitted with a condenser and a stopcock adaptor. The 15% phosgene solution in toluene (39 mL, 55 mmol, 1.3 equiv) was then added dropwise to the dispersion over 2 min, and the reaction was refluxed for 4 h longer under nitrogen atmosphere. The gas outlet was bubbled into a NaOH solution to neutralize HCl gas and phosgene escaping from the flask. The solution became gradually clearer as the reaction proceeded, and transparent when complete. The reaction flask was purged with nitrogen overnight to remove residual phosgene, before evaporating the residual solvent under reduced pressure. The crude product was dissolved in 30 mL of anhydrous THF and recrystallized by adding 150 mL of hexane. The solid was filtered in a Schlenk funnel under N_2 and dried under vacuum overnight. Yield: 9.70 g, 87.4 %. ^{1}H NMR (300 MHz, DMSO-d_6), δ: 1.85 – 2.15 (m, 2H), 2.46 – 2.62 (t, 2H), 4.44 – 4.51 (q, 1H), 5.09 – 5.13 (s, 2H), 7.30 – 7.44 (s, 5H), 9.05 – 9.14 (s, 1H). ^{1}H NMR (300 MHz, $CDCl_3$): δ 2.06 – 2.22 (m, 1H), 2.23 – 2.39 (m, 1H), 2.57 – 2.69 (t, 2H), 4.35 – 4.46 (t, 1H), 5.12 – 5.25 (s, 2H), 6.42 – 6.58 (s, 1H), 7.28 – 7.47 (s, 5H).

2.3 Synthesis of ZLys NCA

The synthesis of ZLys NCA was performed similarly to the BzGlu NCA, starting from ZLys. A typical reaction was performed using ZLys (6.0 g, 35.7 mmol) and phosgene solution (39 mL, 55 mmol, 1.3 equiv) in 300 mL of dry THF. The crude product was dissolved in 18 mL of

anhydrous THF and recrystallized by adding 180 mL of hexane. The solid was filtered in a Schlenk funnel under N_2 and dried under vacuum overnight. Yield: 5.53 g (92.2 %). ^{1}H NMR (300 MHz, DMSO-d_6), δ: 1.17 – 1.50 (m, 4H), 1.55 – 1.84 (m, 2H), 2.92 – 3.07 (q, 2H), 4.36 – 4.51 (t, 1H), 4.93 – 5.12 (s, 2H), 7.19 – 7.30 (s, 1H), 7.30 – 7.44 (s, 5H), 9.02 – 9.14 (s, 1H). ^{1}H-NMR (300 MHz, $CDCl_3$), δ: 1.19 – 1.67 (b, 4H), 1.67 – 2.07 (m, 2H), 3.04 – 3.33 (b, 2H), 4.11 – 4.35 (b, 1H), 4.93 – 5.07 (b, 1H), 5.07 – 5.21 (b, 2H), 7.11 – 7.26 (s, 1H), 7.30 – 7.43 (s, 5H).

2.4 Synthesis of Linear PBG Serving as Side Chains

An ampoule with a polytetrafluoroethylene (PTFE) stopcock, containing a magnetic stirring bar, was attached to a manifold on a high vacuum line and dried by flaming under vacuum. While purging with nitrogen, BzGlu NCA (2.00 g, 7.60 mmol, 22.4 equiv) was added to the ampoule which was then carefully evacuated to remove any moisture adsorbed on the monomer. Dry DMF (3 mL) was added to the ampoule to dissolve the monomer, and the ampoule was placed in an ice bath. *n*-Hexylamine (44.5 μL, 339 μmol, 1.0 equiv) dissolved in 1 mL of dry DMF was added to the monomer solution at 0 °C and after thorough mixing the ampoule was sealed, removed and left in a 0 °C water bath for 3 d. The stopcock was briefly opened after 12 h to release the CO_2 gas produced. After 3 d the solution was stirred at room temperature for 3 h to complete the polymerization, followed by precipitation in chilled methanol, centrifugation, and drying under vacuum overnight. Yield = 1.39 g (82.3%). ^{1}H NMR (300 MHz, DMSO-d_6), X_n = 24.9, δ: 0.78 – 0.86 (t, 3H), 1.13 – 1.48 (b, 10H), 2.68 – 2.63 (b, 100H), 3.78 – 4.34 (b, 25H), 4.83 – 5.15 (s, 50H), 7.09 – 7.44 (b, 125H), 7.85 – 8.60 (b, 25H).

2.5 Synthesis of PBG Serving as Substrate

An ampoule with a PTFE stopcock, containing a magnetic stir bar, was attached to a manifold on a high vacuum line and dried by flaming under vacuum. While purging with nitrogen, BzGlu NCA (2.00 g, 7.60 mmol, 22.5 eq) was added to the ampoule. The ampoule was then carefully evacuated to remove moisture adsorbed on the monomer. Dry DMF (3 mL) was added to dissolve the monomer, and the ampoule was placed in an ice bath. *n*-Hexylamine (44.5 μL, 336 μmol, 1.0 eq) dissolved in 1 mL of DMF was added to the monomer solution, which was mixed thoroughly, and the ampoule was placed in a 0 °C water bath for three days. The ampoule was then removed and stirred at room temperature for 3 h to consume any unreacted monomer. After precipitation in chilled methanol, centrifugation, and drying under vacuum overnight, the polymer was redissolved in 4 mL of dry DMF and 100 μL of acetic anhydride were added. The ampoule was stirred at room temperature for 3 h before precipitation in chilled diethyl ether. The precipitate was recovered by centrifugation and drying under vacuum overnight. Yield = 1.22 g (72.0 %). ^{1}H NMR (300 MHz, DMSO-d_6), X_n = 23.0, δ: 0.78 – 0.86 (t, 3H), 1.13 – 1.48 (b, 10H), 2.68 – 2.63 (b, 95H), 3.78 – 4.34 (b, 23H), 4.83 – 5.15 (s, 46H), 7.09 – 7.44 (b, 115H), 7.85 – 8.60 (b, 23H).

2.6 Synthesis of Linear PZLys

The synthesis of linear PZLys was performed similarly to linear PBG, except that ZLys NCA was used as monomer. The polymerization was carried out with ZLys NCA (2.00 g, 6.53 mmol, 18.8 eq) and hexylamine (44.0 μL, 333 μmol, 1.0 eq) in 4 mL of DMF. After 5 d, the ampoule was left at room temperature for 1 h before the polymer was precipitated in chilled diethyl ether, centrifuged, and dried under vacuum overnight. Yield = 1.39 g (81.2%). ^{1}H NMR (300 MHz,

DMSO-d_6), X_n = 19.3, δ: 0.79 – 0.88 (t, 3H), 1.00 – 2.07 (b, 134H), 2.83 – 3.10 (b, 38H), 3.75 – 4.31 (b, 19H) , 4.84 – 5.12 (b, 38H), 6.97 – 7.46 (b, 114H), 7.66 – 8.30 (b, 19H).

2.7 Synthesis of PEG-CHO Through Direct Oxidation of Terminal Alcohol

The synthesis of PEG-CHO through direct oxidation of the terminal alcohol group of PEG was achieved according to a procedure by Masson *et al.*[105] Briefly, PEG (1.80 g, M_n = 5000 g/mol, 0.360 mmol) was dissolved in 10 mL of dry DCM. TEMPO (11.3 mg, 0.072 mmol) was added to the reaction solution, followed by BAIB (348 mg, 1.080 mmol). The reaction was allowed to run overnight at room temperature before precipitation in diethyl ether. The product was recovered by centrifugation, repeated washing with diethyl ether, and drying under reduced pressure.

2.8 Synthesis of Methoxy Poly(ethylene glycol) Benzaldehyde (PEG-Bz-CHO) Through Esterification with 4-Formylbenzoic Acid (FmBA)

The synthesis of PEG-Bz-CHO through esterification of the hydroxyl end group of PEG monomethyl ether with 4-formylbenzoic acid (FmBA) was performed according to a procedure described by Gu *et al.*[106] Briefly, PEG (1.00 g, M_n = 5000 g/mol, 0.20 mmol), FmBA (120 mg, 0.80 mmol) and DMAP (24 mg, 0.20 mmol) were dissolved in 10 mL of DCM. The reaction mixture was cooled in an ice bath and DCC (165 mg, 0.80 mmol) dissolved in 2 mL of DCM was added dropwise over 2 min. The reaction was allowed to proceed at room temperature for 24 h and filtered to remove the urea side product. The filtrate was concentrated under reduced pressure, redispersed in 2-propanol and cooled to -15 °C overnight. The resulting solid was collected by

suction filtration, washed with diethyl ether and dried under vacuum overnight (Yield: 753 mg, 73.3 %).

2.9 Partial Deprotection of Linear PBG

PBG (1.19 g, X_n = 22.3, 5.35 mmol BzGlu units) was dissolved in TFA (12 mL) and HBr solution (33% w/w) in acetic acid (481 mg, 1.96 mmol HBr) was added. The solution was stirred for 3 h at room temperature under nitrogen atmosphere before precipitation in diethyl ether. The solid was recovered by repeated centrifugation and washing with diethyl ether before drying under vacuum. The final product contained 37 mole% of free glutamic acid moieties.

2.10 Synthesis of G0 Arborescent PBG

Partially deprotected PBG (150 mg, 0.360 mmol -COOH units) and PBG side chain material (1.16 g, 0.176 mmol -NH_2 units) were dissolved in 10 mL of dry DMSO. DIC (278 μL, 1.79 mmol) was added and the solution was stirred for 10 min before HOBt (273 mg, 1.79 mmol) and TEA (182 uL,1.31 mmol) were added, and the solution was stirred for 4 d at room temperature. *n*-Hexylamine (300 μL, 2.27 mmol) was then added to deactivate residual activated carboxylic acid moieties. The solution was dialyzed against 500 mL of DMF (MWCO 1000 Da) for 5 d and the dialysis medium was changed 5 times. The crude polymer solution was purified by preparative SEC to remove unreacted side chains. The purified polymer solution was concentrated under reduced pressure, precipitated in diethyl ether, centrifuged and dried under vacuum overnight.

2.11 Synthesis of G1 Arborescent PBG

G1PBG was synthesized similarly to G0PBG. Briefly, G0PBG (450 mg, 2.05 mmol BzGlu units) was dissolved in 4 mL of TFA and HBr solution (33% w/w) in acetic acid (126 mg, 0.519 mmol HBr) was added with stirring at room temperature under nitrogen for 3 h. The polymer was precipitated in diethyl ether, centrifuged, and dried under vacuum. The partially deprotected G0PBG sample contained 22 mole% of free glutamic acid moieties. Yield = 0.36 g (87.6 %)

In a typical coupling reaction for the synthesis of G1PBG, partially deprotected G0PBG (175 mg, 0.183 mmol free –COOH units) and PBG side chain material (879 mg, 0.158 mmol –NH_2 units) were dissolved in 10 mL of dry DMSO. DIC (115 mg, 0.917 mmol) was added and the solution was stirred for 10 min before HOBt (124 mg, 0.913 mmol) and TEA (92.8 mg, 0.917 mmol) were added with stirring at room temperature. After 4 d, *n*-hexylamine (100 μL, 0.757 mmol) was added to deactivate residual activated carboxylic acid moieties. The solution was dialyzed against 500 mL of DMF (MWCO 1000 Da) for 4 d and the dialysis medium was changed three times. The crude polymer solution was purified by preparative SEC to remove unreacted side chains. The purified polymer was recovered by concentrating the solution under reduced pressure, precipitation in diethyl ether, centrifugation and drying under vacuum overnight.

2.12 Synthesis of G0PBG-*g*-PZLys and G1PBG-*g*-PZLys

The G0PBG-*g*-PZLys and G1PBG-*g*-PZLys samples were prepared by procedures similar to G0PBG and G1PBG. In a typical synthesis for G0PBG-*g*-PZLys, partially deprotected G0PBG (160 mg, 0.176 mmol free –COOH units) and PZLys (824 mg, 0.159 mmol –NH_2 units) were

dissolved in 10 mL of dry DMSO containing 1% DMF. DIC (111 mg, 0.880 mmol) was added with stirring for 10 min, followed by HOBt (195 mg, 0.880 mmol) and TEA (88.8 mg, 0.880 mmol). The reaction was allowed to proceed for one week at room temperature and the polymer solution was dialyzed against 500 mL of DMSO, and subsequently against DMF (MWCO 1000 Da) for 4 d and the dialysis medium was changed four times. The crude polymer solution was purified by preparative SEC to remove unreacted side chains and concentrated under reduced pressure. The polymer was precipitated in diethyl ether, centrifuged and dried under vacuum overnight. The synthesis of G1PBG-*g*-PZLys was performed by a similar procedure, using G1PBG (200 mg, 0.312 mmol –COOH units), PZLys (1.25 g, 0.284 mmol $–NH_2$ units), DIC (197 mg, 1.56 mmol), HOBt (211 mg, 1.56 mmol), and TEA (159 mg, 1.57 mmol).

2.13 Full Deprotection of G0PBG-*g*-PZLys and G1PBG-*g*-PZLys

The deprotection of G0PBG-*g*-PZLys was achieved by a method similar to G0PBG and G1PBG. Briefly, G0PBG-*g*-PZLys (250 mg, 0.953 mmol ZLys units) was dissolved in 5 mL of TFA. A large excess of HBr solution (33% w/w) in acetic acid (769 mg, 9.5 mmol HBr) was added to the solution to fully deprotect the Z groups on lysine. The reaction was allowed to proceed for 3 h before precipitation in diethyl ether. The white powder was collected by centrifugation and dried under vacuum. Yield = 175 mg (70.0 %). The deprotection of G1PBG-g-PZLys was performed in a similar manner using G1PBG-*g*-PZLys (203 mg, 0.598 mmol) and HBr solution in acetic acid (290 mg, 1.20 mmol HBr units).

2.14 Synthesis of Model Imines Using Small Molecule Amines

To study the formation of the imine products between an aromatic aldehyde and a primary amine, several model reactions were performed using small-molecule *n*-hexylamine and linear PLys chains, using a procedure adapted from Gu et al.[106]

2.14.1 Synthesis of *n*-Hexyl Poly(ethylene glycol) Benzylimine (HexNH$_2$-imi-PEG)

A comparative experiment to study the formation of the imine was performed using *n*-hexylamine and PEG-Bz-CHO. Briefly, hexylamine (50 μL, 38 mg, 0.372 mmol) and PEG-Bz-CHO (51 mg, 0.010 mmol) were dissolved in 2 mL of dry DMSO. The reaction mixture was allowed to stir for 5 d. The solvent and excess *n*-hexylamine were evaporated under vacuum and the product was recovered as a white solid. ^{1}H NMR (300 MHz, DMSO-d_6), δ: 3.25 (s, 3H), 3.26 – 3.60 (m, 454H), 7.96 (q, 4H), 8.44 (s, 1H).

2.14.2 Synthesis of *n*-Hexyl Trifluoromethylbenzylimine (HexNH$_2$-imi-TFBA)

n-Hexylamine (50 μL, 38 mg, 0.372 mmol) and TFBA (50 μL, 69 mg, 0.292 mmol) were added to 2 mL of dry DMSO. The reaction mixture was allowed to stir for 4 d. The solvent was then evaporated under vacuum. The final product was obtained as a light-yellow liquid. ^{1}H-NMR, (300 MHz, DMSO-d_6.). δ: 0.85 (t, 3H), 1.16 – 1.39 (m, 6H), 1.61 (quint, 2H), 3.59 (t, 2H), 7.96 (q, 4H), 8.44 (s, 1H).

2.15 Synthesis of PLys-*g*-PEG

The synthesis of model imines using PLys and PEG-Bz-CHO was performed under conditions similar to those described in Section 2.14. Briefly, PLys (50 mg, 0.391 mmol Lys units) and PEG-Bz-CHO (50 mg, 9.8 μmol) were added to 2 mL of DMSO-d_6, The reaction mixture was stirred for 3d at room temperature before magnesium sulfate was added to the solution. The reaction mixture was analyzed by NMR multiple times throughout the reaction time. After two more days of stirring at room temperature, the imine was recovered by evaporation of the solvent.

2.16 Synthesis of G0PBG-*g*-PLys-*g*-PEG and G1PBG-*g*-PLys-*g*-PEG

The syntheses of G0PBG-*g*-PLys-*g*-PEG and G1PBG-*g*-PLys-*g*-PEG were carried out by a method similar to PLys-*g*-PEG. In a typical procedure, fully deprotected G0PBG-*g*-PLys (70 mg, 0.410 mmol Lys units) and PEG-Bz-CHO (50 mg, 0.010 mmol) were dissolved in 1.5 mL of DMSO. $MgSO_4$ (10 mg) was added to the solution and the reaction mixture was stirred at room temperature for 2 d, before it was heated to 40 °C and stirred for 4 h longer. The synthesis of G1PBG-*g*-PLys-*g*-PEG was performed by a similar method, using G1PBG-*g*-PLys-*g*-PEG (44 mg, 0.34 mmol) and PEG-Bz-CHO (44 mg, 8.5 μmol).

2.17 Amine Functionality Analysis

The terminal amine group content of the linear polypeptide chains was determined by ^{19}F NMR spectroscopy by the method of Ji *et al.*[107] In a typical procedure, PBG (12.5 mg, 1.92 μmol)

was dissolved in 2 mL of DMSO-d_6. A solution of BTF (61.3 mg, 420 μmol) and TFBA (57.7 mg, 331 μmol) was prepared in 2 mL of DMSO-d_6, and a 72.4 mg aliquot of that solution (containing 12.4 μmol of BTF and 9.81 mmol of TFBA) was added to the polypeptide solution. The reaction was stirred overnight before performing ^{19}F NMR analysis.

3 Results and Discussion

3.1 Synthesis of BzGlu NCA and ZLysNCA

Peptide synthesis typically relies upon linking the carboxyl group of an N-protected amino acid with the amino functionality of another amino acid containing a protected carboxyl group. The protecting group on the N-terminus of the dipeptide is then removed to expose the free amine, and the coupling and deprotection procedures are repeated to create longer polypeptide chains. This approach to synthesizing polypeptides, while providing precise control over the amino acid sequence, is inefficient for longer polypeptides due to the complicated sequence of deprotection and coupling reactions used, and the significant amount of side products generated due to incomplete coupling in each cycle. A better method to synthesize peptide chains with uniform molecular weight distributions, when amino acid sequence control is not required, is using amino acid *N*-carboxyanhydride (NCA) monomers.[108] Amino acid NCAs were first synthesized by Leuch by heating a solution of the *N*-ethoxycarbonyl or *N*-methoxycarbonyl amino acid.[109] In 1950, Farthing and Reynolds developed a more efficient procedure for N-unsubstituted phenylalanine NCA using phosgene.[110] Phosgenation has since become a common technique to synthesize amino acid NCAs.[111–113] In this project, a 15% phosgene solution in toluene was used. Reactions for the synthesis of BzGluNCA and ZLysNCA are shown in **Scheme 3.1** and **Scheme 3.2**, respectively.

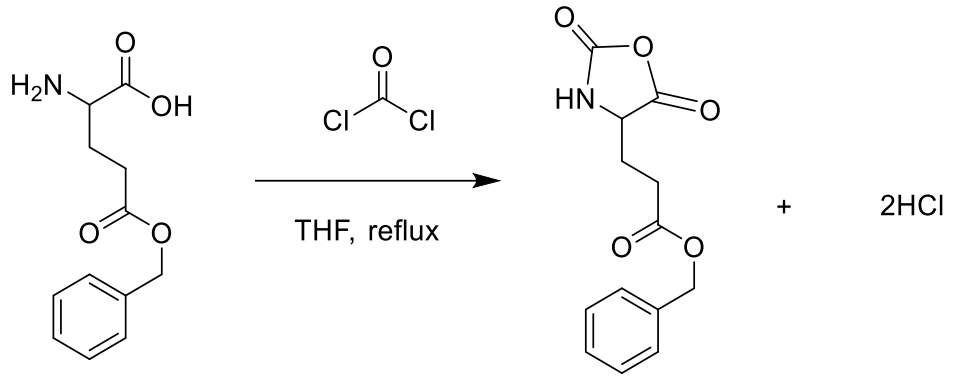

Scheme 3.1 Synthesis of BzGlu NCA.

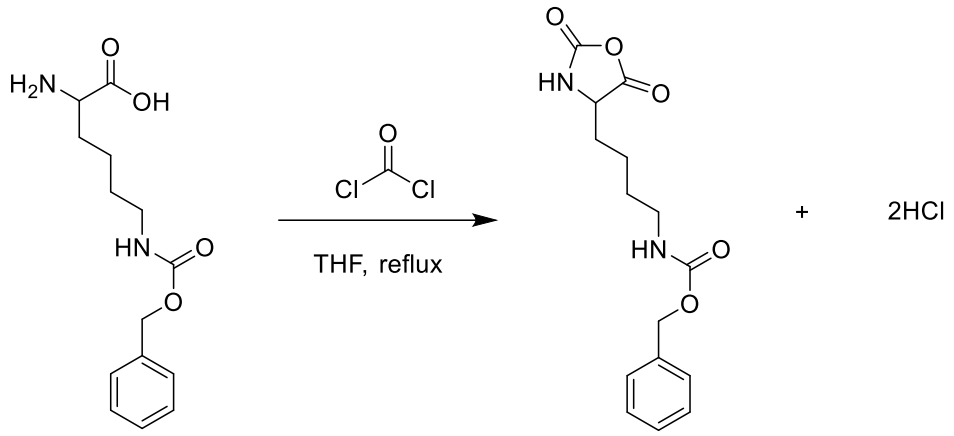

Scheme 3.2 Synthesis of ZLys NCA.

Both amino acid NCAs were characterized by ^{1}H NMR spectroscopy in DMSO-d_6. In the spectrum for BzGlu NCA, the multiplet signal from 1.87–2.13 ppm and the triplet signal from 2.48–2.57 ppm are assigned to the methylene protons of the β- and γ-carbon on the aliphatic side chains of the monomer, respectively. The signal from 4.43–4.53 ppm is assigned to the methine proton. The signal from 5.02–5.15 ppm is for the benzylic protons, and the signals from 7.15–7.55 ppm is for the aromatic protons on the side chains.

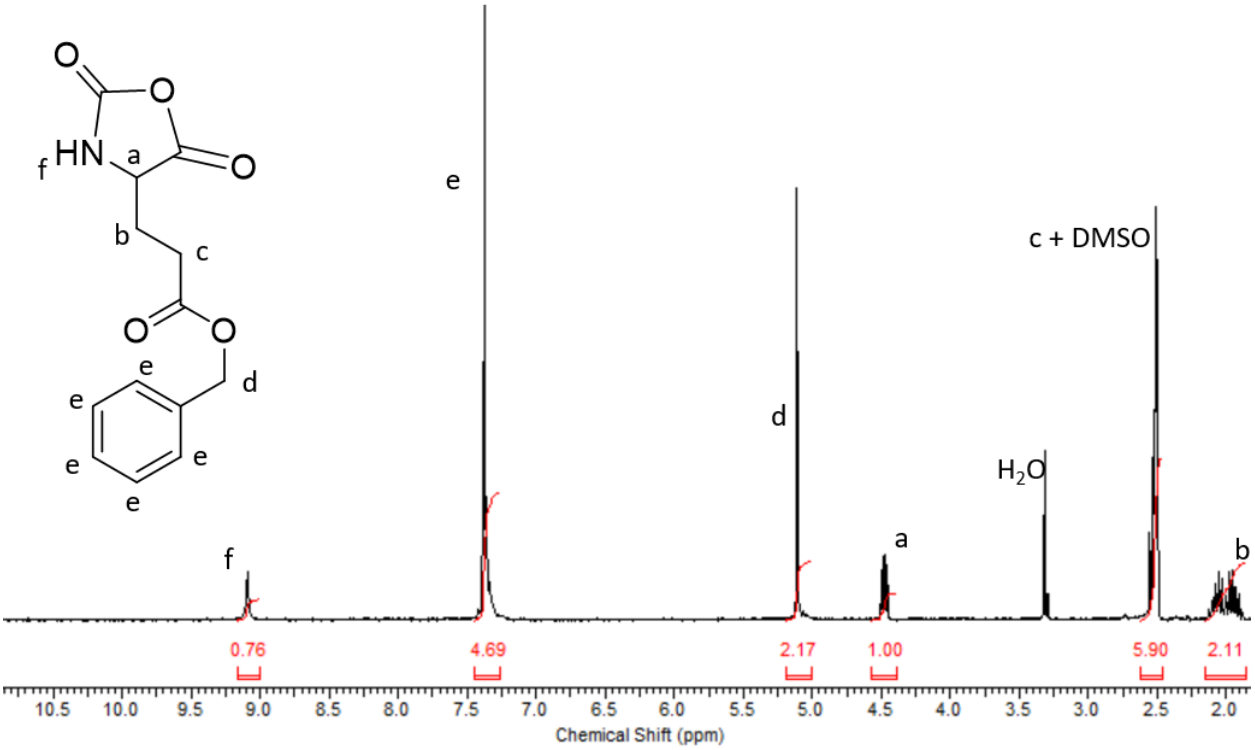

Figure 3.1 ^{1}H NMR spectrum for BzGlu NCA.

The NMR spectrum for the ZLys NCA in DMSO-d_6 is shown in Figure 3.2. The resonance signal for the methine proton can be found at 4.45 pm. The photons from the aliphatic side chains of the lysine units are at 1.14, 1.17 and 2.99 ppm. The peaks at 5.02 and 7.35 ppm are assigned to the benzylic and aromatic protons of the Z protecting group, respectively. Finally, the resonance for the NH group on the NCA ring and the NH group on the side chain of lysine can be found at 9.09 and 7.25 ppm, respectively.

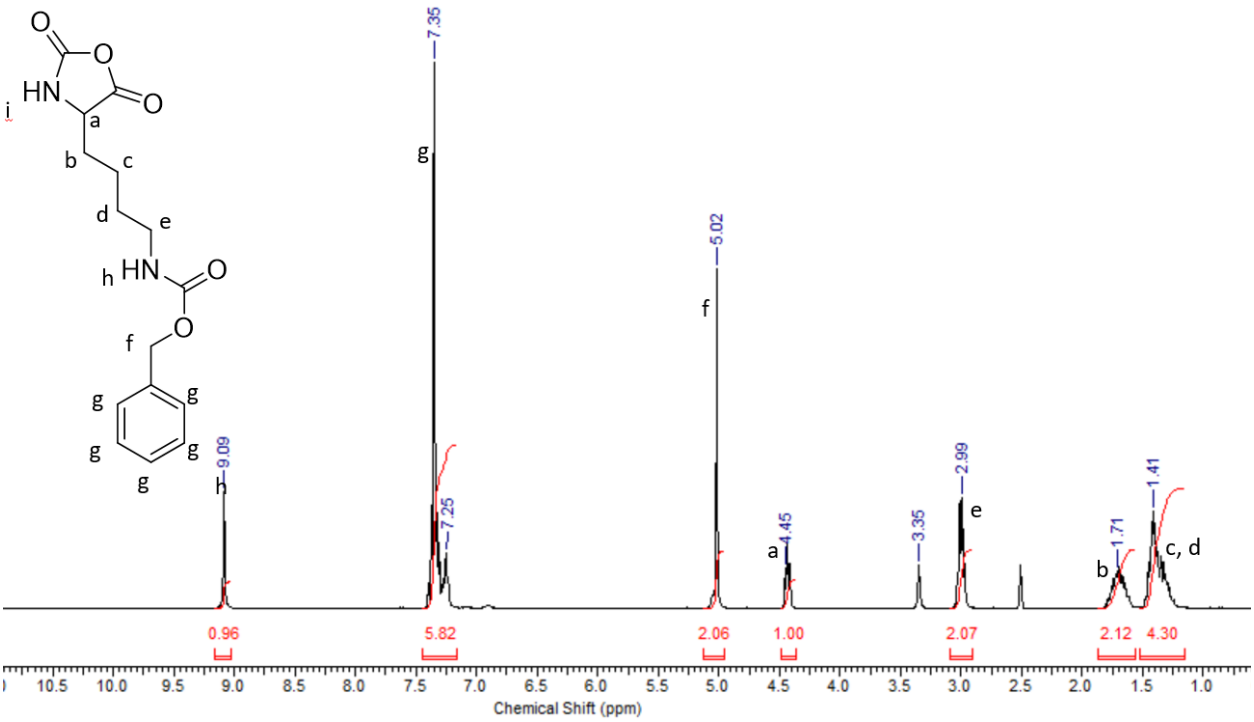

Figure 3.2 ^{1}H NMR spectrum for ZLys NCA.

3.2 Synthesis of PBG and PZLys Serving as Side Chains

Linear polypeptide chains with controllable molecular weights and narrow molecular weight distributions are highly desirable building blocks for the construction of arborescent polymers for drug delivery applications. The polymerization of the NCA monomers can be initiated by Lewis bases such as amines, alkoxides, and hydroxides. There are two major mechanisms for the polymerization of amino acid NCA monomers, namely the amine mechanism and the activated monomer mechanism. These are provided in **Scheme 3.3** and **Scheme 3.4**, respectively. In the amine mechanism, the nucleophilic initiator attacks the C-5 carbon of the monomer to generate a free amine group. Chain propagation occurs by subsequent attack of the

free amine on the C-5 carbon of additional monomers. In the activated mechanism, the initiator serves as a base to deprotonate the NH moiety on the NCA monomer. The anionic NCA monomer can attack another monomer to create a dimer. A new NCA anion is generated by a proton transfer and the release of CO_2. Chain propagation proceeds by the attack of subsequently deprotonated monomers on the anhydride-terminated polymer chain.

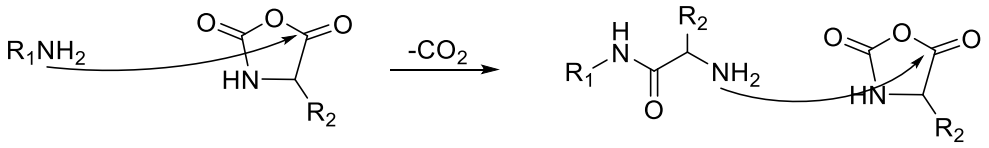

Scheme 3.3 Polymerization of amino acid NCAs by the amine mechanism.

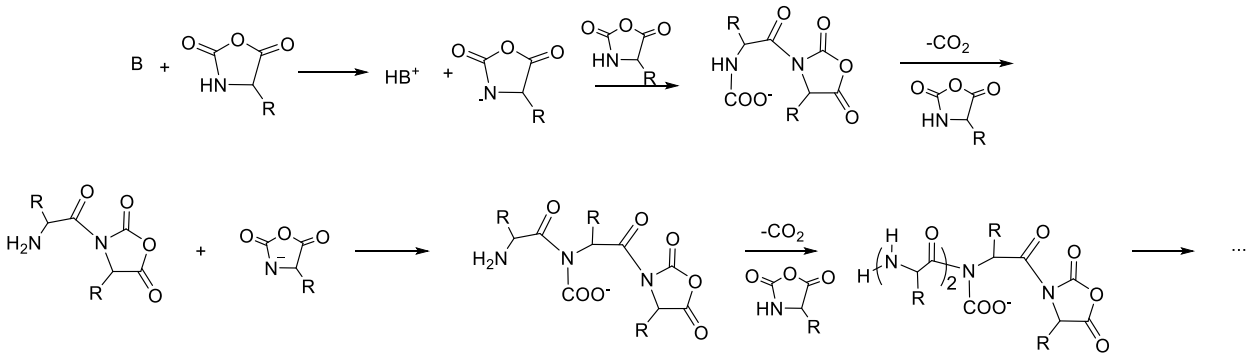

Scheme 3.4 Polymerization of amino acid NCAs by the activated monomer mechanism.

When a primary amine is used as initiator, the polymerization usually occurs via the amine mechanism due to its nucleophilicity. The rate of initiation is faster than the rate of propagation, leading to polypeptides with narrow molecular weight distributions. When an initiator with weaker nucleophilic but stronger base character such as a tertiary amine is used as initiator, polymerization occurs via the activated monomer mechanism. The rate of chain propagation is faster than the rate

of initiation under these conditions, yielding longer polypeptide chains with a broad molecular weight distribution. To construct arborescent polymer structures with a well-defined architecture, it is essential to use linear polypeptide chains with a narrow molecular weight distribution. Consequently, a primary amine was selected as initiator for the polymerization. Schemes for the synthesis of linear PBG and PZLys are provided in **Scheme 3.5** and **Scheme 3.6**, respectively.

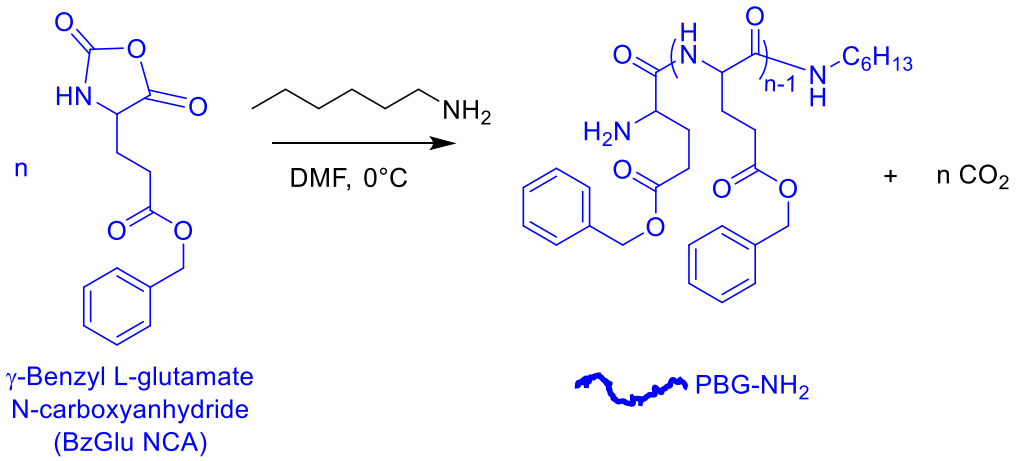

Scheme 3.5 Polymerization of BzGlu NCA with *n*-hexylamine.

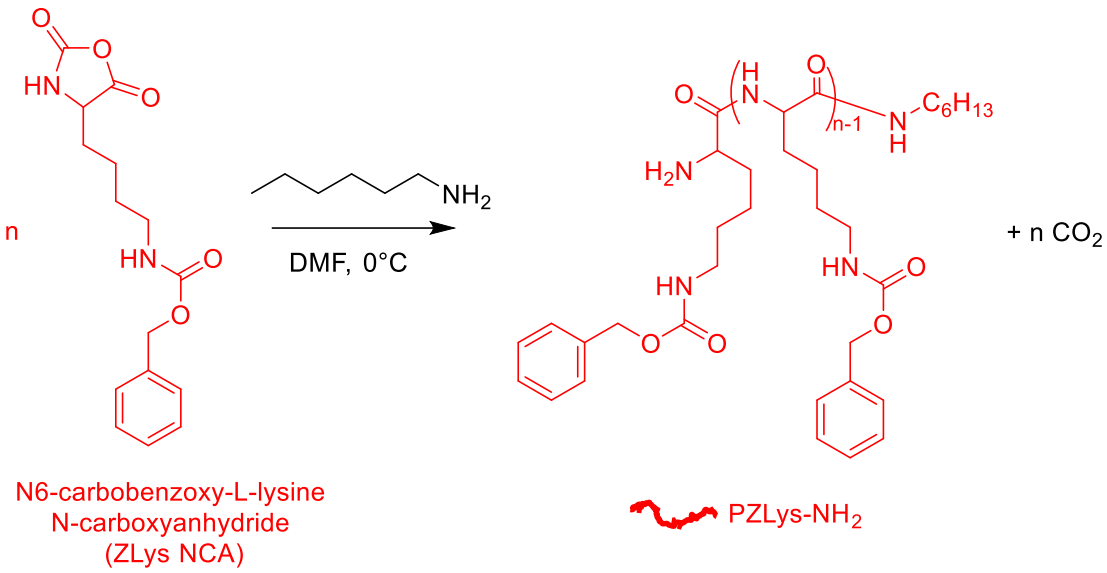

Scheme 3.6 Polymerization of ZLys NCA with *n*-hexylamine.

One very important side reaction in the synthesis of linear PBG is intramolecular cyclization, whereby the terminal amine attacks the ester groups of BzGlu to form a lactam ring (**Scheme 3.7**). This terminates the propagating polypeptide chain, causing broadening of the molecular weight distribution. More importantly, cyclization deactivates the terminal amine group required for the grafting reaction. It was shown previously that decreasing the reaction temperature can effectively suppress chain-end cyclization reactions.[114] Consequently, the polymerizations were performed at 0 °C in a chilled bath. The lower polymerization temperature decreased the rate of chain propagation, but also generated polypeptides with narrower molecular weight distributions.

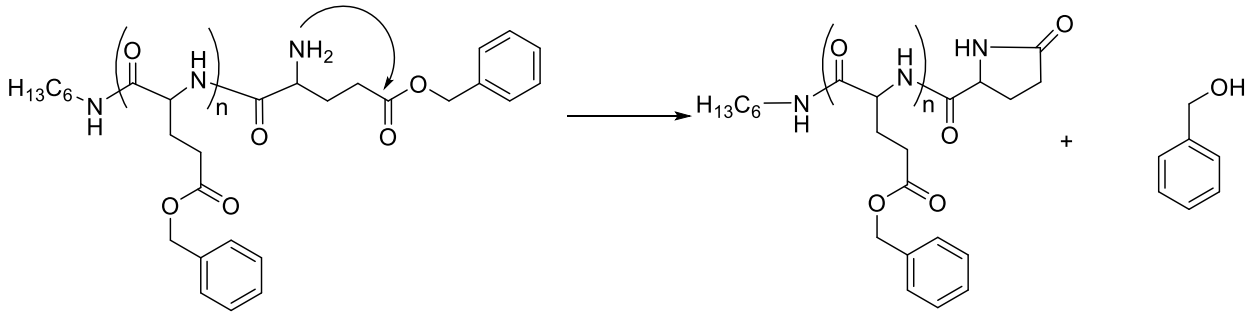

Scheme 3.7 Chain-end cyclization of PBG.

Since water can also initiate the polymerization of amino acid NCAs, the solvent was carefully distilled from a drying agent (CaH_2) prior to the reaction. The degree of polymerization can be controlled through the molar ratio of the monomer to initiator. A ^1H NMR spectrum obtained for PBG is provided in **Figure 3.3**. Comparing the NMR spectra for BzGlu NCA and PBG, the resonance signal at 9.09 ppm corresponding to the NH proton on the NCA is no longer present in the NMR spectrum for the polymer, which shows that the polymer contains no residual monomer. A new broad peak from 7.58–8.41 ppm corresponds to the amide NH group in the polypeptide chain. This shows that the monomer was successfully converted to PBG.

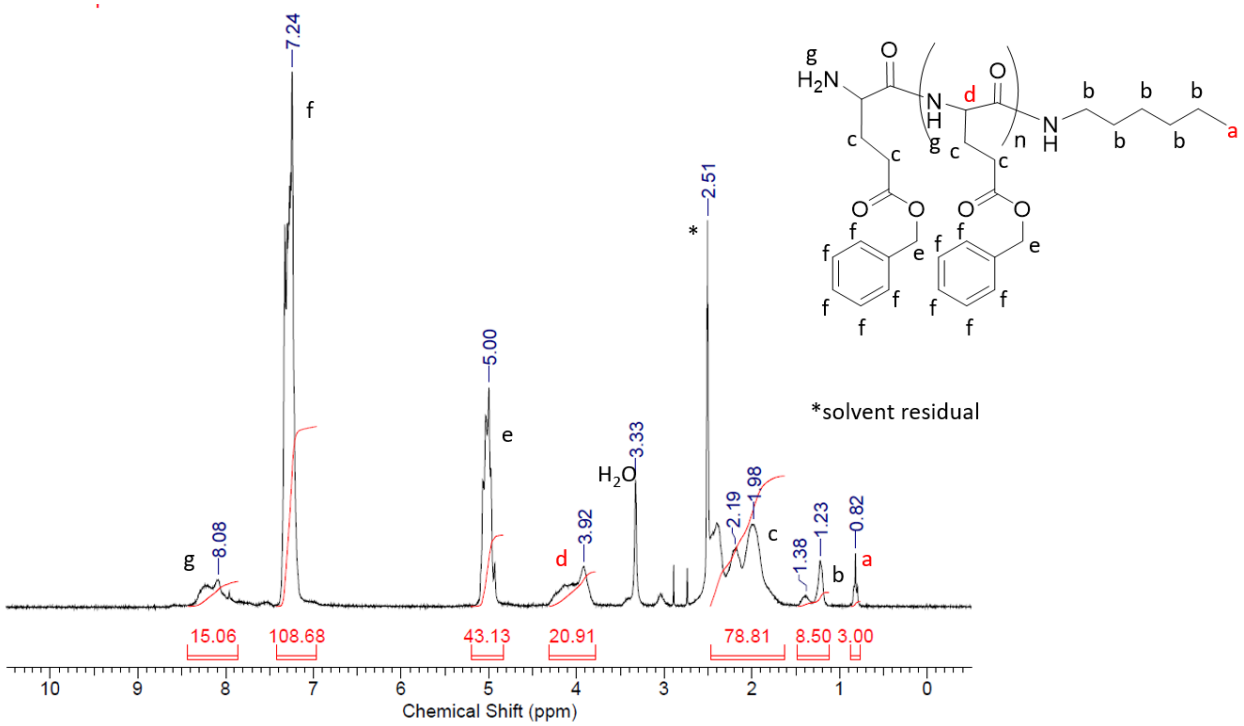

Figure 3.3 ^{1}H NMR spectrum for PBG with X_n = 21.

The number-average degree of polymerization of the PBG chains can be determined from the relative integration areas for the terminal methyl protons and the methine proton in the monomer units. In this specific case, the degree of polymerization of PBG was calculated as:

$$X_n = \left(\frac{Integration\ of\ methine\ proton}{\#\ of\ protons}\right) \Big/ \left(\frac{Integration\ of\ terminal\ methyl\ protons}{\#\ of\ protons\ in\ methyl\ group}\right)$$

$$X_n = \left(\frac{20.91}{1.00}\right) \Big/ \left(\frac{3.00}{3.00}\right) = 20.9$$

The calculated degree of polymerization (X_n = 20.9) is in good agreement with the targeted value (X_n = 22.6), demonstrating that the PBG chain length is effectively controlled by the monomer-to-initiator molar ratio. The corresponding number-average molecular weight (M_n) of

the PBG was 5560 g/mol. The PBG sample was also characterized by GPC analysis (**Figure 3.4**) which yielded a narrow and symmetrical peak corresponding to a polydispersity index M_w/M_n = 1.04, confirming that the ROP of the NCA was well-controlled. The polystyrene equivalent M_n measured by GPC analysis was 11400 g/mol, which is significantly higher than the absolute M_n calculated from NMR. This is because the M_n in GPC analysis is an apparent molecular weight based on the hydrodynamic volume, and the analysis was performed using a linear polystyrene calibration curve. Due to the significant difference in chemical structures between PBG and polystyrene, the apparent molecular weight calculated by GPC using a polystyrene standard is not an accurate representation of the polymer size. Therefore, the absolute M_n determined from NMR analysis was used in subsequent stoichiometric calculations.

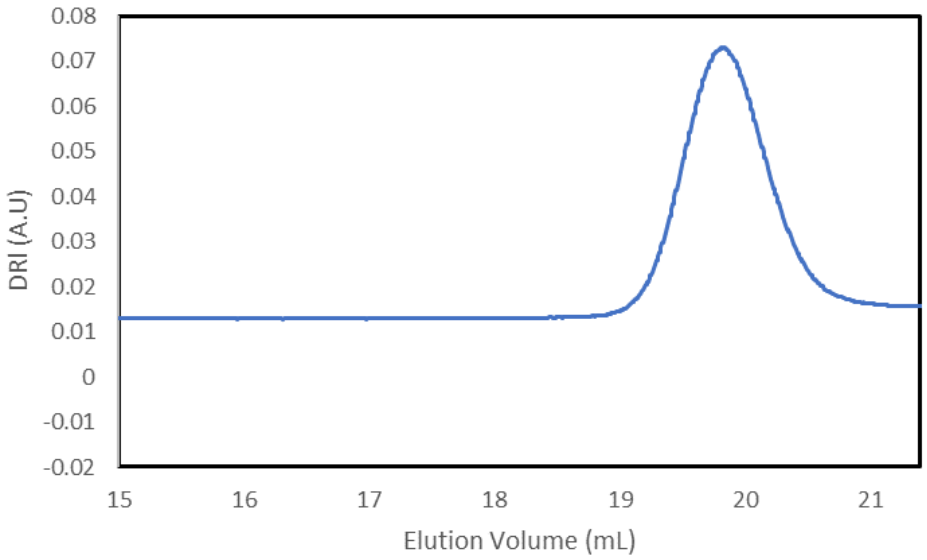

Figure 3.4 SEC analysis of PBG with X_n = 21.

The synthesis of linear PZLys was performed under similar conditions, and the polymer was characterized by ^{1}H NMR and GPC analyses. Comparison of the NMR spectrum obtained for PZLys (**Figure 3.5**) with ZLys NCA shows that the peak at 9.09 ppm for the NH proton on the NCA monomer is not present in the NMR spectrum of the polymer, which shows that the recovered sample contained no residual monomer. A new broad peak from 7.64–8.50 ppm is assigned to the amide NH group in the polypeptide. These confirm that the monomer was successfully converted to PZLys.

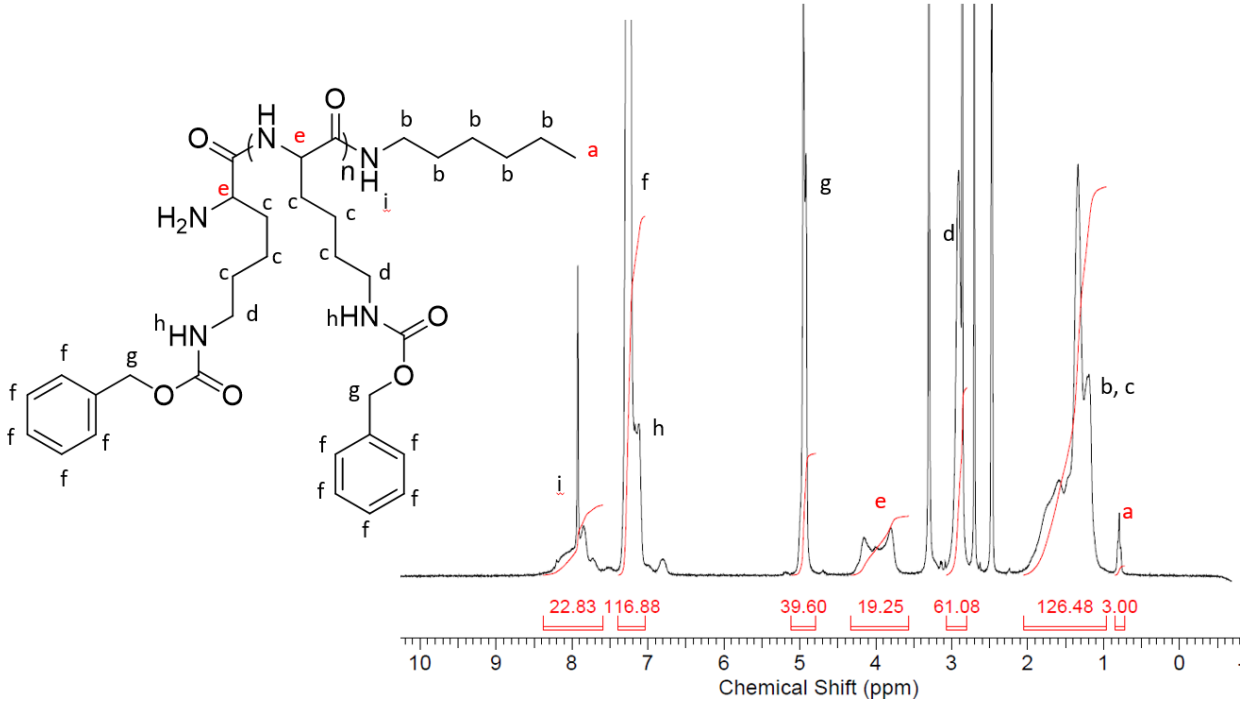

Figure 3.5 ^{1}H NMR spectrum for PZLys with X_n = 19.3.

Similarly to linear PBG, the degree of polymerization was calculated from the relative integration areas for the methine proton and the terminal methyl proton:

$$X_n = \left(\frac{Integration\ of\ methine\ proton}{\#\ of\ protons}\right) \Big/ \left(\frac{Integration\ of\ terminal\ methyl\ protons}{\#\ of\ protons\ in\ methyl\ group}\right)$$

$$X_n = \left(\frac{19.25}{1.00}\right) \Big/ \left(\frac{3.00}{3.00}\right) = 19.3.$$

The calculated number-average degree of polymerization (X_n = 19.3) is in agreement with the targeted value (X_n = 19.6), demonstrating again that the PZLys chain length can be effectively controlled by varying the monomer-to-initiator ratio. This corresponds to a number-average molecular weight of 4890 g/mol. The GPC trace obtained for the PZLys sample, provided in **Figure 3.6**, shows a narrow and relatively symmetrical molecular weight distribution (M_w/M_n = 1.07), with a polystyrene-equivalent M_n = 17490 g/mol. This demonstrates that the ring-opening polymerization of ZLys NCA was controlled, similarly to the BzGlu NCA.

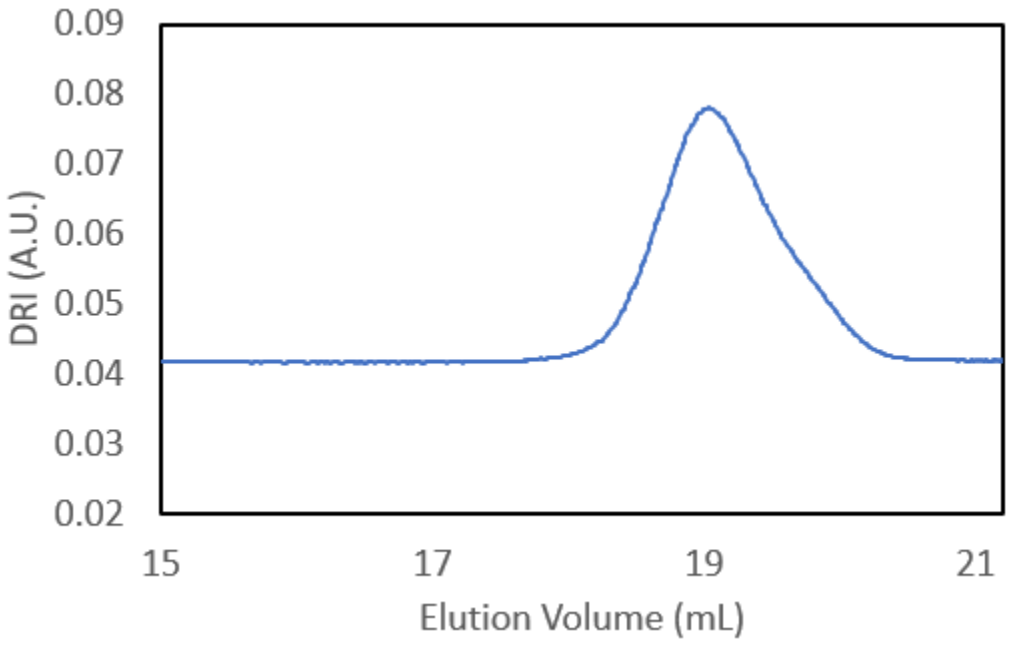

Figure 3.6 SEC analysis of PZLys with X_n = 19.3.

3.3 Synthesis of PEG-CHO Through Direct Oxidation of Terminal Alcohol

To produce a pH-sensitive imine bond between the PEG chains forming the shell and the PLys inner layer, a carbonyl group needed to be generated from the –OH terminus of the PEG monomethyl ether chains. Initially, this was achieved through direct oxidation of the terminal alcohol group into an aldehyde functionality as shown in **Scheme 3.8**, using a TEMPO/BAIB reagent system developed by Masson *et al.*[105] In this procedure a catalytic amount of TEMPO radical is used to oxidize the alcohol group, together with three molar equivalents of BAIB to regenerate the TEMPO as it is consumed (**Scheme 3.9**). The extent of oxidation is controlled by the solvent used. Reactions in a 1:1 mixture of water and acetonitrile selectively yield the carboxylic acid product, while in DCM the aldehyde product is generated without over-oxidation.

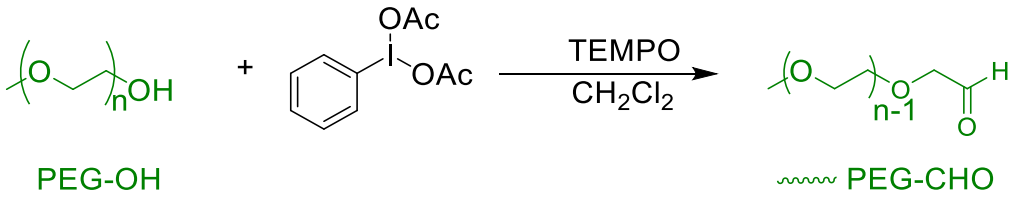

Scheme 3.8 Synthesis of PEG-CHO by TEMPO/BAIB oxidation.

Reprinted with permission from reference 105. Copyright 2001 John Wiley and Sons.

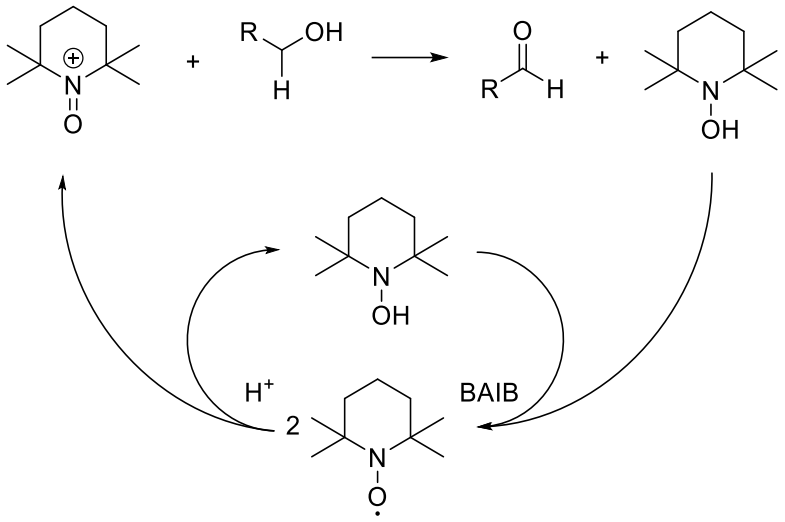

Scheme 3.9 Mechanism of TEMPO/BAIB oxidation to aldehyde.

Reprinted with permission from reference 115. Copyright 1997 American Chemical Society.

After the oxidation was allowed to proceed for 3 h, an aliquot of the reaction mixture was precipitated in diethyl ether. GPC analysis showed a relatively unimodal peak at the elution volume expected for oxidized PEG (**Figure 3.7**). However, a small peak was also observed near an elution volume of 17.8 mL The reaction was allowed to continue overnight before the product was recovered and analyzed again by GPC, but as shown in **Figure 3.7**, two peaks were found on the GPC trace. The apparent (polystyrene-equivalent) molecular weights of the peaks at elution volumes of 17.5 mL and 18.5 mL were found to be 49700 g/mol and 28300 g/mol, respectively. This suggested that the GPC peak at 17.5 mL is due to a dimer of PEG-CHO. This was investigated further in a subsequent experiment where the reaction was monitored by NMR and GPC analyses.

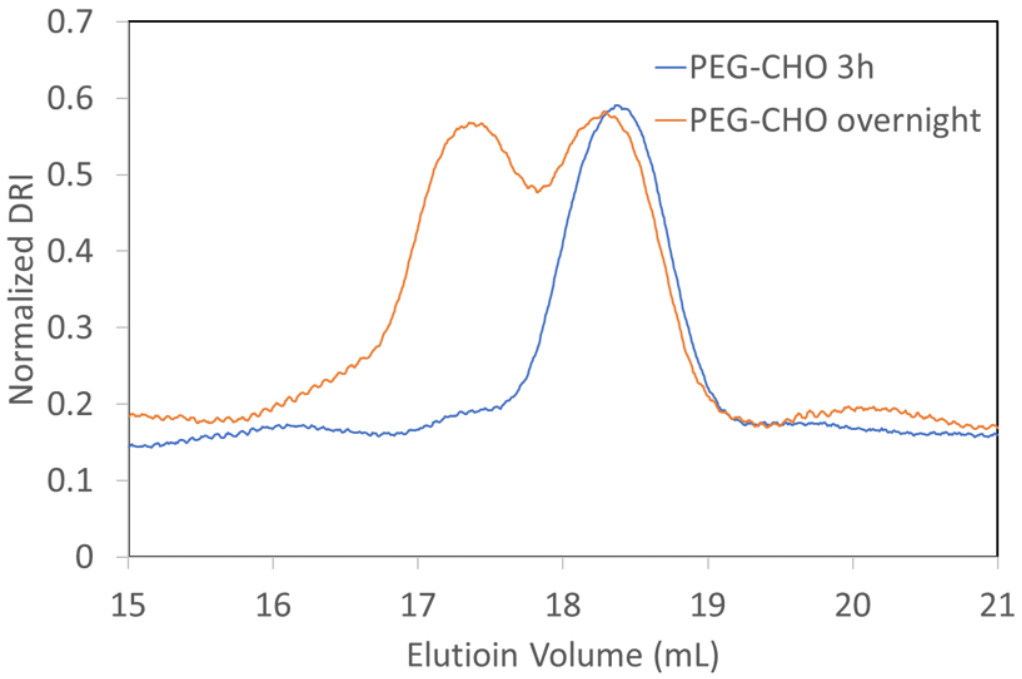

Figure 3.7 Comparison of GPC traces for PEG-CHO after 3 h and overnight reactions.

Using NMR analysis, the fraction of alcohol groups oxidized was monitored using the peak integration area of the protons alpha to the aldehyde group relative to the chain-end methyl protons, near 4.18 and 3.40 ppm, respectively. As shown in **Figure 3.8**, 8% of the alcohol groups were converted to aldehyde functionalities after 4 h. The conversion level increased progressively and approximately 97% conversion was achieved after 18 h. However, in GPC analysis, a peak for dimerized product was present 4 h after starting the reaction. The fraction of the dimer species increased with reaction time from 4 h to 6 h. Then, the fraction of dimeric product started to decrease until 18 h after the beginning of the reaction (**Figure 3.9**). These results show that the reaction is highly sensitive to dimer formation and needs to be closely monitored. After recovering the product by precipitation, centrifugation and drying under vacuum overnight, subsequent NMR

analysis of the PEG-CHO sample showed that only 73% of the aldehyde groups were preserved (**Figure 3.10**). This also showed that the aldehyde groups of PEG-CHO synthesized by this technique were very unstable. Consequently, it would be difficult to obtain reliably large amounts of PEG-CHO with a high aldehyde functionality for subsequent coupling reactions with the PLys side chains by that method. Consequently, an alternate synthetic pathway was investigated for the preparation of aldehyde-terminated PEG.

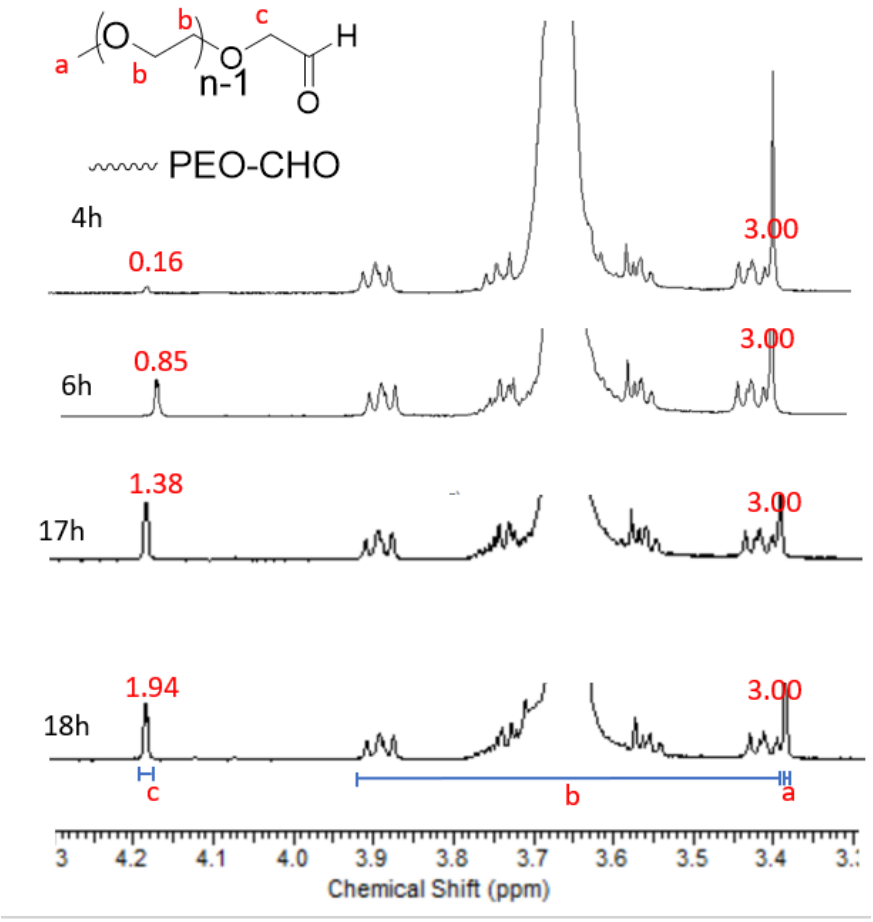

Figure 3.8 ^{1}H NMR spectra for PEG-CHO by direct oxidation at different reaction times.

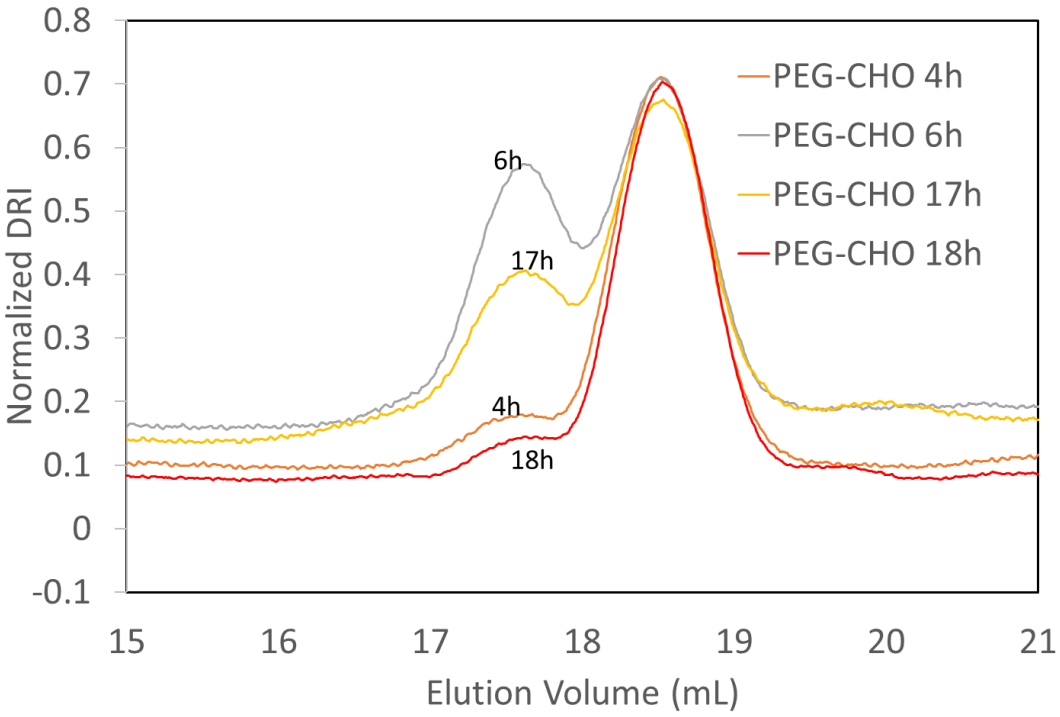

Figure 3.9 Evolution of dimer species of PEG-CHO over time analyzed by GPC.

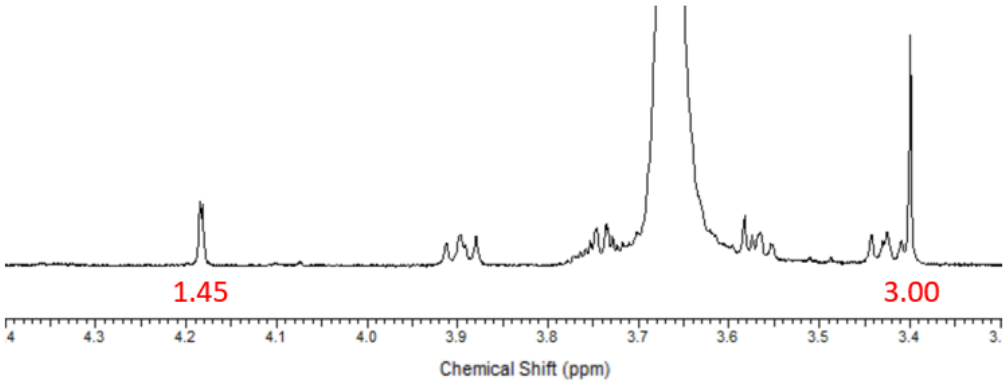

Figure 3.10 ^{1}H NMR spectrum for PEG-CHO prepared by direct oxidation, after purification.

3.4 Synthesis of PEG-Bz-CHO Through Esterification with FmBA

To improve the synthesis efficiency and stability of aldehyde-terminated PEO, another method to modify the PEO chain end was explored. Furthermore, the type of aldehyde reactant used in the synthesis of imines is known to have a significant impact on the efficiency of the reaction. When aromatic aldehydes are used thermodynamics favour the formation of the imine product, while for aliphatic aldehydes the reaction is usually unfavourable unless water is removed from the mixture.[116] Consequently, an aromatic aldehyde was used to modify the chain end of PEG. This was achieved through esterification of the terminal hydroxyl group of PEG monomethyl ether with the carboxyl group of FmBA. The reaction was performed under Steglich esterification conditions in DCM at room temperature, with DCC and DMAP as activating agents. The reaction is shown in **Scheme 3.10**.

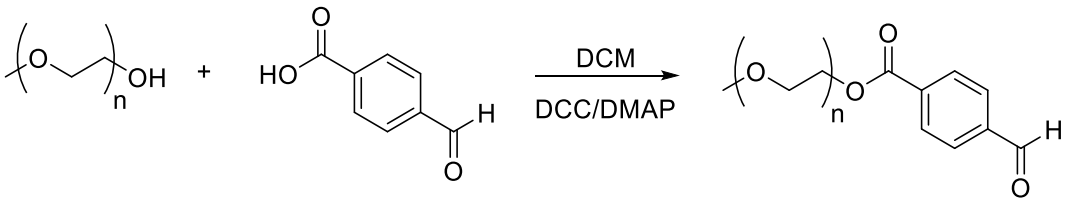

Scheme 3.10 Synthesis of PEG-Bz-CHO.

The PEG-Bz-CHO sample was characterized by ^{1}H NMR analysis in $CDCl_3$ (**Figure 3.11**) The signal at 3.5 ppm is assigned to the methylene protons in the repeating units of PEG. To confirm the success of the esterification reaction, ^{1}H NMR spectra for PEG-Bz-CHO and the PEG monomethyl ether substrate are compared in **Figure 3.11**. In the PEG-Bz-CHO spectrum of **Figure 3.11a**, the resonance signals from the aromatic groups and the aldehyde groups at 8.05 – 8.21 ppm

and 10.13 ppm, respectively, indicate the successful modification of the alcohol chain end of PEG. The expanded region from 3 – 5 ppm of both spectra is compared in **Figure 3.12**. The alcohol signal at 4.57 ppm in the spectrum of PEG monomethyl ether is absent in the spectrum of PEG-Bz-CHO. Instead, a signal corresponding to the alpha protons of the ester group (-COOCH_2-) is found at 4.44 ppm. These results further confirm the successful esterification of the alcohol terminus of PEG. The relative integration areas of the resonance signals for the α-protons of the ester group and the methyl protons at the opposite PEG chain end were used to determine the efficiency of the reaction. As shown in **Figure 3.12**, since the relative integration values were 1.92 and 3.00, the alcohol conversion efficiency was calculated as:

$$\%\ Conversion = \frac{(Integration\ of\ COOC\boldsymbol{H_2}\ proton)/2}{(Integration\ of\ OC\boldsymbol{H_3}\ proton)/3} = \frac{1.92/2}{3.00/3} = 96.0\ \%$$

This shows that most of the alcohol chain ends of PEG were successfully converted to the aldehyde-carrying ester. Similar calculations using the integrated signal for the aldehyde proton at 10.2 ppm likewise yielded a functionalization level of approximately 96%.

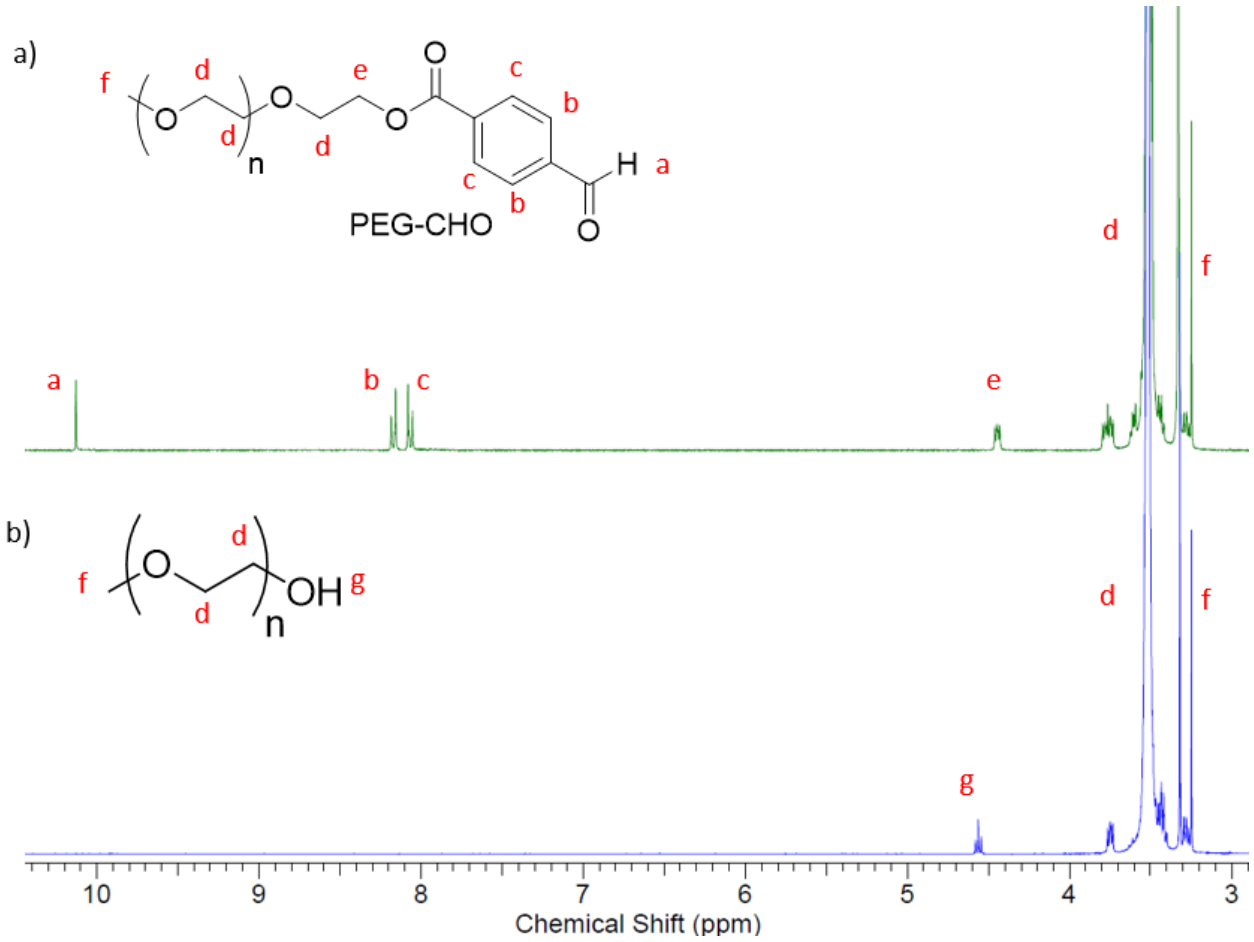

Figure 3.11 ^{1}H NMR spectrum for PEG-Bz-CHO with M_n = 5000 g/mol in DMSO-d_6.

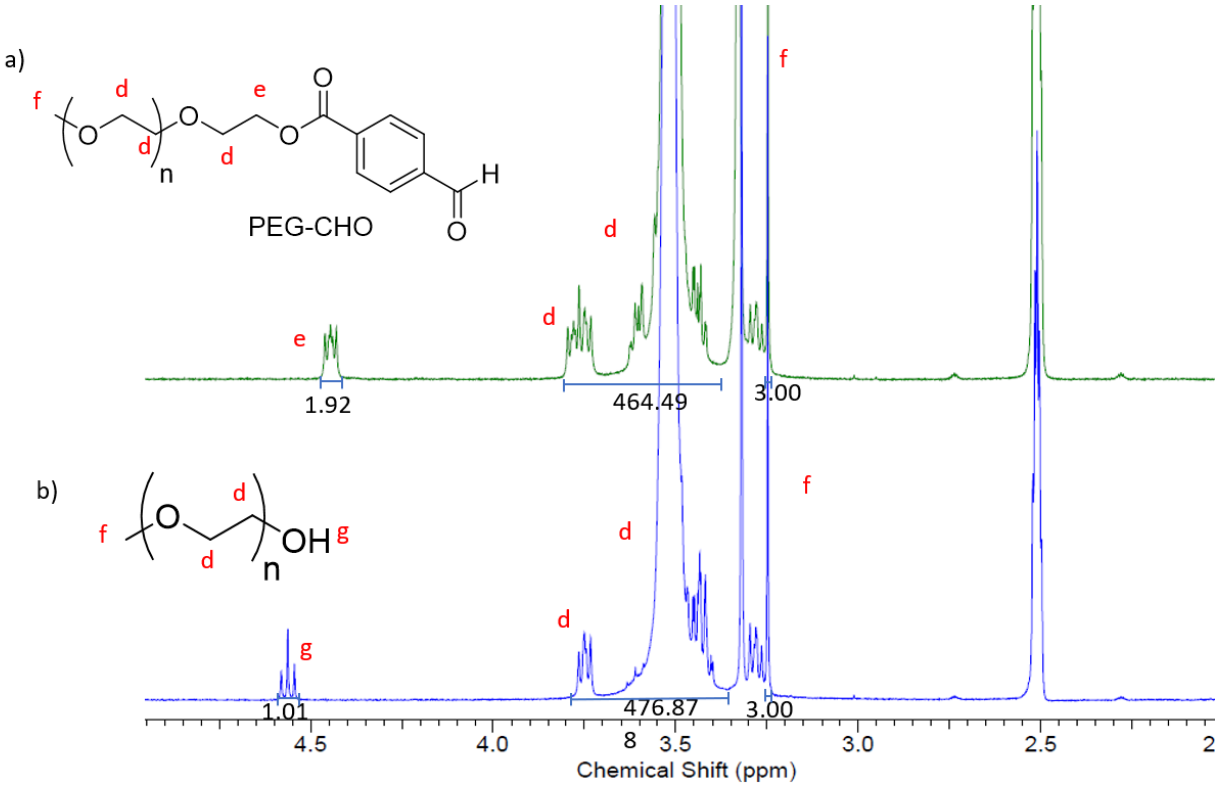

Figure 3.12 Expanded section of ^{1}H NMR spectrum for PEG-Bz-CHO in DMSO-d_6.

3.5 Amine Functionality Analysis

Preserving the primary amine group at the end of the polypeptide side chains is essential for the peptide coupling reactions used in preparing arborescent polymers. As discussed in Section 3.2, an intramolecular cyclization side reaction of PBG can deactivate the terminal amine and limit the grafting efficiency. Therefore, it was essential to determine the amine functionality level of the PBG chains.

The functionality level of the amine terminus (fraction of the chains containing an amine group) was analyzed by the technique developed by Ji *et al.*,[107] using ^{19}F NMR analysis. This

method utilizes the reaction between the primary amine group and an aromatic aldehyde containing three chemically equivalent fluorine atoms to form an imine (**Scheme 3.11**). The fluorine atoms in the imine have a chemical shift appearing downfield relatively to the unreacted aldehyde. The amount of primary amine in the polymer sample can be determined from the fraction of aldehyde reacted. A known amount of benzotrifluoride (BTF) is also added to the solution as an internal standard, such that the amount of primary amine in the polymer sample can be calculated by integrating the fluorine resonance signal from the imine product, and comparing it to the fluorine resonance signal from the known amount of BTF added.

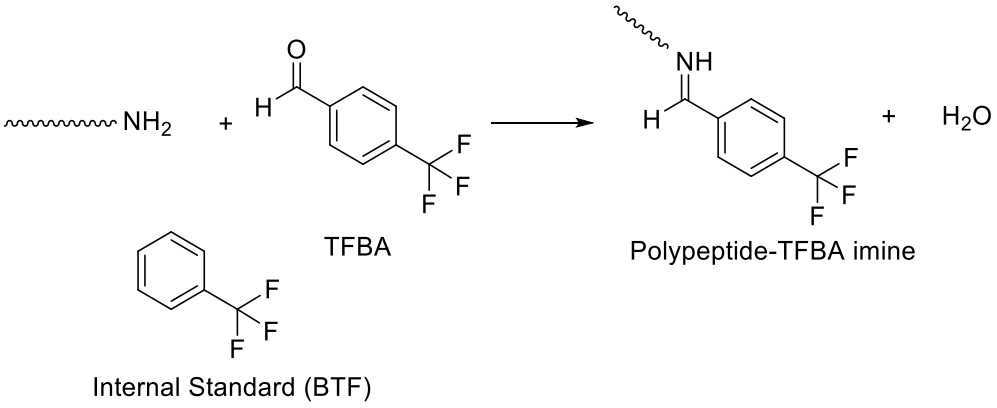

Scheme 3.11 Amine functionality analysis with BTF and TFBA.

An example of a ^{19}F NMR spectrum obtained under these conditions is shown in **Figure 3.13**. The primary amine content in the polymer sample can be determined from the integration values of the resonance peaks for the imine product and the aldehyde relatively to the BTF standard as shown below.[107]

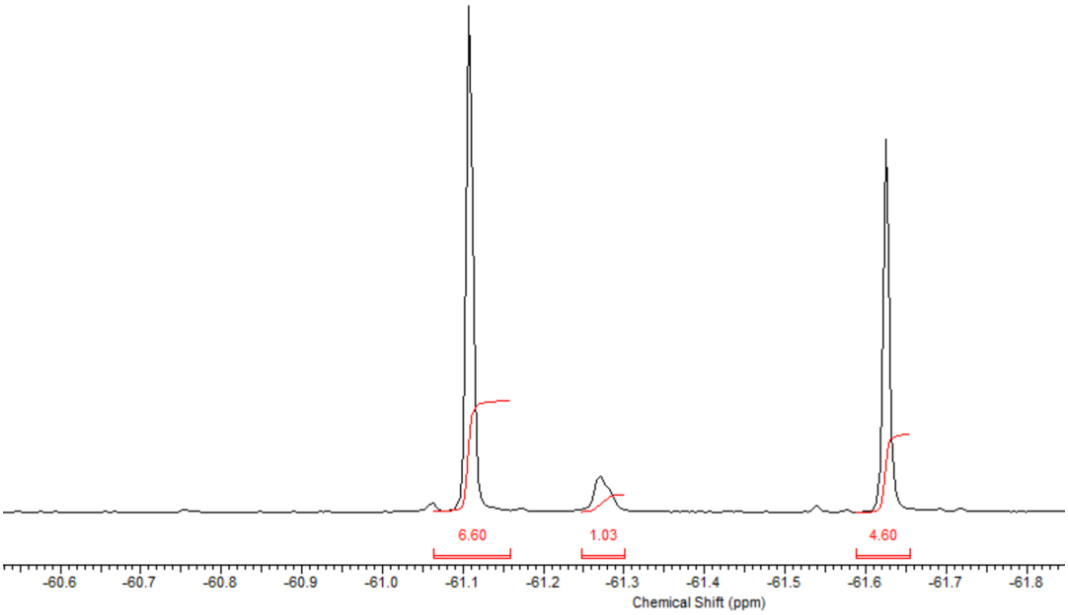

Figure 3.13 ^{19}F NMR spectrum for amine functionality analysis.

$$f_{NH_2} = \frac{integration\ of\ imine\ product}{integration\ of\ BTF} \times \frac{moles\ of\ BTF\ added}{mass\ of\ polymer\ added / M_n\ of\ polymer} \times 100\ \%$$

$$f_{NH_2} = \frac{1.00}{6.60} \times \frac{6.45 \times 10^{-6}\ mol}{12.5 mg / 6500\ \frac{g}{mol}} \times 100\ \% = 97.8\ \%$$

This result indicates that the majority of the chain-end amine groups were active, such that intramolecular cyclization reactions were insignificant and should have minimal impact on the efficiency of the coupling reaction for that sample.

3.6 Synthesis of Linear PBG Serving as Substrate

The arborescent polymers were obtained through coupling reactions between the terminal amine groups on the PBG side chains and the carboxyl groups on partially deprotected PBG substrates. It is important to deactivate the terminal amine group on the linear substrate before performing the coupling reaction for the synthesis of the G0 arborescent polymer, to prevent substrate-to-substrate coupling reactions which could lead to coupled structures and broadened molecular weight distributions. For that reason, the linear PBG serving as substrate was synthesized similarly to PBG used as side chains, except that acetic anhydride was used to quench the amine chain end (**Scheme 3.12**). The ^{1}H NMR spectrum for a PBG sample with a deactivated amine chain end is shown in **Figure 3.14**. Using the resonance signals from the methine proton in the repeating units and the terminal methyl protons from the *n*-hexylamine initiator, the deactivated PBG substrate was found to have X_n = 24.6, in good agreement with the target value X_n = 22.5.

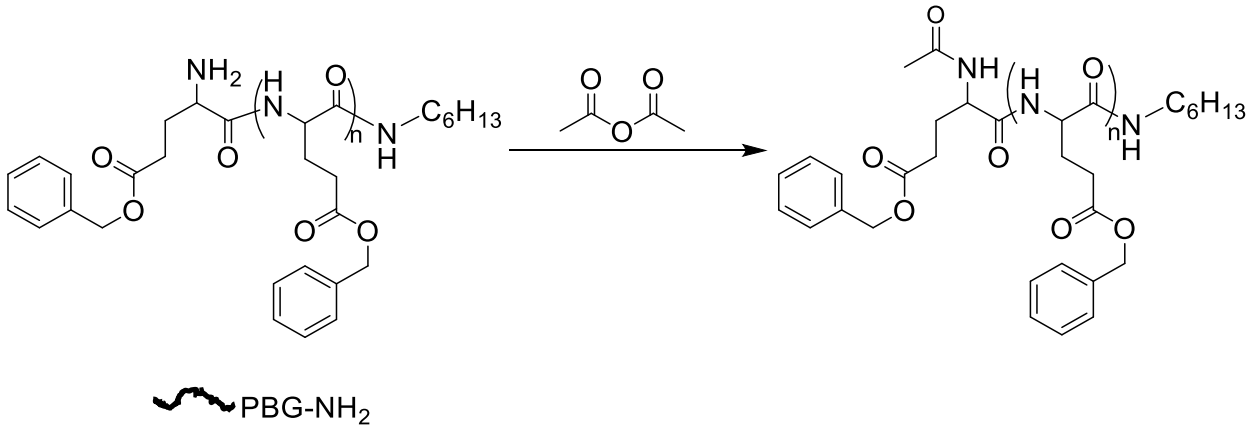

Scheme 3.12 Amine deactivation of linear PBG serving as substrate for the G0PBG synthesis.

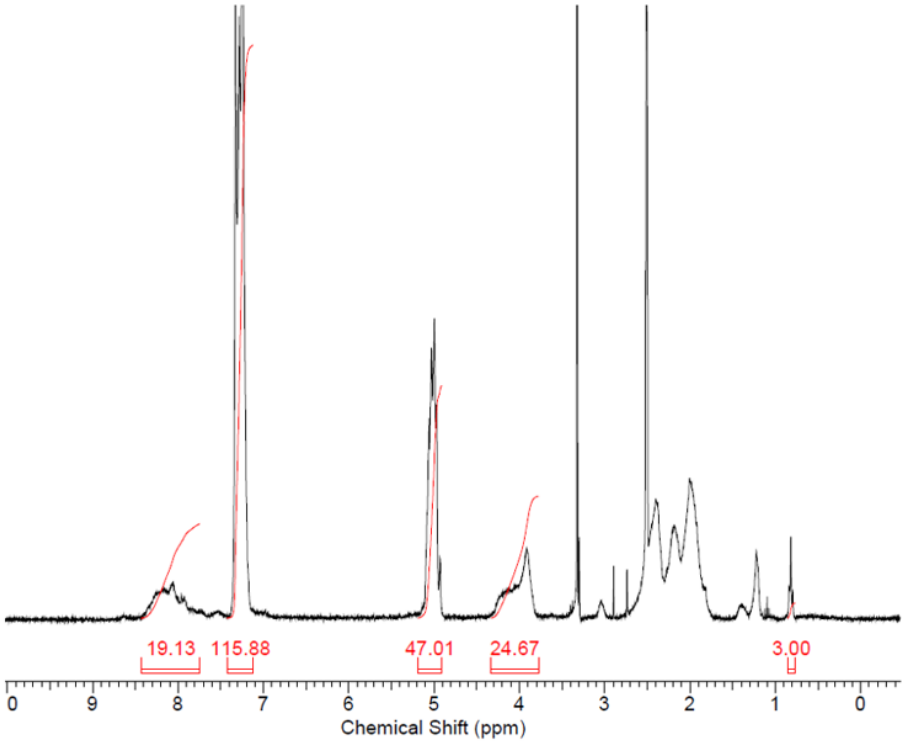

Figure 3.14 ^{1}H NMR spectrum for linear PBG serving as substrate for the G0PBG synthesis.

The acetamide moiety formed by reaction of the amine chain end of PBG with acetic anhydride is difficult to distinguish in the ^{1}H NMR spectrum, as the acyl proton signal around 2 ppm overlaps with the methylene proton resonances in the aminohexyl end group. To confirm the successful deactivation of the terminal amine, ^{19}F NMR analysis was used to determine residual amine functionality in the polymer sample after the reaction, as described in **Section 2.17**. A sample ^{19}F NMR spectrum provided in **Figure 3.15** has no resonance signal near -61.3 ppm corresponding to imine formation. This indicates clearly that no residual amine groups were present in the PBG substrate, and therefore that the chain-end amine groups were successfully deactivated.

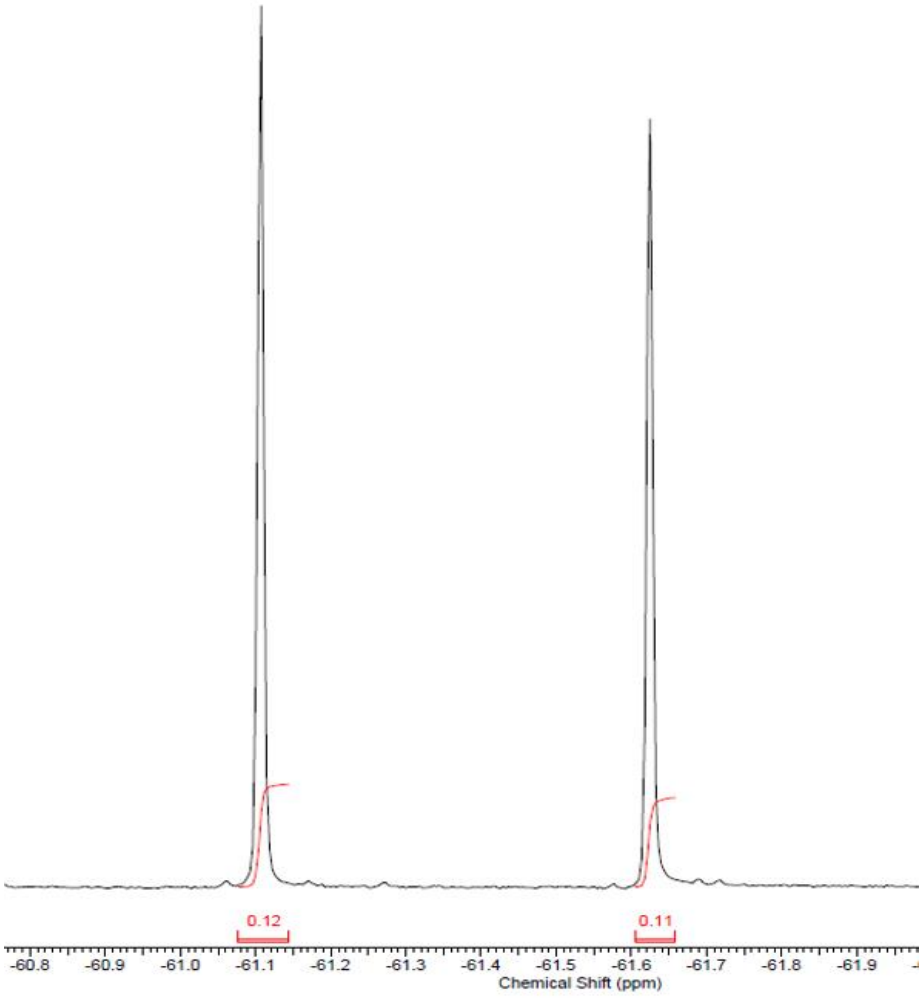

Figure 3.15 ^{19}F NMR amine functionality analysis of linear PBG substrate deactivated with acetic anhydride.

3.7 Partial Deprotection of Linear PBG Serving as Substrate

To create coupling sites for the synthesis of arborescent polymers, a fraction of the benzylic protecting groups on the glutamic acid units needed to be removed to generate free carboxylic acid groups. This was achieved with a hydrobromic acid (HBr) solution in acetic acid.[117] The

deprotection level was controlled by the amount of HBr added. A reaction scheme for the deprotections of the PBG chains with a deactivated amine group is provided in **Scheme 3.13**.

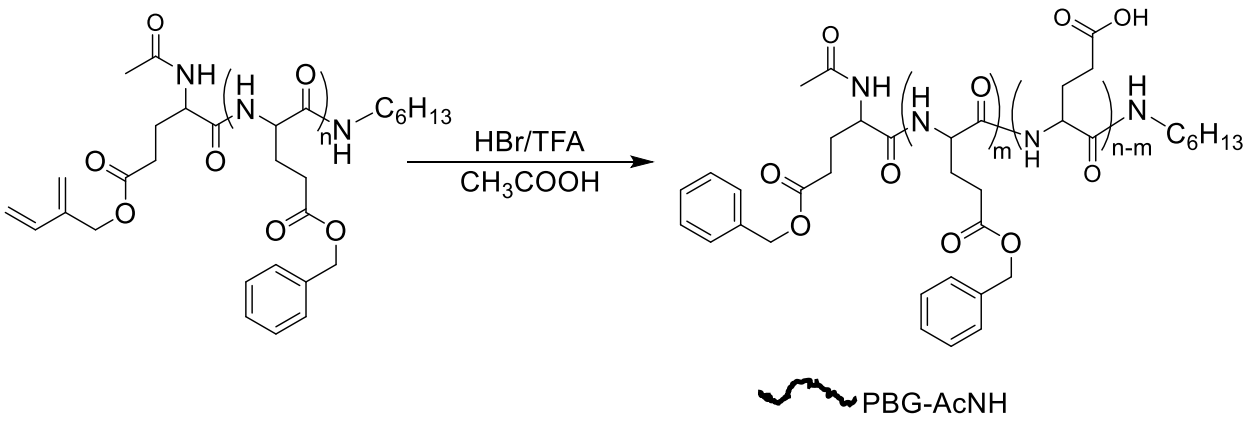

Scheme 3.13 Partial deprotection of PBG with a deactivated amine chain end.

The deprotection reaction was allowed to proceed for three hours before precipitation twice in diethyl ether. The fraction of free carboxylic acid groups in the product was determined by ^{1}H NMR analysis, from the relative integrals for the methine protons on the polymer backbone and the benzylic methylene protons. For the spectrum shown in **Figure 3.16**, the deprotection level was calculated as:

$$\%\ Deprotected = 100\ \% - \left(\frac{Integral\ of\ benzylic\ protons}{integral\ of\ methine\ protons \times 2}\right)$$

$$\%\ Deprotected = 100\ \% - \left(\frac{29.2}{23.0 \times 2}\right) = 36.6\ \%$$

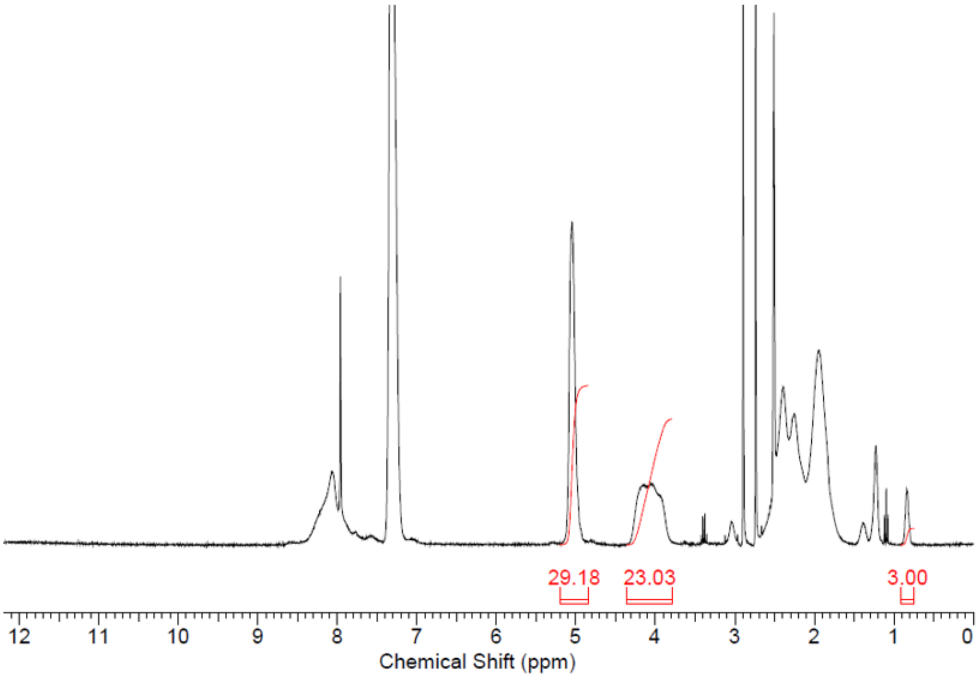

Figure 3.16 ^{1}H NMR spectrum for partially deprotected linear PBG.

3.8 Synthesis of Arborescent G0PBG

The arborescent G0PBG sample was synthesized by grafting PBG side chains containing an amine terminus onto the PBG substrate with carboxylic acid moieties, to create a comb-branched structure. This requires the formation of a peptide bond, promoted by peptide coupling agents. DIC and HOBt, reported to be efficient peptide coupling agents for PBG,[118,100] were used for this reaction. The carbodiimide reagent DIC activates the carboxyl groups on PBG by forming an *O*-acylisourea. This urea derivative acts as a good leaving group, allowing the amine-terminated PBG to attack the carbonyl bond and generate a peptide bond (**Scheme 3.14**). Unfortunately, the *O*-acylisourea is also susceptible to an intramolecular rearrangement to form an *N*-isourea (**Scheme 3.15**). This side product cannot form a peptide bond with a PBG side chain, and therefore

limits the efficiency of the coupling reaction. For this reason, HOBt was used as a peptide coupling additive that reacts with the *O*-acylisourea to form a species less susceptible to isomerization, thereby allowing more efficient peptide coupling. TEA was also added in the coupling reaction, as a base to deprotonate any protonated terminal amine groups potentially present, which would also limit the efficiency of the grafting reaction.

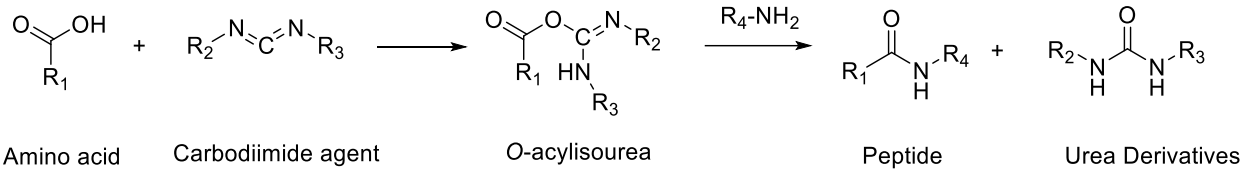

Scheme 3.14 Peptide coupling reactions with a carbodiimide coupling agent.

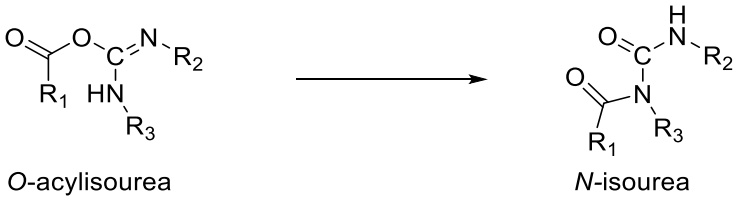

Scheme 3.15 Intramolecular rearrangement of *O*-acylisourea.

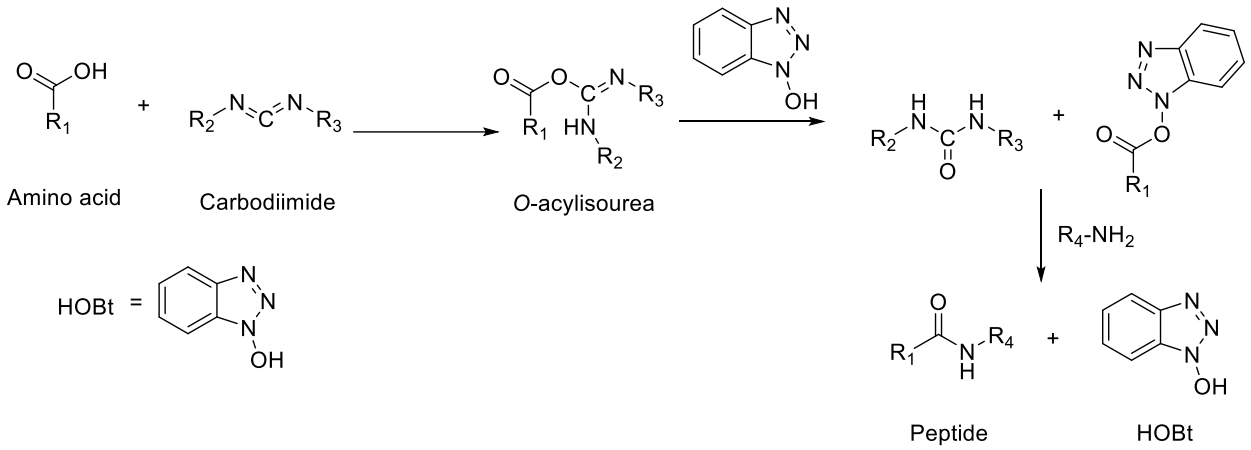

Scheme 3.16 Peptide coupling reaction with HOBt.

The overall reaction for the synthesis of G0PBG with DIC and HOBt as peptide coupling agents is shown in **Scheme 3.17**. The reaction was carried out in dry DMSO, using a 5:1 molar ratio of peptide coupling agents to –COOH units, so as to maximize the efficiency of the grafting reaction. To the same end, a 1.5:1 molar ratio of COOH:NH_2 was used.[100]

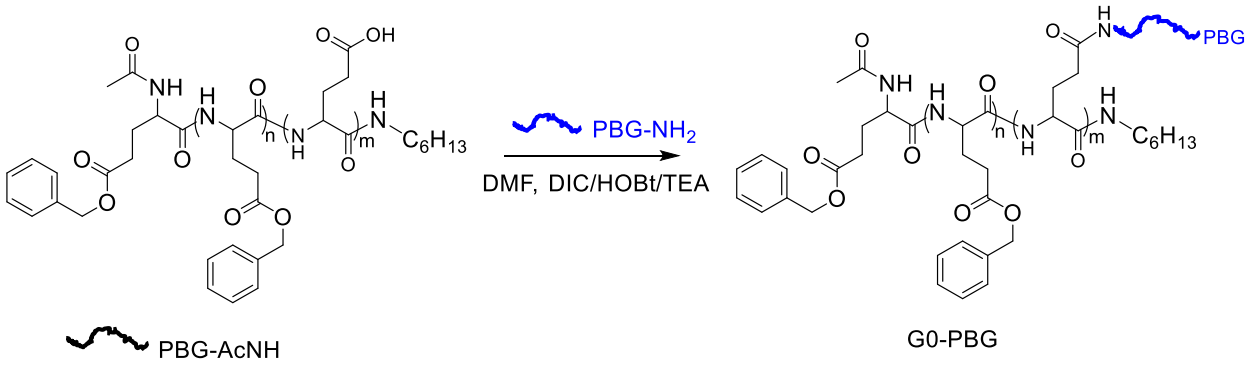

Scheme 3.17 Synthesis for G0PBG with DIC/HOBt as peptide coupling agents.

After 4 days, a small aliquot of the reaction solution was sampled for SEC analysis. SEC traces for the crude arborescent G0 polymer and the linear PBG side chain are compared in **Figure 3.17**. Two species can be observed in the SEC trace: The SEC peak at an elution volume of 17.5 mL corresponds to the graft polymer, while the peak at 18.5 mL is for unreacted PBG side chains.

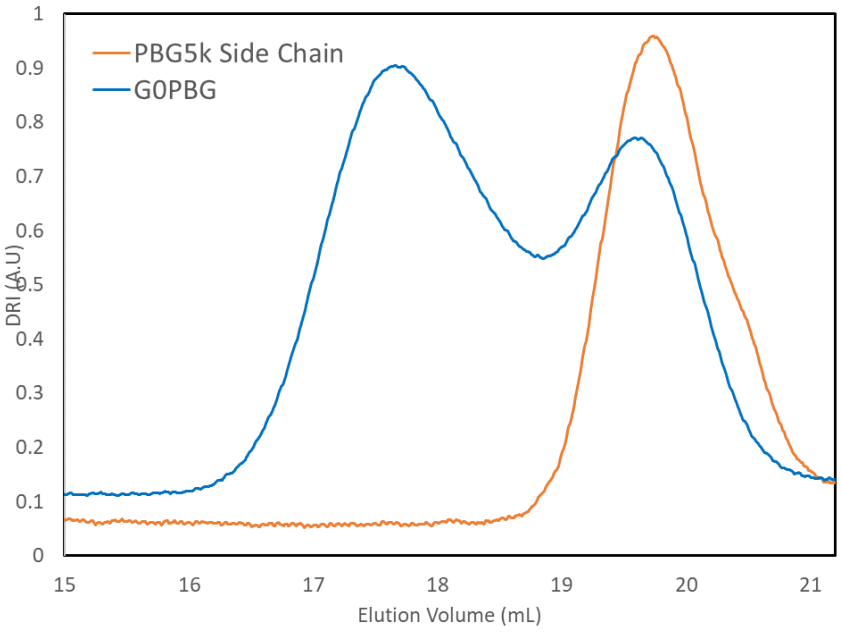

Figure 3.17 Comparison of SEC traces for G0PBG and PBG side chain material.

The crude G0PBG sample needed to be purified to remove unreacted side chains before the next grafting cycle. Since both the arborescent G0PBG and the linear PBG side chains contain BzGlu units, it would be difficult to remove unreacted PBGs chains by precipitation fractionation. Therefore, the side chain material was removed by preparative SEC. Traces obtained for purified and crude G0PBG samples are compared in **Figure 3.18**. It is clear that the purified product was

free of residual linear polymer. The purified G0PBG sample had an apparent $M_n = 5.1 \times 10^4$ g/mol and a narrow molecular weight distribution ($M_w/M_n = 1.08$).

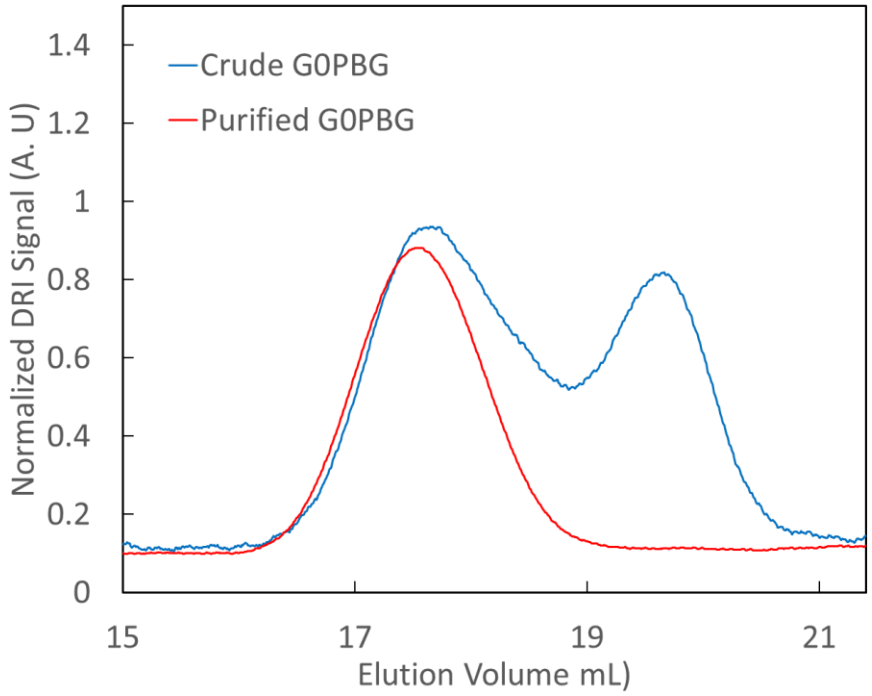

Figure 3.18 Comparison of SEC traces for crude and purified G0PBG.

For linear polymers, the absolute number-average molecular weight can be determined by NMR analysis from the relative intensities of NMR resonance signals from the structural units and the end groups. This is not possible for arborescent polymers, since more than one end group is present in each molecule. The absolute M_n of G0PBG was rather determined by SEC-MALLS analysis in DMSO, and found to be 3.3×10^4 g/mol. From this value the number-average branching functionality (f_n), defined as the number of side chains grafted onto the polymer

substrate, was calculated using the absolute M_n of the substrate, the side chains and the graft polymer:

$$f_n = \frac{M_{\mathrm{n}}\ of\ graft\ polymer - M_{\mathrm{n}}\ of\ substrate}{M_{\mathrm{n}}\ of\ side\ chains} = \frac{3.3 \times 10^4 \frac{\mathrm{g}}{\mathrm{mol}} - 4390 \frac{\mathrm{g}}{\mathrm{mol}}}{6550 \frac{g}{mol}} = 4.3$$

The efficiency of the coupling reaction was quantified with two parameters, namely the grafting yield and the coupling efficiency. The grafting yield is defined as the fraction of side chains successfully grafted onto the polymer substrate in the reaction. This can be calculated from the relative areas of the SEC peaks for the graft polymer and the unreacted side chains. It is clear from the SEC trace shown in **Figure 3.17** that the peaks corresponding to G0PBG and the linear PBG side chains overlap strongly, which limits the accuracy of such calculations. Approximating the peak areas by drawing a vertical line in the valley between the two peaks, peak areas of 213 and 136 arbitrary units were obtained for the graft polymer and the side chains, respectively. The weight fraction of the substrate in the graft polymer was 4390 / 33000 = 13.3%. The grafting yield was then calculated as (213 × (1 - 0.133) / (213 × (1 - 0.133) + 136) = 58 %. The coupling efficiency is defined as the fraction of coupling sites consumed on the substrate. For the G0PBG sample, an average of 4.3 polymer side chains were grafted onto a polymer substrate containing 8.4 free carboxylic acid groups, yielding a coupling efficiency of (4.3 / 8.4) = 51 %.

3.9 Synthesis of Higher Generation Arborescent Polymers

An arborescent G1PBG sample was prepared by synthesis and purification methods similar to G0PBG. The G0PBG and G1PBG samples were then partially deprotected, and grafted with

PZLys chains to obtain G0PBG-*g*-PZLys and G1PBG-*g*-PZLys, respectively. An example of a reaction for the synthesis of G0PBG-*g*-PZLys is provided in **Scheme 3.18**. For all the grafting reactions, the substrates were partially deprotected to generate 20 –30 % of free carboxylic acid moieties, and the coupling reactions were performed at a COOH:NH_2 molar ratio of 1.15:1. Molar ratios of 5:1 were used for the coupling agents (DIC and HOBt) and TEA to COOH moieties on the substrate for all the grafting reactions. The molecular weight of the side chains used, as well as substrate molecular weight, deprotection level, and number of COOH units are summarized in **Table 3.1**. The branching functionality, grafting yield, and coupling efficiency, determined similarly to G0PBG, are provided in **Table 3.2**.

Table 3.1 Deprotection level of substrates and molecular weight of side chains used to prepare PBG and PZLys polypeptides.

Polymer Sample	Substrate M_n	Substrate Deprotection %	Substrate COOH Units	Side Chain M_n
G0PBG	4.4×10^3	44	8.4	6.5×10^3
G0PBG-*g*-PZLys	3.0×10^4	21	31	5.5×10^3
G1PBG	3.0×10^4	21	31	5.5×10^3
G1PBG-*g*-PZLys	1.1×10^5	30	167	4.7×10^3

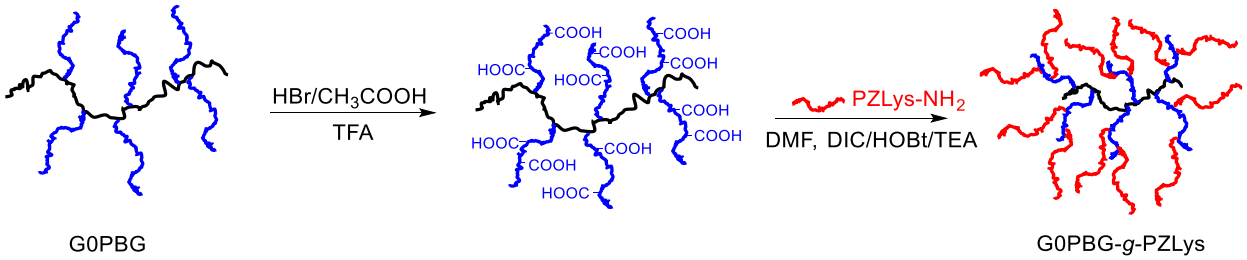

Scheme 3.18 Synthesis of G0PBG-*g*-PZLys.

Table 3.2 Characteristics of arborescent polypeptides and copolypeptides of PBG and PLys.

Polymer Sample	M_n	M_w/M_n	f_n	Coupling Efficiency (%)	Grafting Yield (%)
Linear PBG	5.5×10^3	1.07	--	--	
G0PBG	3.3×10^4	1.08	4.2	51	58
G0PBG-*g*-PZLys	1.2×10^5	1.09	16.3	52	46
G1PBG	1.2×10^5	1.07	16.6	53	37
G1PBG-*g*-PZLys	4.7×10^5	1.07	76.6	46	38

As seen in **Table 3.2**, the molecular weight of the arborescent polymers increased rapidly over successive generations, and narrow molecular weight distributions (M_w/M_n < 1.10) were maintained for all the samples. Correspondingly, the higher generation polymers eluted at significantly lower elution volumes than the lower generation polymers, as shown in **Figure 3.19**.

The higher generation arborescent polymers also had higher branching functionalities as expected, due to the larger number of coupling sites created on the substrates serving in their synthesis. The grafting yield was found to be lower for the higher generation structures, which is attributed to greater steric hindrance due to the highly branched structure of arborescent polymers.[97] The coupling efficiency also decreased for sample G1PBG-*g*-PZLys for similar reasons, albeit the variations in coupling efficiency over successive generations are not as pronounced as for the grafting yield. The coupling efficiency was lower for G0PBG, likely because a 1.5:1 molar ratio of COOH:NH_2 was used in the grafting reaction, so as to maximize the grafting yield. As a result, the maximum coupling efficiency for G0PBG would have been 67% if all the side chains were grafted (Grafting yield = 100%).

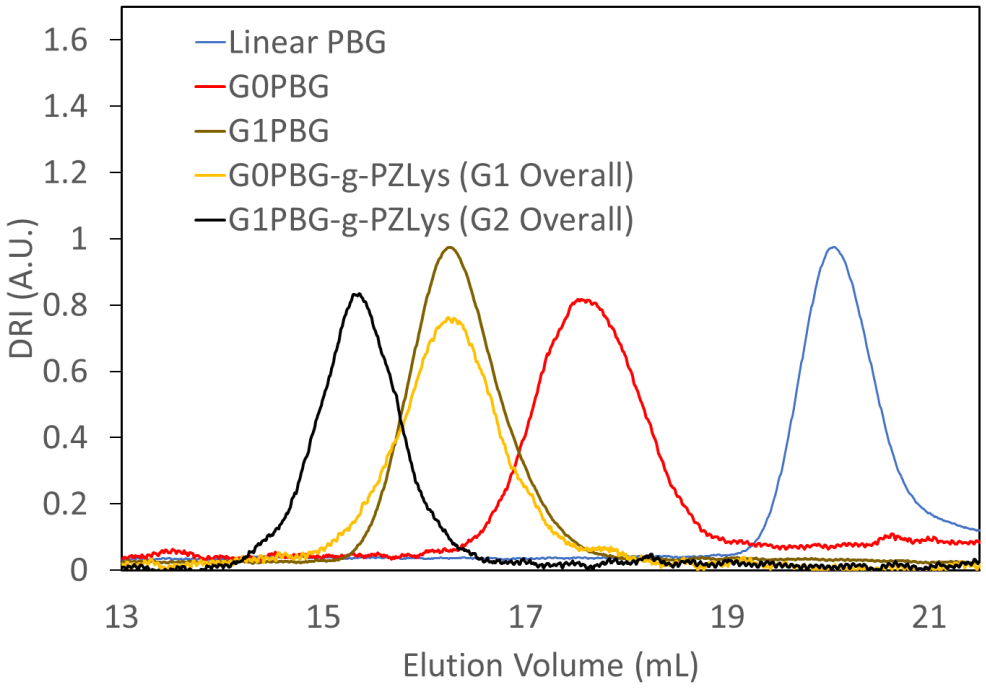

Figure 3.19 SEC traces for linear PBG and the different arborescent polymers synthesized.

3.10 Deprotection of G0PBG-*g*-PZLys and G1PBG-*g*-PZLys

The arborescent copolymers G0PBG-*g*-PZLys and G1PBG-*g*-PZLys needed to be deprotected to generate free amine groups on the lysine units and allow grafting of the PEO segments forming a shell. The benzyloxycarbonyl (Z) protecting groups on PZLys were cleaved with a large excess of HBr solution in acetic acid (**Scheme 3.19**).[117] ^{1}H NMR spectra for G0PBG-*g*-PZLys (before deprotection) and G0PBG-*g*-PLys (after deprotection) are compared in **Figure 3.20**. No resonance signal corresponding to the aromatic protons of the carbobenzoxy groups (7.0–7.5 ppm) or the benzylic methylene protons (4.7–5.1 ppm) are observed for G0PBG-*g*-PLys, confirming the full deprotection of the PZLys chains.

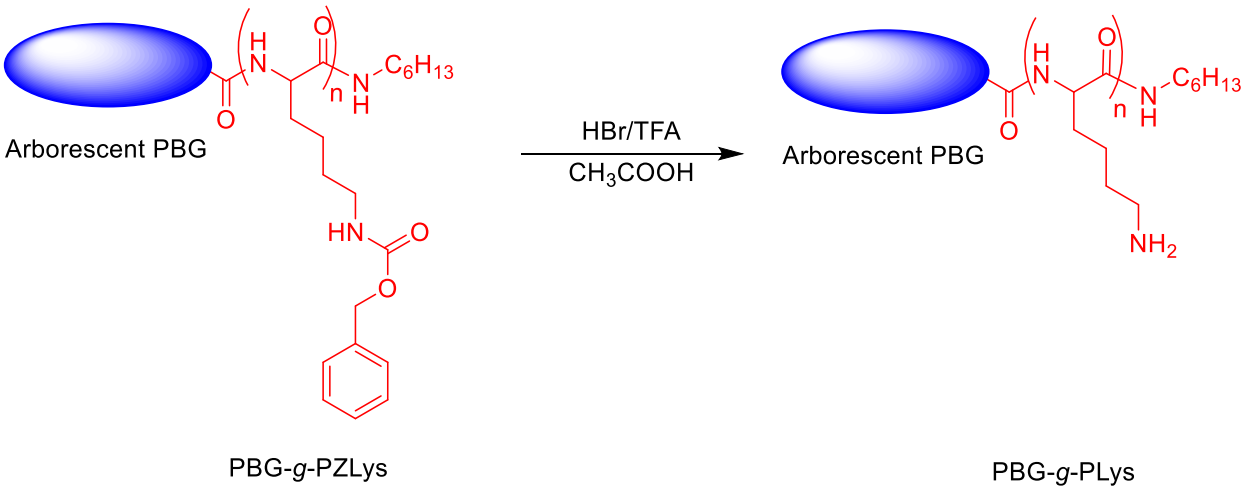

Scheme 3.19 Deprotection of arborescent PBG-*g*-PZLys.

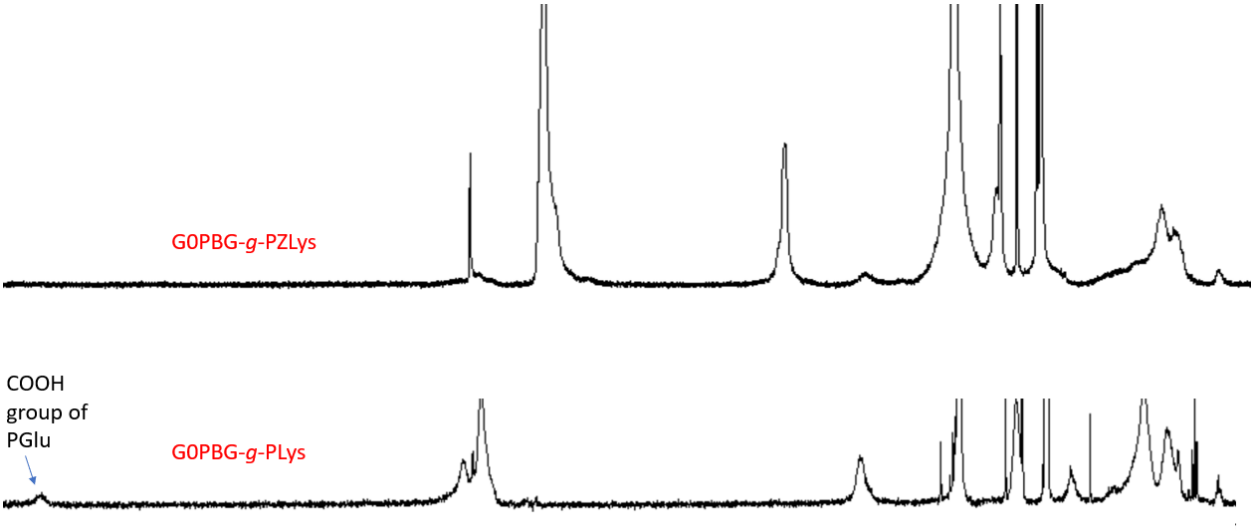

Figure 3.20 Comparison of ^{1}H NMR spectra for Z-protected G0PBG-*g*-PZLys (top) and deprotected G0PBG-*g*-PLys (bottom).

However, NMR signals for aromatic protons corresponding to the benzyl protecting groups inside the PBG core were likewise absent, indicating that these were cleaved as well. This inadvertent deprotection was further supported by the resonance signals near 12.1 ppm, corresponding to the carboxylic acid protons on the PBG units. This is because the reaction conditions used for the deprotection for the Z groups of PZLys were identical with those used to remove the benzyl protecting groups of PBG. Lysine with a different type of side-chain protecting groups could be used in the future to prepare the PLys chains, such that removal of the protecting groups on PZLys does not affect the benzylic groups of PBG. Potential protecting groups to achieve this include Boc, which can be deprotected using a 25% - 50 % TFA solution in

DCM,[119,120] and Fmoc, which can be removed using a 25% piperidine solution in DMF.[121] The benzylic groups are stable under such conditions.

To minimize the deprotection of benzylic units inside the PBG core, a lower stoichiometric amount of HBr was used in the deprotection of G1PBG-*g*-PZLys. NMR spectra for G1PBG-*g*-PLys and G1PBG-*g*-PLys are compared in **Figure 3.21**. Resonance signals for the aromatic protons in the protecting groups can be found near 7.19 to 7.50 ppm, which indicates that a fraction of the Z and benzylic protecting groups remained on the polymer. The deprotection level can be calculated using the relative integration values for the methine proton signals and the benzylic protons signals (from both PBG and ZLys units):

$$Deprotection\ \% = 1 - \frac{integration\ of\ benzylic\ protons\ /\#\ of\ protons}{integration\ of\ methine\ protons/\#\ of\ protons}$$

$$Deprotection\ \% = 1 - \frac{4.15/2}{10.00/1} = 79.3\ \%$$

This is approximately equal to the fraction of PZLys units in the arborescent structure G1PBG-*g*-PZLys. Based on information provided in **Table 3.1** and **Table 3.2**, G1PBG-*g*-PZLys contained approximately 3.6×10^5 Da of ZLys units, which corresponds to 1374 ZLys units per molecule. The BzGlu and Glu units account for 1.1×10^5 Da in the partially deprotected G1PBG substrate. Since a deprotection level of 30% was used for the synthesis of G1PBG-*g*-PZLys, the average molecular weight of the BzGlu and Glu repeating units was calculated as (219 × 0.7 + 129 × 0.3) = 192 Da. The average number of BzGlu units per G1PBG substrate molecule was calculated as 1.1×10^5 Da / 192 Da = 572 units. Therefore, the fraction of PZLys repeating units in G1PBG-*g*-PZLys was approximately 1374 / (1374 + 572) = 71%. Furthermore, in **Figure 3.21**,

no resonance peaks corresponding to the free carboxylic acid groups could be observed near 12 ppm. This suggests that deprotection of the benzylic groups in the interior core of the micelles was insignificant. Since the deprotection level was close to the fraction of ZLys repeating units in G1PBG-*g*-PZLys, and no significant deprotection of the benzylic protecting groups of PBG occurred based on NMR analysis, it was concluded that the majority of the Z groups on PZLys were successfully removed under the modified conditions using a decreased amount of HBr.

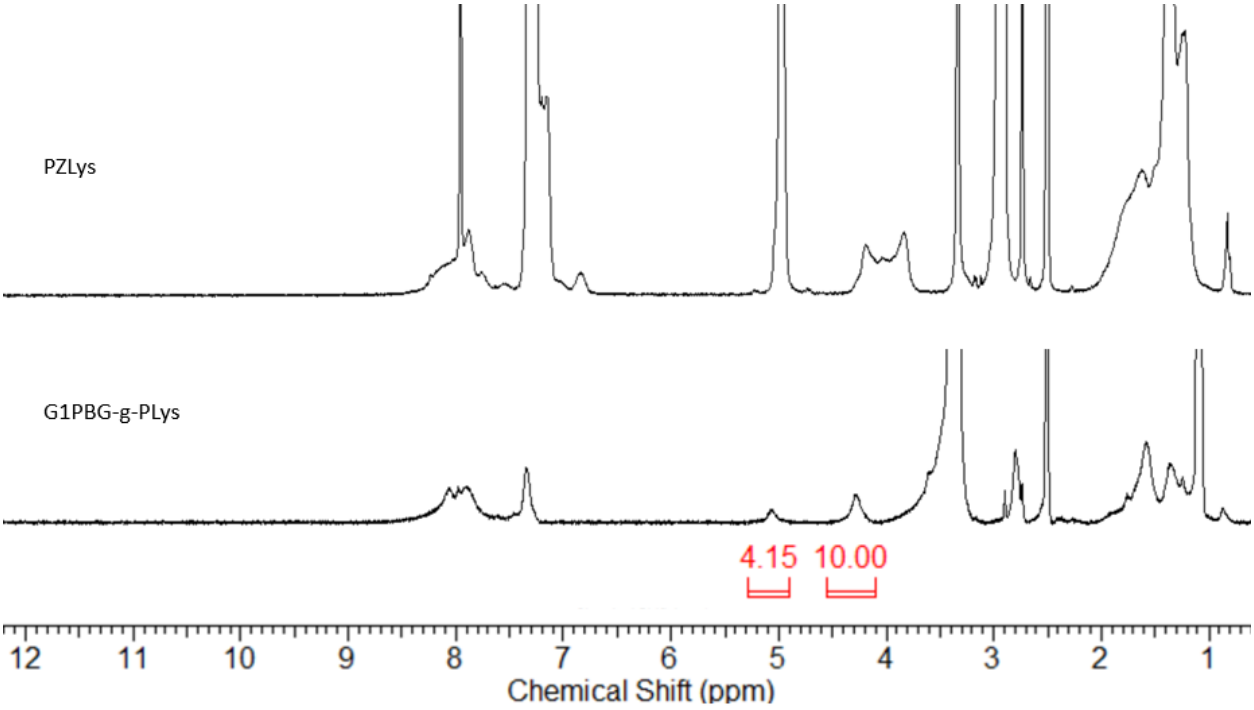

Figure 3.21 Comparison of ^{1}H NMR spectra for PZLys (top) and deprotected G1PBG-*g*-PLys (bottom).

3.11 Synthesis of Model Imines Using Small-molecule Amines

To determine the characteristics of imine products formed between a primary amine and an aldehyde, hexylamine was used as a model small molecule to investigate the efficiency of imine formation. Hexylamine was mixed with either TFBA or PEG-Bz-CHO in DMSO to prepare the corresponding imine products, as shown in **Scheme 3.20**. The NMR spectra for $HexNH_2$-imi-PEG and $HexNH_2$-imi-TFBA are provided in **Figure 3.22** and **Figure 3.23**, respectively.

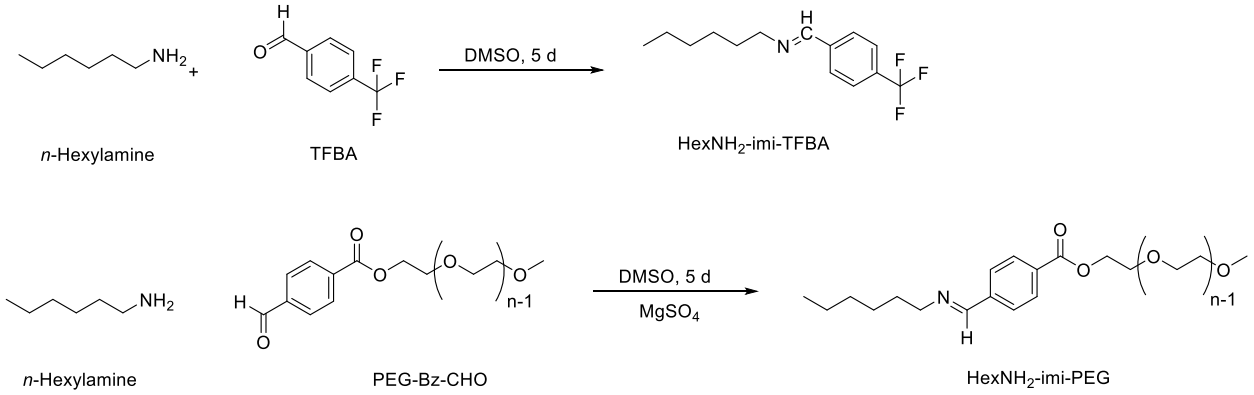

Scheme 3.20 Synthesis of model imine products $HexNH_2$-imi-TFBA and $HexNH_2$-imi-PEG.

In **Figure 3.22**, the resonance signals from the aromatic protons of TFBA shifted from 7.96 and 8.07 ppm to 7.77 and 7.93 ppm. A new resonance appearing at 8.42 ppm was assigned to the -C*H*N- proton of the imine group, while the aldehyde resonance peak at 10.09 ppm in the spectrum of TFBA vanished in the spectrum obtained for the imine. In addition, the α- and β-protons of hexylamine shifted downfield from near 1.24 ppm (overlapping with the other methylene protons) to 1.61 ppm and 3.59 ppm, respectively, which further confirmed the successful formation of $HexNH_2$-imi-TFBA.

Similarly, NMR spectra for PEG-Bz-CHO and HexNH$_2$-imi-PEG are compared in **Figure 3.23**. The resonance signal for the aromatic groups shifted from 8.15 ppm and 8.08 ppm in PEG-Bz-CHO to 8.01 ppm and 7.89 ppm in HexNH$_2$-imi-PEG, respectively. A new resonance signal also appeared at 8.42 ppm, which was assigned to the -C*H*N- proton of the imine group, while the aldehyde resonance peak at 10.09 ppm for PEG-Bz-CHO vanished. In addition, the protons of PEG-Bz-CHO α- to the aromatic ring shifted slightly upfield from 4.44 ppm to 4.41 ppm. These results suggest that the imine product was successfully prepared from PEG-Bz-CHO and hexylamine, and that a resonance signal for the α-proton of benzylimine can be expected near 8.44 ppm in DMSO.

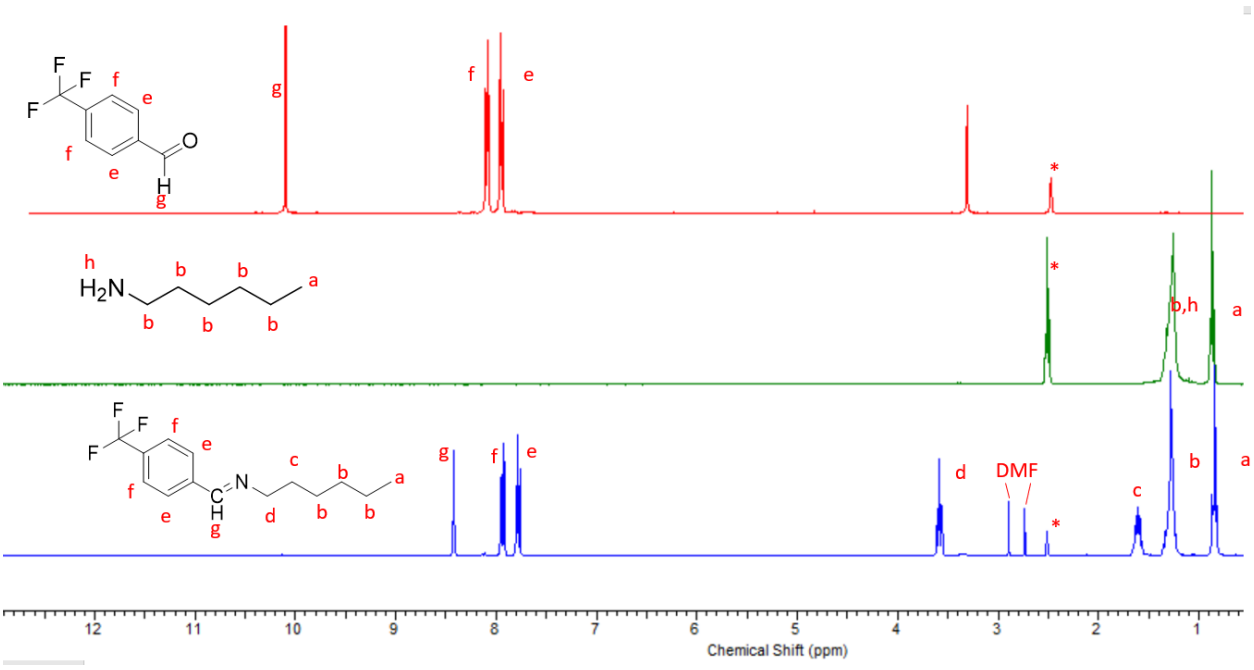

Figure 3.22 Comparison of NMR spectra for TFBA, hexylamine and HexNH$_2$-imi-TFBA in DMSO-d_6.

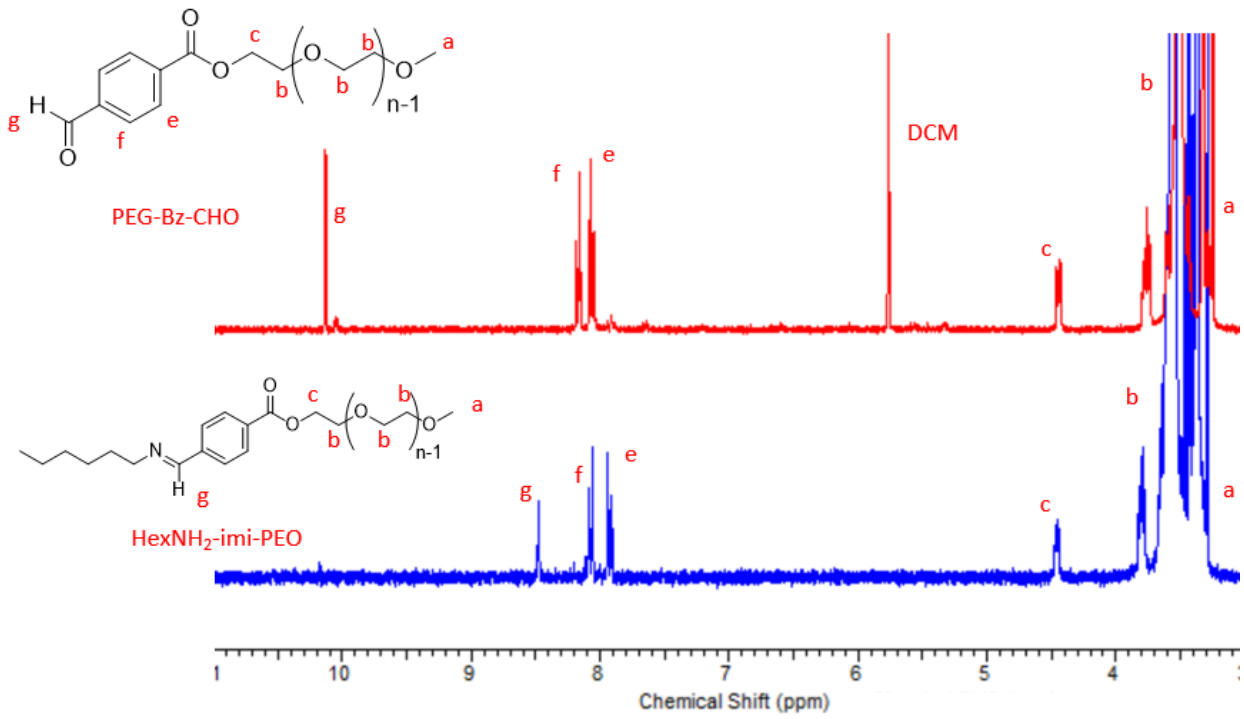

Figure 3.23 Comparison of NMR spectra for PEG-Bz-CHO, hexylamine and $HexNH_2$-imi-TFBA in DMSO-d_6.

3.12 Synthesis of PLys-*g*-PEG

Owing to the promising results obtained in the synthesis of $HexNH_2$-imi-PEG and $HexNH_2$-imi-TFBA, the preparation of PLys-*g*-PEG was performed under similar reaction conditions. The corresponding reaction scheme is shown in **Scheme 3.21** Synthesis of PLys-*g*-PEG. The structure contains a PLys backbone and PEG side chains grafted onto the PLys chains via imine bonds.

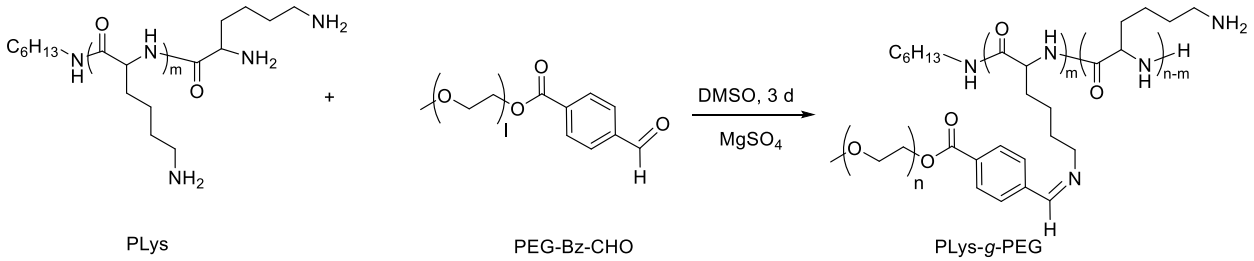

Scheme 3.21 Synthesis of PLys-*g*-PEG.

The NMR spectrum obtained for PLys-*g*-PEG is shown in **Figure 3.24**. The resonance signals from 1.18 – 1.89 ppm and near 2.79 ppm are assigned to the side chain methylene protons of PLys, while the signals from 3.16 – 3.83 ppm are for the methylene protons of the PEG chains, and the resonance near 4.43 ppm is attributed to the α-methylene protons of the PEG-Bz-CHO ester. Unfortunately, the aromatic proton signals from the aromatic aldehyde moiety in PEG overlaps with the side chain amine protons of PLys near 7.6 to 8.2 ppm. The sharp resonance peak at 10.11 ppm is from the unreacted aldehyde.

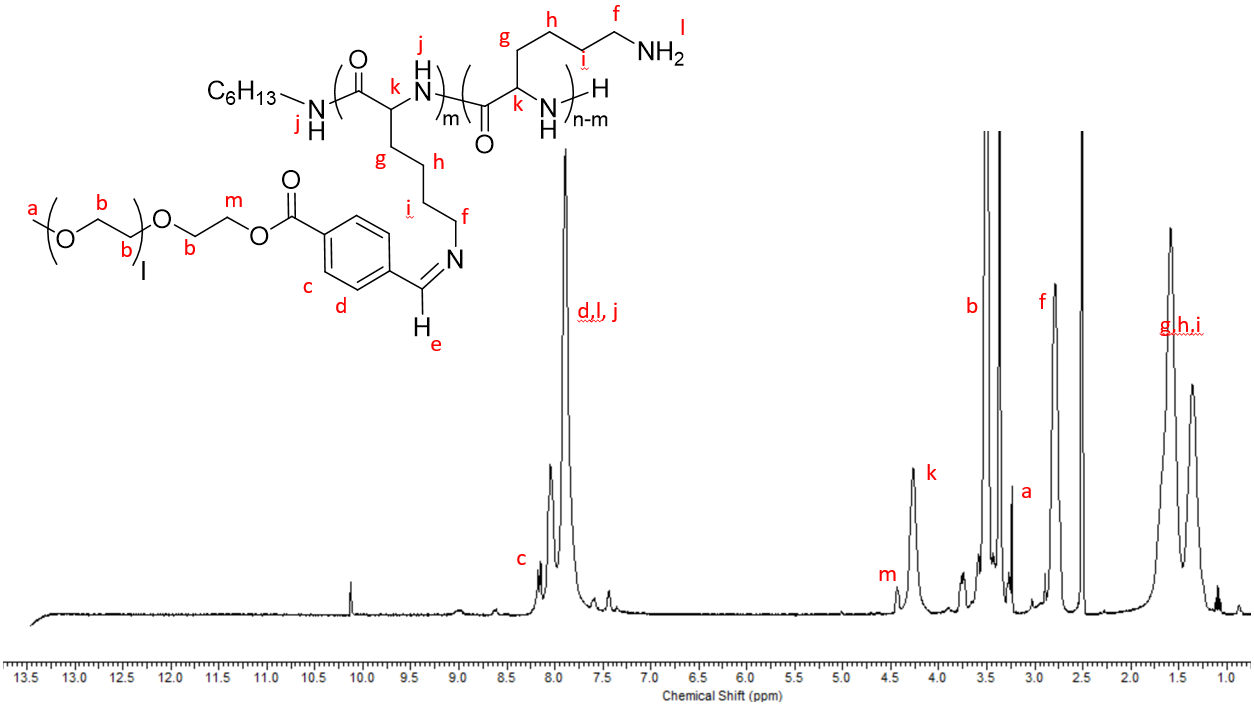

Figure 3.24 ^{1}H NMR spectrum for PLys-*g*-PEG in DMSO-d_6.

Imine formation with PLys-*g*-PEG was monitored by NMR analysis throughout the reaction (**Figure 3.25**). The amounts of imine product formed and unreacted aldehyde were determined from the spectra. After the reaction was allowed to proceed for 3 d, no signal corresponding to an imine proton was observed near 8.5 ppm (**Figure 3.25a**). Since water is a by-product of imine formation, $MgSO_4$ was added to the reaction mixture to remove water and drive the reaction to the desired product. After continuing stirring of the reaction mixture for 2 d, a new NMR resonance signal was observed at 8.48 ppm (**Figure 3.25b**). This is approximately the same chemical shift observed for the imine protons of HexNH_2-*g*-TFBA and HexNH_2-*g*-PEG (8.42 – 8.44 ppm) in **Section 3.11**. The amount of imine formed was quantified using the integration areas

for resonance signals of the imine and the α-methylene protons of the benzyl ester. For example, the fraction of imine products was determined from **Figure 3.25c** as follows:

$$\%\ imine = \frac{integration\ of\ imine\ proton}{\#\ of\ protons} \times \frac{integration\ of\ \alpha - proton\ of\ ester}{\#\ of\ protons}$$

$$\%\ imine = \frac{0.24}{1} \times \frac{2.00}{2} = 24\ \%$$

Therefore, when linear PLys chains were used as substrate, only 24 % of the PEG-Bz-CHO chains were grafted even after $MgSO_4$ was added to the reaction to drive it in the forward direction. The yield of PLys-*g*-PEG was significantly lower than for the $HexNH_2$-imi-PEG synthesis discussed earlier, for which almost quantitative yield was achieved without removal of the water by-product.

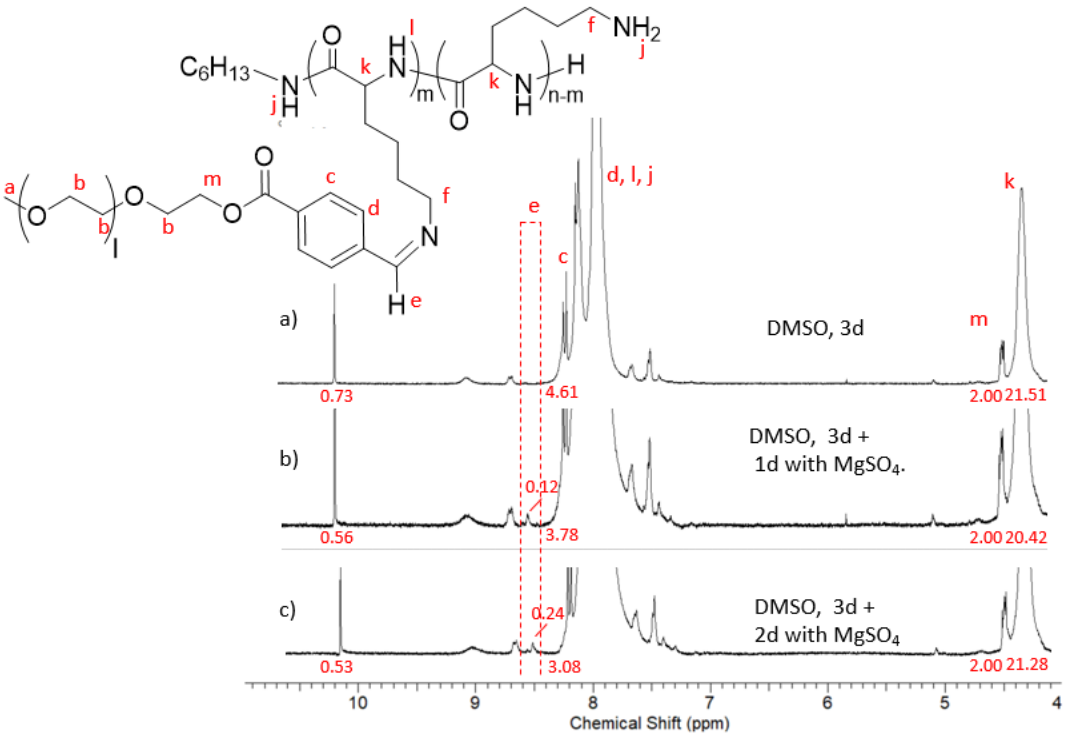

Figure 3.25 ^{1}H NMR spectra for PLys-*g*-PEG at different reaction times.

3.13 Synthesis of G0PBG-*g*-PLys-*g*-PEG and G1PBG-*g*-PLys-*g*-PEG

Attempts were also made to graft the aldehyde-terminated PEG chains onto G0PBG-*g*-PLys and G1PBG-*g*-PLys via the free amine groups on the PLys side chains. These should form pH-sensitive imine bonds with the aldehyde functionalities of PEG-Bz-CHO as shown in **Scheme 3.22**.

The synthesis of G0PBG-*g*-PLys-*g*-PEG was performed by a method similar to the model imines using small-molecule amines and the linear PLys chains. The ^{1}H NMR spectrum obtained for G0PBG-*g*-PLys-*g*-PEG (**Figure 3.26**) was similar to that of PLys-*g*-PEG.

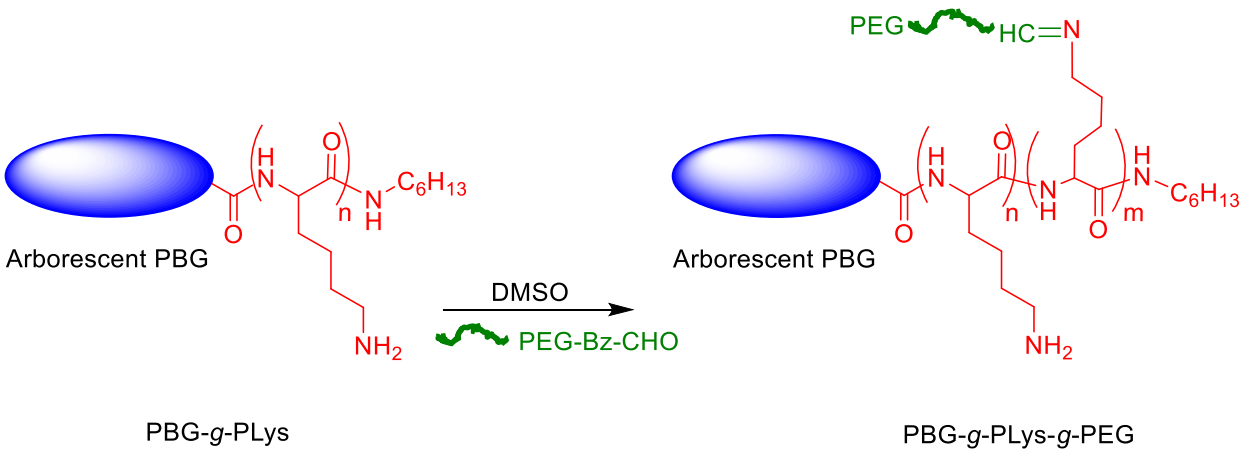

Scheme 3.22 Grafting of aldehyde-terminated PEG chains onto G0PBG-*g*-PLys and G1PBG-*g*-PLys via a pH-sensitive imine bond.

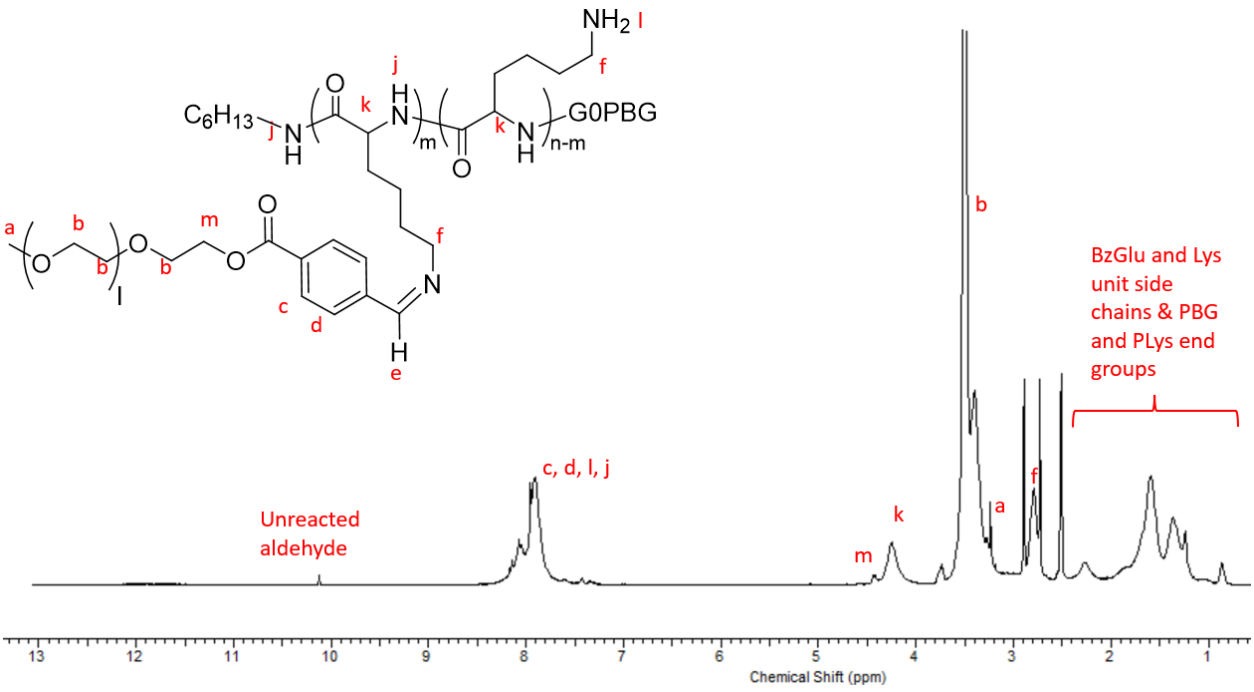

Figure 3.26 ^{1}H NMR spectrum for G0PBG-*g*-PLys-*g*-PEG.

Imine formation for G0PBG-*g*-PLys-*g*-PEG was monitored by NMR spectroscopy at different reaction times (**Figure 3.27**). The resonance signals between 8.00 and 8.20 ppm, attributed to the aromatic protons of unreacted PEG-Bz-CHO, became gradually less distinct as the reaction proceeded. By setting the integration area of the signal for the α-methylene protons of the benzoic ester near 4.5 ppm to 2.00, the aromatic signals of the unreacted PEG-Bz-CHO were integrated and normalized. The integrated areas for the aromatic proton signals in **Figure 3.27a-d** were found to be 25.0, 27.8, 18.8, and 17.6 units, respectively. This shows that some of the PEG-Bz-CHO was consumed after stirring with $MgSO_4$ and 4A molecular sieves overnight (**Figure 3.27c**), and that more reactants were consumed after stirring at 40 °C for 4 h (**Figure 3.27d**). Similarly, the aldehyde signals from unreacted PEG-Bz-CHO near 10.1 ppm in **Figure 3.27a-d** were found to be 0.70, 0.63, 0.42, and 0.41 units, respectively, likewise suggesting consumption of the aldehyde in the reaction. It should be noted that the signals for the α-methylene protons of

the benzoic acid ester overlapped with the methine protons of the Lys units, and the aromatic protons signal overlapped with the amine protons signal for the PLys side chains. Consequently, these integration values are very approximate and do not reflect the absolute PEG-Bz-CHO content in the reaction mixtures. To confirm the formation of the imine, the region from 7.5 to 8.5 ppm was expanded in **Figure 3.28** for clarity. It can be seen that an imine signal started appearing when the reaction mixture was stirred at room temperature with a combination of $MgSO_4$ and 4A molecular sieves overnight (**Figure 3.28c**), and that the signal intensity was slightly increased after heating at 40 °C for 4 h (**Figure 3.28d**). The amount of imine formed under these conditions nevertheless remained minimal. This is attributed to lower accessibility of the amine groups in the arborescent structures as compared to amines in small molecules and the linear PLys chains.

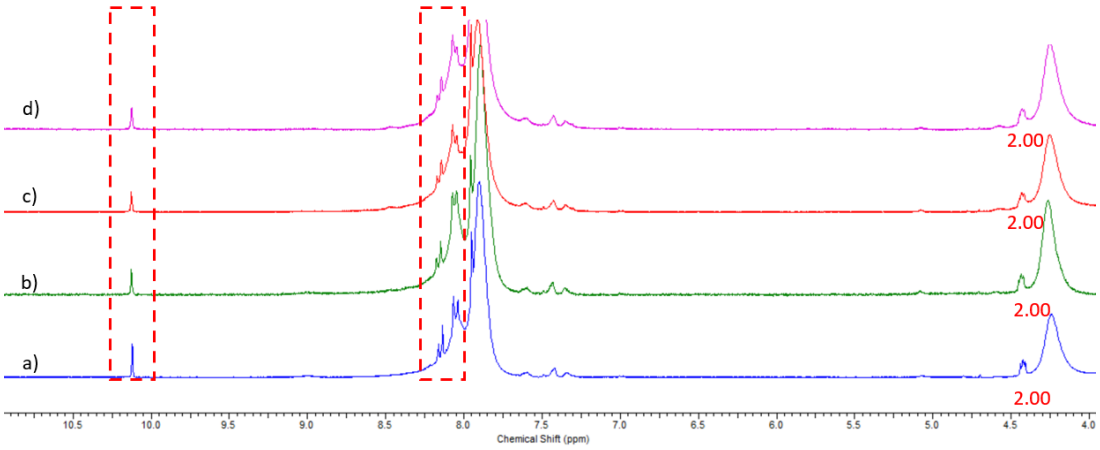

Figure 3.27 ^{1}H NMR spectra for G0PBG-*g*-PLys-*g*-PEG after a) stirring with $MgSO_4$ for 2 d; b) stirring with $MgSO_4$ for 2 d and then with 4A molecular sieves for 4 h; c) stirring with $MgSO_4$ for 2 d and then with 4A molecular sieves overnight; d) stirring with $MgSO_4$ for 2 d, with 4A molecular sieves overnight, and then heating to 40 °C for 4 h.

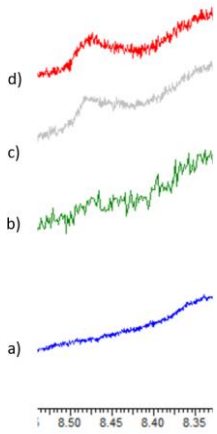

Figure 3.28 Zoomed ^{1}H NMR spectra near the chemical shift of the imine for G0PBG-*g*-PLys-*g*-PEG after a) stirring with $MgSO_4$ for 2 d; b) stirring with $MgSO_4$ for 2 d and then with 4A molecular sieves for 4 h; c) stirring with $MgSO_4$ for 2 d and then with 4A molecular sieves overnight; d) stirring with $MgSO_4$ for 2 d, with 4A molecular sieves overnight, and then heating to 40 °C for 4 h.

To prepare G1PBG-*g*-PLys-*g*-PEG, G1PBG-*g*-PLys and PEG-Bz-CHO were dissolved in DMSO, first stirred with $MgSO_4$ and 4A molecular sieves at room temperature, and then stirred at 40 °C for 4 h. The final NMR spectrum obtained for G1PBG-*g*-PLys-*g*-PEG is shown in **Figure 3.29**. The spectrum for G1PBG-*g*-PLys-*g*-PEG is similar to G0PBG-*g*-PLys-*g*-PEG, except for the benzylic and aromatic resonance signals near 7 – 7.5 ppm and 4.8 – 5.2 ppm, respectively. A more prominent signal for the imine proton in G1PBG-*g*-PLys as compared with G0PBG-*g*-PLys can also be found near 8.5 ppm. By setting the integration area for the α-methylene protons of the benzoic ester to 2.00, the relative integrations of the imine signals in G0PBG-*g*-PLys and G1PBG-*g*-PLys were found to be 0.29 and 0.61, respectively. This shows that imine formation in G1PBG-*g*-PLys was more efficient than in G0PBG-*g*-PLys. Enhanced imine formation in G1PBG-*g*-PLys could be due to the lower amount of carboxylate groups in the PBG core, potentially interfering

with the coupling reaction, or else to a higher local concentration of amine groups in the G1PBG-*g*-PLys substrate.

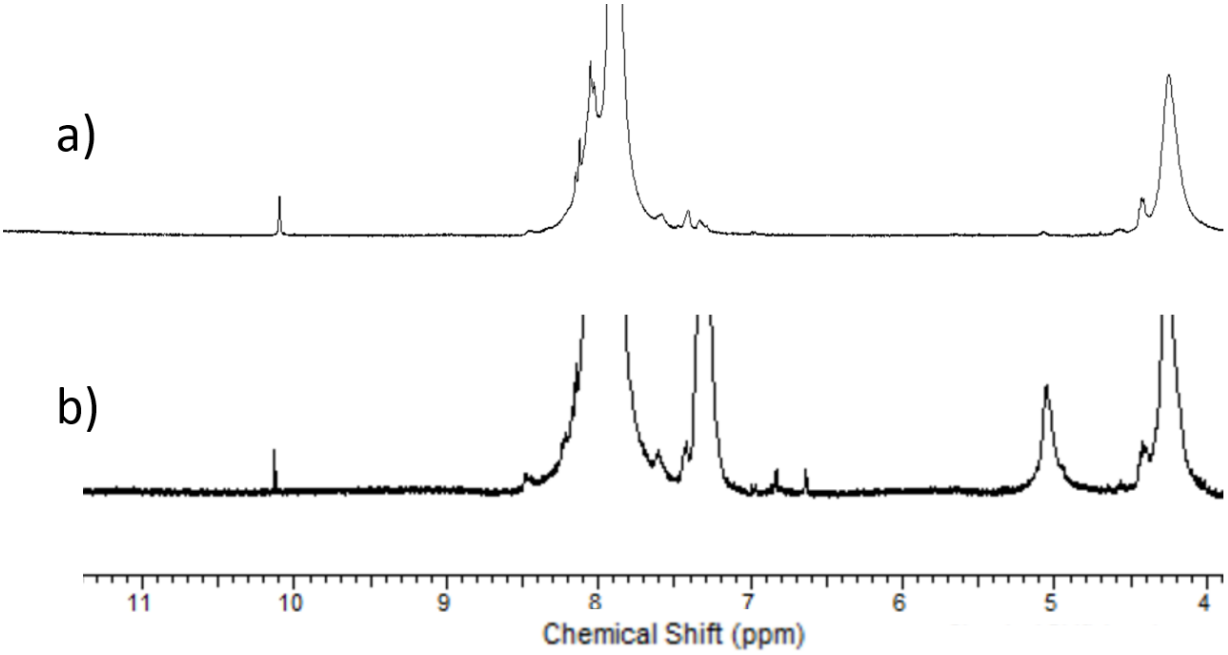

Figure 3.29 ^{1}H NMR spectra of a) G0PBG-*g*-PLys-*g*-PEG and b) G1PBG-*g*-PLys-*g*-PEG.

3.14 Size and Zeta Potential Measurements for the Arborescent Polymers

The arborescent copolymers G0PBG-*g*-PLys and G1PBG-*g*-PLys were analyzed by DLS to determine their size and zeta potential. Higher generation polymers are expected to have larger sizes. Positive zeta potential values are also expected for G0PBG-*g*-PLys and G1PBG-*g*-PLys, due to protonation of the amine groups on the lysine units. Conversely, grafting PEG chains onto the PLys-containing substrates would be expected to provide partial shielding of the charges on the protonated amine groups, and therefore a decrease in zeta potential.

Size and zeta potential measurements for G0PBG-*g*-PLys were first performed in deionized water and PBS, and the results obtained are summarized in **Table 3.3** and **Figure 3.30**. It should be noted that these measurements did not meet the data quality statistics standards of the Zetasizer software, so they are not considered very reliable and provided only for information. Large particles with a size around 100 nm were observed in both media, indicating the presence of aggregated species. Since the benzyl protecting groups in the PBG cores were also removed in the deprotection of PZLys, electrostatic interaction may have occurred not only between the anionic carboxyl groups of the PBG core and the cationic amine groups of the PZLys internal layer, but also intermolecularly, which would lead to aggregation. The results obtained in water suggest that more aggregation was present in that medium as compared with PBS, which makes sense because the salts in the PBS solution should partially shield the charges on the polymers, and thereby reduce the extent of intermolecular aggregation.

Table 3.3 Size and zeta potential of G0PBG-*g*-PLys in water and PBS.

Sample	D_h Number (nm)	D_h Volume (nm)	D_h Intensity (nm)	PDI	Zeta Potential (mV)
Water	81	89	97	0.27	+20
PBS	7.1	8.4	125	0.38	+15

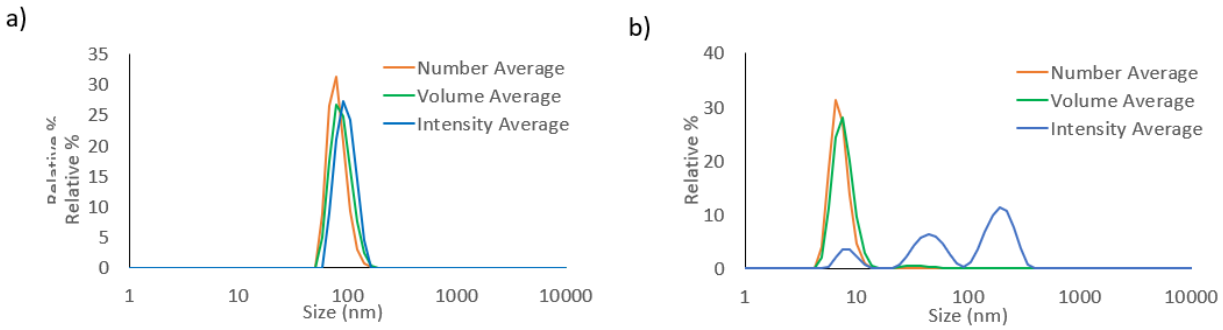

Figure 3.30 Size distributions for G0PBG-*g*-PLys in a) water and b) PBS.

The size data for G0PBG-*g*-PLys and G1PBG-*g*-PLys in PBS are compared in **Table 3.4** and **Figure 3.31**. As expected, the hydrodynamic diameters of G1PBG-*g*-PLys were higher than for G0PBG-*g*-PLys. It can also be seen in **Figure 3.31** that the extent of aggregation observed in the intensity distribution for G1PBG-*g*-PLys was significantly lower than for G0PBG-*g*-PLys, which indicates that G1PBG-*g*-PLys is less prone to aggregation as compared with G0PBG-*g*-PLys. This is also confirmed by the lower standard deviations (errors) in the number- and volume-average diameters for G1PBG-*g*-PLys over three measurements. The higher colloidal stability of G1PBG-*g*-PLys in PBS could be due to a majority of the BzGlu units in the micelle cores remaining protected, or at least isolated from the Lys units, which minimized electrostatic interactions between the carboxylic acids and the amines.

The zeta potential values for G0PBG-*g*-PLys and G1PBG-*g*-PLys are compared in **Table 3.4**. The zeta potential for G1PBG-*g*-PLys is significantly higher than for G0PBG-*g*-PLys, due to its larger number of amine groups at the periphery of the molecules. In addition, G0PBG-*g*-PLys

also contains a significant number of negatively charged carboxylate units inside the micelle cores, which may have partially decreased the surface charge of the micelles.

Table 3.4 Particle size and zeta potential comparisons for the arborescent copolymers in PBS.

Sample	D_h number	D_h volume	D_h intensity	PDI	Zeta Potential
G0PBG-*g*-PLys	8 ± 1	10 ± 2	120 ± 30	0.49	13 ± 3
G1PBG-*g*-PLys	14 ± 1	16 ± 1	160 ± 50	0.51	21 ± 1

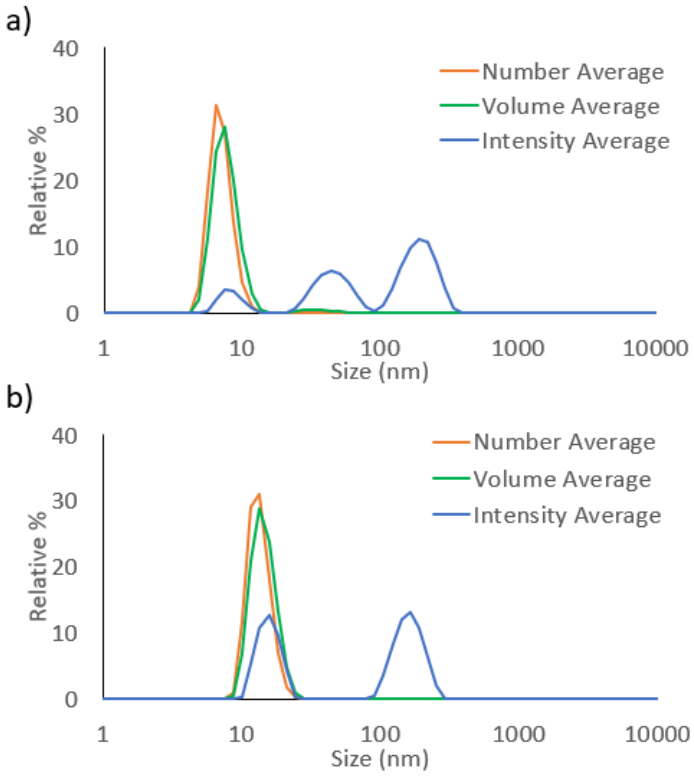

Figure 3.31 Size distributions for a) G0PBG-*g*-PLys and b) G1PBG-*g*-PLys in PBS.

In an attempt to further minimize electrostatic interactions and prevent aggregation of the arborescent molecules, size measurements were performed under acidic conditions to protonate the carboxyl groups in the PBG core. To this end, G0PBG-*g*-PLys was dissolved in different media containing HCl, and the size was determined by DLS analysis. When the polymer was dissolved in 20% v/v PBS (1:5 dilution relatively to the PBS stock solution) in 1 mM HCl, 20% v/v PBS in 10 mM HCl, and in 10 mM HCl, the sizing results were still very irreproducible. Somewhat more reliable (reproducible) results were obtained when using a 0.1 M HCl solution as dispersion medium, however. The results for the size and zeta potential measurements in 0.1 M HCl for G0PBG-*g*-PLys are summarized in **Table 3.5**.

Table 3.5 Particle size and zeta potential of G0PBG-*g*-PLys in 0.1 M HCl.

Sample	D_h Number	D_h Volume	D_h Intensity	PDI	Zeta-Potential
G0PBG-*g*-PLys	10.2 ± 0.9	12.2 ± 1.0	278 ±1530	0.58	+31 ± 3

The corresponding size distributions for G0PBG-*g*-PLys in 0.1 M HCl are provided in **Figure 3.32**. Some aggregated species with diameters greater than 100 nm were still observed in the intensity-weighted distributions, and the hydrodynamic diameters were still slightly larger than in PBS. This could be explained by the non-aggregated unimolecular G0PBG-*g*-PLys micelles having the Lys units on the exterior of the molecules fully protonated, which forced the PLys chains to adopt a more extended conformation due to electrostatic repulsions between the Lys units. The higher surface charge on the outside PLys chains is also supported by the significantly higher zeta potential of G0PBG-*g*-PLys in 0.1M HCl as compared with PBS.

The aggregated species in the intensity distribution are likely due to residual intermolecular electrostatic interactions between the protonated lysine units and the carboxylate groups of glutamic acid moieties. As compared with the size distribution for G1PBG-*g*-PLys in PBS, however, the extent of aggregation was significantly lower. Based on these results it appears that even in 0.1 M HCl, electrostatic interactions cause a small amount of aggregation. As stated earlier, different protecting groups such as Fmoc could be selected to protect the PLys units, to allow their selective deprotection without affecting the benzyl groups in the PBG core.[122] Alternate procedures allowing the selective deprotection of the Z groups of Lys, without tampering with the benzylic groups of the glutamate units, could also be considered to resolve this issue.

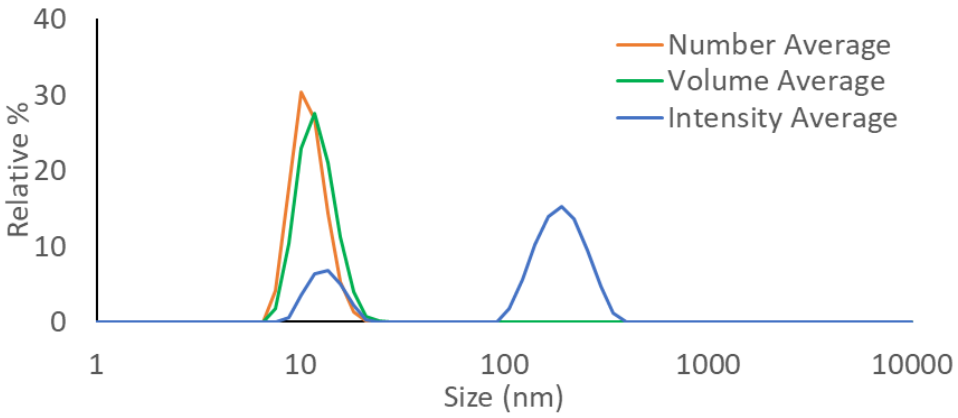

Figure 3.32 Size distributions for G0PBG-*g*-PLys in 0.1 M HCl.

While arborescent copolymer micelles G0PBG-*g*-PLys-*g*-PEG and G1PBG-*g*-PLy-*g*-PEG were also prepared with some degree of success, they could not be isolated in quantities sufficient for size and zeta potential analyses. Increasing the efficiency of imine formation should allow the larger scale synthesis of these micelles in the future.

4 Conclusions and Future Work

In this investigation, the synthesis of arborescent copolymers of G0PBG-*g*-PLys and G1PBG-*g*-PLys with well-defined architectures and controlled molecular weights was accomplished. Relatively narrow molecular weight distributions ($M_w/M_n < 1.10$) were obtained for all the arborescent structures. The molecular weight of the polymers increased with the generation number as expected for arborescent structures.

During deprotection of the Z groups in the PLys layer in G0PBG-*g*-PLys, it was noticed that the benzyl protecting groups on the PBG chains in the core of the micelles were also inadvertently deprotected. This is because the conditions used to deprotect the Z groups of PZLys were identical to those used to cleave the benzyl groups of PBG. This issue was partially addressed by using a lower amount of HBr in the deprotection of G1PBG-*g*-PZLys. In the future, lysine NCA monomers with different protecting groups, requiring deprotection conditions different from the benzylic units of PBG, should be considered to prepare the PLys chains. Protecting groups potentially useful for this purpose include Boc and Fmoc groups.

PEG-Bz-CHO chains with an aromatic aldehyde chain end were prepared through esterification with 4-formylbenzoic acid. These chains were successfully coupled with hexylamine in almost quantitative yield. In contrast, the preparation of the PLys-*g*-PEG imine was incomplete and required the addition of a drying agent to remove water from the system. For G0PBG-*g*-PLys-*g*-PEG and G1PBG-*g*-PLys-*g*-PEG, an insignificant amount of imine was formed even after heating the reaction mixture with a drying agent. These results can be explained by the lesser accessibility of the amine units in PLys and the arborescent structures compared to the small-molecule amines. More stringent reaction conditions, such as heating to higher temperatures and

for longer times with 4A molecular sieves, may help to increase the yield of the coupling reaction between the PBG-*g*-PLys substrates and PEG-Bz-CHO.

The DLS size measurements were also challenging due to the tendency of the copolymer micelles to aggregate in water and in PBS. This was attributed to intermolecular electrostatic interactions between the lysine and glutamic acid units. When comparing the non-aggregated species, G1PBG-*g*-PLys was found to have larger hydrodynamic diameter and more positive zeta potential values as compared with G0PBG-*g*-PLys, as expected. To improve the size characterization results, a different type of protecting group for PLys may be used to facilitate the preservation of the PBG units, which should minimize micelle aggregation due to intermolecular electrostatic interactions.

G0PBG-*g*-PLys-*g*-PEG and G1PBG-*g*-PLys-*g*-PEG could not be isolated in sufficient quantities for size and zeta potential analysis. Increasing the efficiency of imine formation would allow the preparation of these micelles on a larger scale in the future.

References

(1) Ferlay, J.; Colombet, M.; Soerjomataram, I.; Mathers, C.; Parkin, D. M.; Piñeros, M.; Znaor, A.; Bray, F. Estimating the Global Cancer Incidence and Mortality in 2018: GLOBOCAN Sources and Methods. *Int. J. Cancer* **2019**, *144* (8), 1941–1953.

(2) Pérez-Herrero, E.; Fernández-Medarde, A. Advanced Targeted Therapies in Cancer: Drug Nanocarriers, the Future of Chemotherapy. *Eur. J. Pharm. Biopharm.* **2015**, *93*, 52–79.

(3) Seyfried, T. N.; Huyentruyt, L. C. On the Origin of Cancer Metastasis. *Crit. Rev. Oncog.* **2013**, *18* (1–2), 43–73.

(4) Sutradhar, K. B.; Amin, M. L. Nanotechnology in Cancer Drug Delivery and Selective Targeting. *ISRN Nanotechnol.* **2014**, *2014*, 1–12.

(5) Thomas, T. J.; Tajmir-Riahi, H. A.; Pillai, C. K. S. Biodegradable Polymers for Gene Delivery. *Molecules* **2019**, *24* (20), 3744.

(6) Zhang, Y.; Satterlee, A.; Huang, L. In Vivo Gene Delivery by Nonviral Vectors: Overcoming Hurdles. *Mol. Ther.* **2012**, *20* (7), 1298–1304.

(7) Bono, N.; Ponti, F.; Mantovani, D.; Candiani, G. Non-Viral in Vitro Gene Delivery: It Is Now Time to Set the Bar! *Pharmaceutics* **2020**, *12* (2), 183.

(8) Sriraman, S. K.; Aryasomayajula, B.; Torchilin, V. P. Barriers to Drug Delivery in Solid Tumors. *Tissue Barriers* **2014**, *2* (3), e29528-1-e29528-10.

(9) Cabral, H.; Miyata, K.; Osada, K.; Kataoka, K. Block Copolymer Micelles in Nanomedicine

Applications. *Chem. Rev.* **2018**, *118* (14), 6844–6892.

(10) Schmaljohann, D. Thermo- and PH-Responsive Polymers in Drug Delivery. *Adv. Drug Deliv. Rev.* **2006**, *58* (15), 1655–1670.

(11) Wang, Z.; Deng, X.; Ding, J.; Zhou, W.; Zheng, X.; Tang, G. Mechanisms of Drug Release in PH-Sensitive Micelles for Tumour Targeted Drug Delivery System: A Review. *Int. J. Pharm.* **2018**, *535* (1–2), 253–260.

(12) Ganta, S.; Devalapally, H.; Shahiwala, A.; Amiji, M. A Review of Stimuli-Responsive Nanocarriers for Drug and Gene Delivery. *J. Control. Release* **2008**, *126* (3), 187–204.

(13) Dadwal, A.; Baldi, A.; Kumar Narang, R. Nanoparticles as Carriers for Drug Delivery in Cancer. *Artif. Cells, Nanomedicine Biotechnol.* **2018**, *46* (sup2), 295–305.

(14) Maeda, H. The Enhanced Permeability and Retention (EPR) Effect in Tumor Vasculature: The Key Role of Tumor-Selective Macromolecular Drug Targeting. *Adv. Enzyme Regul.* **2001**, *41* (1), 189–207.

(15) Lu, Z. R.; Qiao, P. Drug Delivery in Cancer Therapy, Quo Vadis? *Mol. Pharm.* **2018**, *15* (9), 3603–3616.

(16) Ding, Y.; Xu, Y.; Yang, W.; Niu, P.; Li, X.; Chen, Y.; Li, Z.; Liu, Y.; An, Y.; Liu, Y.; et al. Investigating the EPR Effect of Nanomedicines in Human Renal Tumors via Ex Vivo Perfusion Strategy. *Nano Today* **2020**, *35*, 100970.

(17) Park, K. Facing the Truth about Nanotechnology in Drug Delivery. *ACS Nano* **2013**, *7* (9), 7442–7447.

(18) Shi, Y.; van der Meel, R.; Chen, X.; Lammers, T. The EPR Effect and beyond: Strategies to Improve Tumor Targeting and Cancer Nanomedicine Treatment Efficacy. *Theranostics* **2020**, *10* (17), 7921–7924.

(19) Peer, D.; Karp, J. M.; Hong, S.; Farokhzad, O. C.; Margalit, R.; Langer, R. Nanocarriers as an Emerging Platform for Cancer Therapy. *Nat. Nanotechnol.* **2007**, *2* (12), 751–760.

(20) Sercombe, L.; Veerati, T.; Moheimani, F.; Wu, S. Y.; Sood, A. K.; Hua, S. Advances and Challenges of Liposome Assisted Drug Delivery. *Front. Pharmacol.* **2015**, *6*, 286.

(21) Ahmad, M. Z.; Akhter, S.; Jain, G. K.; Rahman, M.; Pathan, S. A.; Ahmad, F. J.; Khar, R. K. Metallic Nanoparticles: Technology Overview and Drug Delivery Applications in Oncology. *Expert Opin. Drug Deliv.* **2010**, *7* (8), 927–942.

(22) Ahmad, Z.; Shah, A.; Siddiq, M.; Kraatz, H. B. Polymeric Micelles as Drug Delivery Vehicles. *RSC Adv.* **2014**, *4* (33), 17028–17038.

(23) Zhou, Z.; Liu, X.; Zhu, D.; Wang, Y.; Zhang, Z.; Zhou, X.; Qiu, N.; Chen, X.; Shen, Y. Nonviral Cancer Gene Therapy: Delivery Cascade and Vector Nanoproperty Integration. *Adv. Drug Deliv. Rev.* **2017**, *115*, 115–154.

(24) Samal, S. K.; Dash, M.; Vlierberghe, S. Van; Kaplan, D. L.; Chiellini, E.; Blitterswijk, C. van; Moroni, L.; Dubruel, P. Cationic Polymers and Their Therapeutic Potential. *Chem. Soc. Rev.* **2012**, *41* (21), 7147–7194.

(25) Hong, S. J.; Ahn, M. H.; Sangshetti, J.; Choung, P. H.; Arote, R. B. Sugar-Based Gene Delivery Systems: Current Knowledge and New Perspectives. *Carbohydr. Polym.* **2018**,

181, 1180–1193.

(26) Teixeira, H. F.; Bruxel, F.; Fraga, M.; Schuh, R. S.; Zorzi, G. K.; Matte, U.; Fattal, E. Cationic Nanoemulsions as Nucleic Acids Delivery Systems. *Int. J. Pharm.* **2017**, *534* (1–2), 356–367.

(27) Owens, D. E.; Peppas, N. A. Opsonization, Biodistribution, and Pharmacokinetics of Polymeric Nanoparticles. *Int. J. Pharm.* **2006**, *307* (1), 93–102.

(28) Kweon, D. K.; Kang, D. O. O. W. Drug-Release Behavior of Chitosan-g-Poly(Vinyl Alcohol) Copolymer Matrix. *J. Appl. Polym. Sci.* **1999**, *74*, 458–464.

(29) Inoue, T.; Chen, G.; Nakamae, K.; Hoffman, A. S. An AB Block Copolymer of Oligo(Methyl Methacrylate) and Poly(Acrylic Acid) for Micellar Delivery of Hydrophobic Drags. *J. Control. Release* **1998**, *51* (2–3), 221–229.

(30) Scales, C. W.; Huang, F.; Li, N.; Vasilieva, Y. A.; Ray, J.; Convertine, A. J.; McCormick, C. L. Corona-Stabilized Interpolyelectrolyte Complexes of SiRNA with Nonimmunogenic, Hydrophilic/Cationic Block Copolymers Prepared by Aqueous RAFT Polymerization. *Macromolecules* **2006**, *39* (20), 6871–6881.

(31) Kabanov, A. V.; Chekhonin, V. P.; Alakhov, V. Y.; Batrakova, E. V.; Lebedev, A. S.; Melik-Nubarov, N. S.; Arzhakov, S. A.; Levashov, A. V.; Morozov, G. V.; Severin, E. S.; et al. The Neuroleptic Activity of Haloperidol Increases after Its Solubilization in Surfactant Micelles. Micelles as Microcontainers for Drug Targeting. *FEBS Lett.* **1989**, *258* (2), 343–345.

(32) Zhang, X.; Jackson, J. K.; Burt, H. M. Development of Amphiphilic Diblock Copolymers as Micellar Carriers of Taxol. *Int. J. Pharm.* **1996**, *132*, 195–206.

(33) Pişkin, E.; Kaitian, X.; Denkbaş, E. B.; Küçükyavuz, Z. Novel PDLLA/PEG Copolymer Micelles as Drug Carriers. *J. Biomater. Sci. Polym. Ed.* **1995**, *7* (4), 359–373.

(34) Kadam, Y.; Yerramilli, U.; Bahadur, A.; Bahadur, P. Micelles from PEO-PPO-PEO Block Copolymers as Nanocontainers for Solubilization of a Poorly Water Soluble Drug Hydrochlorothiazide. *Colloids Surfaces B Biointerfaces* **2011**, *83* (1), 49–57.

(35) Kataoka, K.; Matsumoto, T.; Yokoyama, M.; Okana, T.; Yasuhisa, S.; Fukushima, S.; Okamoto, K.; Kwon, G. S. Doxorubicin-Loaded Poly(Ethylene Glycol)–Poly(b-Benzyl-L-Aspartate) Copolymer Micelles: Their Pharmaceutical Characteristics and Biological Significance. *J. Control. Release* **2000**, *64* (1–3), 143–153.

(36) Cabral, H.; Kataoka, K. Progress of Drug-Loaded Polymeric Micelles into Clinical Studies. *J. Control. Release* **2014**, *190*, 465–476.

(37) Hamaguchi, T.; Kato, K.; Yasui, H.; Morizane, C.; Ikeda, M.; Ueno, H.; Muro, K.; Yamada, Y.; Okusaka, T.; Shirao, K.; et al. A Phase I and Pharmacokinetic Study of NK105, a Paclitaxel-Incorporating Micellar Nanoparticle Formulation. *Br. J. Cancer* **2007**, *97* (2), 170–176.

(38) Kim, J. O.; Oberoi, H. S.; Desale, S.; Kabanov, A. V.; Bronich, T. K. Polypeptide Nanogels with Hydrophobic Moieties in the Cross-Linked Ionic Cores: Synthesis, Characterization and Implications for Anticancer Drug Delivery. *J. Drug Target.* **2013**, *21* (10), 981–993.

(39) Ohya, Y.; Takeda, S.; Shibata, Y.; Ouchi, T.; Kano, A.; Iwata, T.; Mochizuki, S.; Taniwaki, Y.; Maruyama, A. Evaluation of Polyanion-Coated Biodegradable Polymeric Micelles as Drug Delivery Vehicles. *J. Control. Release* **2011**, *155* (1), 104–110.

(40) Fan, X.; Li, Z.; Loh, X. J. Recent Development of Unimolecular Micelles as Functional Materials and Applications. *Polym. Chem.* **2016**, *7* (38), 5898–5919.

(41) Yuan, X.; Harada, A.; Yamasaki, Y.; Kataoka, K. Stabilization of Lysozyme-Incorporated Polyion Complex Micelles by the ω-End Derivatization of Poly(Ethylene Glycol)-Poly(α,β-Aspartic Acid) Block Copolymers with Hydrophobic Groups. *Langmuir* **2005**, *21* (7), 2668–2674.

(42) Tomalia, D. A.; Baker, H.; Dewald, J.; Hall, M.; Kallos, G.; Martin, S.; Roeck, J.; Ryder, J.; Smith, P. A New Class of Polymers: Starburst-Dendritic Macromolecules. *Polym. J.* **1985**, *17* (1), 117–132.

(43) Esfand, R.; Tomalia, D. A. Poly(Amidoamine) (PAMAM) Dendrimers: From Biomimicry to Drug Delivery and Biomedical Applications. *Drug Discov. Today* **2001**, *6* (8), 427–436.

(44) Kojima, C.; Kono, K.; Maruyama, K.; Takagishi, T. Synthesis of Polyamidoamine Dendrimers Having Poly(Ethylene Glycol) Grafts and Their Ability to Encapsulate Anticancer Drugs. *Bioconjug. Chem.* **2000**, *11* (6), 910–917.

(45) Patri, A. K.; Kukowska-Latallo, J. F.; Baker, J. R. Targeted Drug Delivery with Dendrimers: Comparison of the Release Kinetics of Covalently Conjugated Drug and Non-Covalent Drug Inclusion Complex. *Adv. Drug Deliv. Rev.* **2005**, *57* (15), 2203–2214.

(46) Morgan, M. T.; Nakanishi, Y.; Kroll, D. J.; Griset, A. P.; Carnahan, M. A.; Wathier, M.; Oberlies, N. H.; Manikumar, G.; Wani, M. C.; Grinstaff, M. W. Dendrimer-Encapsulated Camptothecins: Increased Solubility, Cellular Uptake, and Cellular Retention Affords Enhanced Anticancer Activity in Vitro. *Cancer Res.* **2006**, *66* (24), 11913–11921.

(47) Kim, Y. H.; Webster, O. W. Water-Soluble Hyperbranched Polyphenylene; "A Unimolecular Micelle"? *J. Am. Chem. Soc.* **1990**, *112* (11), 4592–4593.

(48) Kurniasih, I. N.; Keilitz, J.; Haag, R. Dendritic Nanocarriers Based on Hyperbranched Polymers. *Chem. Soc. Rev.* **2015**, *44* (12), 4145–4164.

(49) Gauthier, M.; Möller, M. Uniform Highly Branched Polymers by Anionic Grafting: Arborescent Graft Polymers. *Macromolecules* **1991**, *24* (16), 4548–4553.

(50) Tomalia, D. A.; Hedstrand, D. M.; Ferritto, M. S. Comb-Burst Dendrimer Topology. New Macromolecular Architecture Derived from Dendritic Grafting. *Macromolecules* **1991**, *24* (6), 1435–1438.

(51) Teertstra, S. J.; Gauthier, M. Dendrigraft Polymers: Macromolecular Engineering on a Mesoscopic Scale. *Prog. Polym. Sci.* **2004**, *29* (4), 277–327.

(52) Gauthier, M.; Tichagwa, L.; Downey, J. S.; Gao, S. Arborescent Graft Copolymers: Highly Branched Macromolecules with a Core-Shell Morphology. *Macromolecules* **1996**, *29* (2), 519–527.

(53) Kee, R. A.; Gauthier, M. Arborescent Polystyrene-Graft-Poly(2-Vinylpyridine) Copolymers: Synthesis and Enhanced Polyelectrolyte Effect in Solution. *Macromolecules*

2002, *35* (17), 6526–6532.

(54) Collier, L. Determination of Bis-Chloromethyl Ether at the Ppb Level in Air Samples by High-Resolution Mass Spectroscopy. *Environ. Sci. Technol.* **1972**, *6* (10), 930–932.

(55) Li, J.; Gauthier, M. A Novel Synthetic Path to Arborescent Graft Polystyrenes. *Macromolecules* **2001**, *34* (26), 8918–8924.

(56) Gauthier, M.; Li, J.; Dockendorff, J. Arborescent Polystyrene-Graft-Poly(2-Vinylpyridine) Copolymers as Unimolecular Micelles. Synthesis from Acetylated Substrates. *Macromolecules* **2003**, *36* (8), 2642–2648.

(57) Yuan, Z.; Gauthier, M. Synthesis of Arborescent Isoprene Homopolymers. *Macromolecules* **2005**, *38* (10), 4124–4132.

(58) Zhang, H.; Li, Y.; Zhang, C.; Li, Zh.; Li, X.; Wang, Y. Synthesis of Dendrigraft Star-Comb Polybutadienes by Anionic Polymerization and Grafting-onto Methodology. *Macromolecules* **2009**, *42* (14), 5073–5079.

(59) Gauthier, M.; Aridi, T. Synthesis of Arborescent Polystyrene by "Click" Grafting. *J. Polym. Sci. Part A Polym. Chem.* **2019**, *57* (16), 1730–1740.

(60) Yuan, Z.; Gauthier, M. One-Pot Synthesis of Arborescent Polystyrenes. *Macromolecules* **2006**, *39* (6), 2063–2071.

(61) Vivek, A. V.; Babu, K.; Dhamodharan, R. Arborescent Polystyrene via Ambient Temperature ATRP: Toward Ordered Honeycomb Microstructured Templates. *Macromolecules* **2009**, *42* (6), 2300–2303.

(62) Feng, X. S.; Taton, D.; Chaikof, E. L.; Gnanou, Y. Toward an Easy Access to Dendrimer-like Poly(Ethylene Oxide)S. *J. Am. Chem. Soc.* **2005**, *127* (31), 10956–10966.

(63) Grasmiiller, M.; Puskas, J. E. Star-Brached and Hyperbranched Polyisobutylenes. *Macromol. Symp.* **1998**, *132* (1), 117–126.

(64) Karimi, M.; Ghasemi, A.; Sahandi Zangabad, P.; Rahighi, R.; Moosavi Basri, S. M.; Mirshekari, H.; Amiri, M.; Shafaei Pishabad, Z.; Aslani, A.; Bozorgomid, M.; et al. Smart Micro/Nanoparticles in Stimulus-Responsive Drug/Gene Delivery Systems. *Chem. Soc. Rev.* **2016**, *45* (5), 1457–1501.

(65) Wang, Y. C.; Wang, F.; Sun, T. M.; Wang, J. Redox-Responsive Nanoparticles from the Single Disulfide Bond-Bridged Block Copolymer as Drug Carriers for Overcoming Multidrug Resistance in Cancer Cells. *Bioconjug. Chem.* **2011**, *22* (10), 1939–1945.

(66) Li, Y.; Lokitz, B. S.; Armes, S. P.; McCormick, C. L. Synthesis of Reversible Shell Cross-Linked Micelles for Controlled Release of Bioactive Agents. *Macromolecules* **2006**, *39* (8), 2726–2728.

(67) Yan, B.; Boyer, J. C.; Branda, N. R.; Zhao, Y. Near-Infrared Light-Triggered Dissociation of Block Copolymer Micelles Using Upconverting Nanoparticles. *J. Am. Chem. Soc.* **2011**, *133* (49), 19714–19717.

(68) Son, S.; Shin, E.; Kim, B. S. Light-Responsive Micelles of Spiropyran Initiated Hyperbranched Polyglycerol for Smart Drug Delivery. *Biomacromolecules* **2014**, *15* (2), 628–634.

(69) Devalapally, H.; Shenoy, D.; Little, S.; Langer, R.; Amiji, M. Poly(Ethylene Oxide)-Modified Poly(Beta-Amino Ester) Nanoparticles as a PH-Sensitive System for Tumor-Targeted Delivery of Hydrophobic Drugs: Part 3. Therapeutic Efficacy and Safety Studies in Ovarian Cancer Xenograft Model. *Cancer Chemother. Pharmacol.* **2007**, *59* (4), 477–484.

(70) Keeney, M.; Ong, S. G.; Padilla, A.; Yao, Z.; Goodman, S.; Wu, J. C.; Yang, F. Development of Poly(β-Amino Ester)-Based Biodegradable Nanoparticles for Nonviral Delivery of Minicircle DNA. *ACS Nano* **2013**, *7* (8), 7241–7250.

(71) Bae, Y.; Fukushima, S.; Harada, A.; Kataoka, K. Design of Environment-Sensitive Supramolecular Assemblies for Intracellular Drug Delivery: Polymeric Micelles That Are Responsive to Intracellular PH Change. *Angew. Chemie - Int. Ed.* **2003**, *42* (38), 4640–4643.

(72) Lee, E. S.; Shin, H. J.; Na, K.; Bae, Y. H. Poly(L-Histidine)–PEG Block Copolymer Micelles and PH-Induced Destabilization. **2003**, *90*, 363–374.

(73) Sun, Y.; Li, Y.; Nan, S.; Zhang, L.; Huang, H.; Wang, J. Synthesis and Characterization of PH-Sensitive Poly(Itaconic Acid)-Poly(Ethylene Glycol)-Folate-Poly(L-Histidine) Micelles for Enhancing Tumor Therapy and Tunable Drug Release. *J. Colloid Interface Sci.* **2015**, *458*, 119–129.

(74) Zhang, Y.; Li, P.; Pan, H.; Liu, L.; Ji, M.; Sheng, N.; Wang, C.; Cai, L.; Ma, Y. Retinal-Conjugated PH-Sensitive Micelles Induce Tumor Senescence for Boosting Breast Cancer Chemotherapy. *Biomaterials* **2016**, *83*, 219–232.

(75) Zhou, T.; Llizo, A.; Wang, C.; Xu, G.; Yang, Y. Nanostructure-Induced DNA Condensation.

Nanoscale **2013**, *5* (18), 8288–8306.

(76) Venkiteswaran, S.; Thomas, T.; Thomas, T. J. Selectivity of Polyethyleneimines on DNA Nanoparticle Preparation and Gene Transport. *ChemistrySelect* **2016**, *1* (6), 1144–1150.

(77) Pandey, A. P.; Sawant, K. K. Polyethylenimine: A Versatile, Multifunctional Non-Viral Vector for Nucleic Acid Delivery. *Mater. Sci. Eng. C* **2016**, *68*, 904–918.

(78) Lee, Y.; Mo, H.; Koo, H.; Park, J. Y.; Cho, M. Y.; Jin, G. W.; Park, J. S. Visualization of the Degradation of a Disulfide Polymer, Linear Poly(Ethylenimine Sulfide), for Gene Delivery. *Bioconjug. Chem.* **2007**, *18* (1), 13–18.

(79) Gou, M.; Men, K.; Zhang, J.; Li, Y.; Song, J.; Luo, S.; Shi, H.; Wen, Y.; Guo, G.; Huang, M.; et al. Efficient Inhibition of C-26 Colon Carcinoma by VSVMP Gene Delivered by Biodegradable Cationic Nanogel Derived from Polyethyleneimine. *ACS Nano* **2010**, *4* (10), 5573–5584.

(80) Liu, L.; Zheng, M.; Librizzi, D.; Renette, T.; Merkel, O. M.; Kissel, T. Efficient and Tumor Targeted SiRNA Delivery by Polyethylenimine-Graft-Polycaprolactone-Block-Poly(Ethylene Glycol)-Folate (PEI-PCL-PEG-Fol). *Mol. Pharm.* **2016**, *13* (1), 134–143.

(81) Tripathi, S. K.; Goyal, R.; Kashyap, M. P.; Pant, A. B.; Haq, W.; Kumar, P.; Gupta, K. C. Depolymerized Chitosans Functionalized with BPEI as Carriers of Nucleic Acids and Tuftsin-Tethered Conjugate for Macrophage Targeting. *Biomaterials* **2012**, *33* (16), 4204–4219.

(82) Kang, J. H.; Tachibana, Y.; Kamata, W.; Mahara, A.; Harada-Shiba, M.; Yamaoka, T.

Liver-Targeted SiRNA Delivery by Polyethylenimine (PEI)-Pullulan Carrier. *Bioorganic Med. Chem.* **2010**, *18* (11), 3946–3950.

(83) Parhiz, H.; Hashemi, M.; Hatefi, A.; Shier, W. T.; Amel Farzad, S.; Ramezani, M. Arginine-Rich Hydrophobic Polyethylenimine: Potent Agent with Simple Components for Nucleic Acid Delivery. *Int. J. Biol. Macromol.* **2013**, *60*, 18–27.

(84) Liu, Y.; Li, Y.; Keskin, D.; Shi, L. Poly(β-Amino Esters): Synthesis, Formulations, and Their Biomedical Applications. *Adv. Healthc. Mater.* **2019**, *8* (2), 1–24.

(85) Bhise, N. S.; Shmueli, R. B.; Gonzalez, J.; Green, J. J. A Novel Assay for Quantifying the Number of Plasmids Encapsulated by Polymer Nanoparticles. *Small* **2012**, *8* (3), 367–373.

(86) Guerrero-Cázares, H.; Tzeng, S. Y.; Young, N. P.; Abutaleb, A. O.; Quiñones-Hinojosa, A.; Green, J. J. Biodegradable Polymeric Nanoparticles Show High Efficacy and Specificity at DNA Delivery to Human Glioblastoma in Vitro and in Vivo. *ACS Nano* **2014**, *8* (5), 5141–5153.

(87) Wang, W.; Zhou, D.; Cutlar, L.; Gao, Y.; Wang, W.; O'Keeffe-Ahern, J.; McMahon, S.; Duarte, B.; Larcher, F.; Rodriguez, B. J.; et al. The Transition from Linear to Highly Branched Poly(β-Amino Ester)s: Branching Matters for Gene Delivery. *Sci. Adv.* **2016**, *2* (6), 1–15.

(88) Lopez-bertoni, H.; Kozielski, K. L.; Rui, Y.; Lal, B.; Wilson, D. R.; Mihelson, N.; Eberhart, C. G.; Green, J. J. Bioreducible Polymeric Nanoparticles Containing Multiplexed Cancer Stem Cell-Regulating MiRNAs Inhibit Glioblastoma Growth and Prolong Survival. **2019**, *18* (7), 4086–4094.

(89) Segovia, N.; Dosta, P.; Cascante, A.; Ramos, V.; Borrós, S. Oligopeptide-Terminated Poly(β-Amino Ester)s for Highly Efficient Gene Delivery and Intracellular Localization. *Acta Biomater.* **2014**, *10* (5), 2147–2158.

(90) Kodama, Y.; Nakamura, T.; Kurosaki, T.; Egashira, K.; Mine, T.; Nakagawa, H.; Muro, T.; Kitahara, T.; Higuchi, N.; Sasaki, H. Biodegradable Nanoparticles Composed of Dendrigraft Poly-l-Lysine for Gene Delivery. *Eur. J. Pharm. Biopharm.* **2014**, *87* (3), 472–479.

(91) Tian, H.; Lin, L.; Jiao, Z.; Guo, Z.; Chen, J.; Gao, S.; Zhu, X.; Chen, X. Polylysine-Modified Polyethylenimine Inducing Tumor Apoptosis as an Efficient Gene Carrier. *J. Control. Release* **2013**, *172* (2), 410–418.

(92) Benns, J. M.; Choi, J. S.; Mahato, R. I.; Park, J. S.; Sung Wan Kim. PH-Sensitive Cationic Polymer Gene Delivery Vehicle: N-Ac-Poly(L-Histidine)-Graft-Poly(L-Lysine) Comb Shaped Polymer. *Bioconjug. Chem.* **2000**, *11* (5), 637–645.

(93) Xu, H.; Yao, Q.; Cai, C.; Gou, J.; Zhang, Y.; Zhong, H.; Tang, X. Amphiphilic Poly(Amino Acid) Based Micelles Applied to Drug Delivery: The in Vitro and in Vivo Challenges and the Corresponding Potential Strategies. *J. Control. Release* **2015**, *199*, 84–97.

(94) Koizumi, F.; Kitagawa, M.; Negishi, T.; Onda, T.; Matsumoto, S. I.; Hamaguchi, T.; Matsumura, Y. Novel SN-38-Incorporating Polymeric Micelles, NK012, Eradicate Vascular Endothelial Growth Factor-Secreting Bulky Tumors. *Cancer Res.* **2006**, *66* (20), 10048–10056.

(95) Klok, H. A.; Rodríguez-Hernández, J. Dendritic-Graft Polypeptides. *Macromolecules* **2002**,

35 (23), 8718–8723.

(96) Collet, H.; Souaid, E.; Cottet, H.; Deratani, A.; Boiteau, L.; Dessalces, G.; Rossi, J. C.; Commeyras, A.; Pascal, R. An Expeditious Multigram-Scale Synthesis of Lysine Dendrigraft (DGL) Polymers by Aqueous n-Carboxyanhydride Polycondensation. *Chem. - A Eur. J.* **2010**, *16* (7), 2309–2316.

(97) Whitton, G.; Gauthier, M. Arborescent Polypeptides from γ-Benzyl l -Glutamic Acid. *J. Polym. Sci. Part A Polym. Chem.* **2013**, *51*, 5270–5279.

(98) Whitton, G.; Gauthier, M. Arborescent Micelles: Dendritic Poly(γ-Benzyl l -Glutamate) Cores Grafted with Hydrophilic Chain Segments. *J. Polym. Sci. Part A Polym. Chem.* **2016**, *54* (9), 1197–1209.

(99) Gauthier, M.; Whitton, G. Arborescent Unimolecular Micelles: Poly(γ-Benzyl L-Glutamate) Core Grafted with a Hydrophilic Shell by Copper(I)-Catalyzed Azide-Alkyne Cycloaddition Coupling. *Polymers (Basel).* **2017**, *9* (10), 540–555.

(100) Alsehli, M.; Gauthier, M. Arborescent Polypeptides for Sustained Drug Delivery Applications, University of Waterloo, 2017.

(101) Sokalingam, S.; Raghunathan, G.; Soundrarajan, N.; Lee, S. G. A Study on the Effect of Surface Lysine to Arginine Mutagenesis on Protein Stability and Structure Using Green Fluorescent Protein. *PLoS One* **2012**, *7* (7), e40410.

(102) Nayvelt, I.; Thomas, T.; Thomas, T. J. Mechanistic Differences in DNA Nanoparticle Formation in the Presence of Oligolysines and Poly-L-Lysine. *Biomacromolecules* **2007**, *8*

(2), 477–484.

(103) Wan, Y.; Alterman, M.; Larhed, M.; Hallberg, A. Dimethylformamide as a Carbon Monoxide Source in Fast Palladium-Catalyzed Aminocarbonylations of Aryl Bromides. *J. Org. Chem.* **2002**, *67* (17), 6232–6235.

(104) Kramer, J. R.; Deming, T. J. General Method for Purification of α-Amino Acid-N-Carboxyanhydrides Using Flash Chromatography. *Biomacromolecules* **2010**, *11* (12), 3668–3672.

(105) Masson, C.; Scherman, D.; Bessodes, M. 2,2,6,6-Tetramethyl-1-Piperidinyl-Oxyl/[Bis(Acetoxy)-Iodo]Benzene-Mediated Oxidation: A Versatile and Convenient Route to Poly(Ethylene Glycol) Aldehyde or Carboxylic Acid Derivatives. *J. Polym. Sci. Part A Polym. Chem.* **2001**, *39* (22), 4022–4024.

(106) Gu, J.; Cheng, W. P.; Liu, J.; Lo, S. Y.; Smith, D.; Qu, X.; Yang, Z. PH-Triggered Reversible "Stealth" Polycationic Micelles. *Biomacromolecules* **2008**, *9* (1), 255–262.

(107) Ji, S.; Hoye, T. R.; Macosko, C. W. Primary Amine (-NH 2) Quantification in Polymers: Functionality by 19F NMR Spectroscopy. *Macromolecules* **2005**, *38* (11), 4679–4686.

(108) Deming, T. J. Facile Synthesis of Block Copolypeptides of Defined Architecture. *Nature* **1997**, *390* (6658), 386–389.

(109) Leuchs, H. Ueber Die Glycin-carbonsäure. *Berichte der Dtsch. Chem. Gesellschaft* **1906**, *39* (1), 857–861.

(110) Farthing, A. C. Synthetic Polypeptides. Part I. Synthesis of Oxazolid-2 : 5-Diones and a

New Reaction of Glycine. *J. Chem. Soc.* **1950**, 3213–3217.

(111) Farthing, A. C.; Reynolds, R. J. W. Anhydro-N-Carboxy-DL-Beta-Phenylalanine. **1950**, No. 4199, 647.

(112) Levy, A. L. Anhydro-N-Carboxy-DL-Beta-Phenylalanine. **1950**, *165*, 152.

(113) Semple, J. E.; Sullivan, B.; Sill, K. N. Large-Scale Synthesis of α-Amino Acid-N-Carboxyanhydrides. *Synth. Commun.* **2017**, *47* (1), 53–61.

(114) Habraken, G. J. M.; Peeters, M.; Dietz, C. H. J. T.; Koning, C. E.; Heise, A. How Controlled and Versatile Is N-Carboxy Anhydride (NCA) Polymerization at 0 °C? Effect of Temperature on Homo-, Block- and Graft (Co)Polymerization. *Polym. Chem.* **2010**, *1* (4), 514–524.

(115) De Mico, A.; Margarita, R.; Parlanti, L.; Vescovi, A.; Piancatelli, G. A Versatile and Highly Selective Hypervalent Iodine (III)/ 2,2,6,6-Tetraniethyl-1-Piperidinyloxyl-Mediated Oxidation of Alcohols to Carbonyl Compounds. *J. Org. Chem.* **1997**, *62* (20), 6974–6977.

(116) Xin, Y.; Yuan, J. Schiff's Base as a Stimuli-Responsive Linker in Polymer Chemistry. *Polym. Chem.* **2012**, *3* (11), 3045–3055.

(117) Ben-Ishai, D. The Use of Hydrogen Bromide in Acetic Acid for the Removal of Carbobenzoxy Groups and Benzyl Esters of Peptide Derivatives. *J. Org. Chem.* **1954**, *19* (1), 62–66.

(118) El-Faham, A.; Albericio, F. Peptide Coupling Reagents, More than a Letter Soup. *Chem. Rev.* **2011**, *111* (11), 6557–6602.

(119) Schwyzer, R.; Rittel, W. Synthese von Peptid-Zwischenprodukten Für Den Aufbau Eines Corticotrop Wirksamen Nonadecapeptids. I. Nϵ-t-Butyloxycarbonyl-L-lysin, Nϵ-(Nϵ-t-Butyloxycarbonyl-L-lysyl)-Nϵ-t-butyloxycarbonyl-L-lysin, Nϵ-t-Butyloxycarbonyl-L-lysyl-L-prolyl-L-valyl-glycin Und. *Helv. Chim. Acta* **1961**, *44* (1), 159–169.

(120) Isidro-Llobet, A.; Álvarez, M.; Albericio, F. Amino Acid-Protecting Groups. *Chem. Rev.* **2009**, *109* (6), 2455–2504.

(121) Dölling, R.; Beyermann, M.; Haenel, J.; Kernchen, F.; Krause, E.; Franke, P.; Brudel, M.; Bienert, M. Piperidine-Mediated Side Product Formation for Asp(OBut)- Containing Peptides. *J. Chem. Soc. Chem. Commun.* **1994**, *20* (7), 853–854.

(122) Luna, O. F.; Gomez, J.; Cárdenas, C.; Albericio, F.; Marshall, S. H.; Guzmán, F. Deprotection Reagents in Fmoc Solid Phase Peptide Synthesis: Moving Away from Piperidine? *Molecules* **2016**, *21* (11), 1542–1533.